UNIVERSIDADE FEDERAL DE MINAS GERAIS

Instituto de Geociências

Programa de Pós-Graduação em Geologia

Júlia Mattioli Rolim

First U-Pb age constraints from plutonic xenoliths preserved in alkaline volcanic rocks of the Brazilian Fernando de Noronha Archipelago, Southwest Atlantic Ocean

N° 232

Belo Horizonte
DATA (02/02/2022)

Júlia Mattioli Rolim

First U-Pb age constraints from plutonic xenoliths preserved in alkaline volcanic rocks of the Brazilian Fernando de Noronha Archipelago, Southwest Atlantic Ocean

Versão Final

Dissertação apresentada ao Programa de Pós-Graduação em Geologia da Universidade Federal de Minas Gerais como requisito parcial para obtenção do título de Mestre em Geologia.

Área de Concentração: Geologia Regional

Orientador: Prof. Dr. Tiago Amâncio Novo

Coorientador: Prof. Dr. Fábio Soares de Oliveira e Prof. Dr. Ross Stevenson

Belo Horizonte
2022

R748f
2022

Rolim, Júlia Mattioli.

First U-Pb age constraints from plutonic xenoliths preserved in alkaline volcanic rocks of the Brazilian Fernando de Noronha Archipelago, Southwest Atlantic Ocean [manuscrito] / Júlia Mattioli Rolim. – 2022.

81 f., enc. il. (principalmente color.)

Orientador: Tiago Amâncio Novo.

Coorientadores: Fábio Soares de Oliveira e Ross Stevenson.

Dissertação (mestrado) – Universidade Federal de Minas Gerais, Instituto de Geociências, 2022.

Área de concentração: Geologia Regional.

Bibliografia: f. 42-52.

Inclui anexos e apêndice.

1. Rochas plutônicas – Teses. 2. Apatita – Fernando de Noronha, Arquipélago (PE) – Teses. 3. Tempo geológico – Teses. I. Novo, Tiago Amâncio. II. Oliveira, Fábio Soares de. III. Stevenson, Ross. IV. Universidade Federal de Minas Gerais. Instituto de Geociências. V. Título.

CDU: 552.321(813.6)

Ficha catalográfica elaborada por Elisabete Quatrini Vieira – CRB6 2210

UNIVERSIDADE FEDERAL DE MINAS GERAIS

PROGRAMA DE PÓS-GRADUAÇÃO EM GEOLOGIA DO IGC-UFMG

FOLHA DE APROVAÇÃO

New U-Pb age constraints from plutonic enclaves preserved in alkaline volcanic rocks of the Brazilian oceanic Fernando de Noronha Archipelago, Southwest Atlantic Ocean

JÚLIA MATTIOLI ROLIM

Dissertação submetida à Banca Examinadora designada pelo Colegiado, como requisito para obtenção do grau de Mestre em GEOLOGIA, área de concentração GEOLOGIA REGIONAL, pelo Programa de Pós-graduação em Geologia do Instituto de Geociências da Universidade Federal de Minas Gerais.

Aprovada em 02 de fevereiro de 2022, pela banca constituída pelos membros:

Prof. Tiago Amâncio Novo - Orientador
UFMG

Profa. Mahyra Ferreira Tedeschi
UFMG

Prof. Matheus Henrique Kuchenbecker do Amaral
UFVJM

Belo Horizonte, 2 de fevereiro de 2022.

To my parents, Rosangela Mattioli Silva and Clauder Teixeira Rolim, for all their love and support.

ACKNOWLEDGMENTS

Firstly, I would like to thank my parents, Rosangela and Clauder, for all their support, encouragement, and understanding, and for being present throughout my academic career. I also thank my brothers, Vitor, Camila, and Lucas, and my grandparents, Nilza, Onofre, Marjô, and Deck, for always guiding me and celebrating my achievements, even if from afar away, as well as my family. Thanks to my friends, especially Maria Clara and Ana Paula for the friendship and thanks to Angelo Santos, Danielle, and Lora for the endless support and friendship, especially throughout my stay in Canada.

Thanks to *"Pró-reitoria de Pós-graduação (PRPg) UFMG"* and the *"Programa de Pós-graduação em Geologia do Instituto de Geociências (IGC-UFMG)".* Also thanks to Prof. Tiago Novo, for always giving necessary support for the project's development, and Prof. Fábio Soares de Oliveira, for always encouraging me and for all the amazing opportunities during my academic career. Porf. Ross Stevenson for all support, learnings and for providing the opportunity of an internship and a life-change experience in Montreal. Thanks also Prof. Joshua Davies for all the teachings, for the supportive review and opportunities, as well as Prof. Antônio Pedrosa-Soares for support, comments and review. Also thanks to Prof. Mahyra Tedeschi, for all the teachings and support, and Prof. Anderson Santos, for always being available and helping us to understanding the complexity of the Brazilian volcanic islands and Prof. Matheus Kuchenbecker for the comments and review.

To ICMBio and ATDEFN for the authorization and collaboration that made it possible to carry out the activities of the field. To CPMTC for sample preparation support and facilities, as well as Profa. Gláucia Queiroga (LMIC) and Prof. Cristiano Lana (LOPAG) for the analytical support at UFOP. Thanks to Geotop, especially to Andre Poirier, Daniele Pinti, Julien Gogot, Diogo Barnetche, and Sandrine, for the support and the learnings. Thanks also to Global Affairs Canada.

This work is part of the Project *"Geomorfologia Ambiental das Ilhas Oceânicas Fernando de Noronha e Trindade: compartimentação do relevo, evolução quaternária e interações solo-água"*, coordinated by Prof. Dr. Fábio Soares de Oliveira (IGC-UFMG). This study was financed in part by the Coordenação de Aperfeiçoamento de Pessoal de Nível Superior - Brasil (CAPES) - Finance Code 001, CNPq (Nº 28/2018 – Edital Universal) and research funding to RS was provided by an NSERC Discovery grant.

Do not let anyone rob you of your imagination, your creativity, or your curiosity. It is your place in the world; it is your life. Go on and do all you can with it, and make it the life you want to live."
- Mae Jemison, first African American woman astronaut in space

RESUMO

Os xenólitos plutônicos são fonte de informações e evidências sobre processos magmáticos que ocorrem em profundidade, nas zonas alimentadoras de edifícios vulcânicos. Novos dados petrográficos, geoquímicos, isotópicos e geocronológicos são apresentados para um xenólito classificado como kaersutita diorito, do depósito piroclástico da unidade basal do Arquipélago de Fernando de Noronha (FNA), no Sudoeste do Oceano Atlântico. A amostra é formada principalmente por kaersutita, andesina, diopsídeo e flogopita, associado com magnetita e ilmenita, juntamente com minerais acessórios, como apatita, titanita e zircão. As assinaturas de elementos principais e traços das análises de rocha total apresentam composições subsaturadas em sílica e padrões enriquecidos de ETR leves (La/Yb_N = 13-14) que são semelhantes às outras rochas da FNA. As análises de isótopos de Nd produzem valores de ε_{Nd} de +1,7 a +2,2. Análises de U-Pb em zircão obtidas a partir do kaersutita diorito forneceram uma idade de cristalização de 13,69 ± 0,07 Ma, enquanto uma idade U-Pb calculada utilizando titanita e apatita registra uma idade U-Pb mais recente de 9,76 ± 0,94 Ma, refletindo um evento térmico mais jovem, provavelmente relacionado ao magmatismo explosivo que formou o depósito piroclástico da unidade basal da FNA. Essas idades também indicam que o magmatismo da FNA foi contemporâneo com o magmatismo continental terrestre encontrado no nordeste do Brasil.

PALAVRAS-CHAVES: ROCHAS PLUTÔNICAS, APATITA, TITANITA, ZIRCÃO

ABSTRACT

Plutonic xenoliths are a potential wealth of information and evidence about magmatic processes that occur at depth, in the feeder zones of volcanic edifices. New petrographic, geochemical, isotopic, and geochronology data are presented for kaersutite diorite derived from a pyroclastic deposit from the basal unit of the Fernando de Noronha Archipelago (FNA), in the Southwest Atlantic Ocean. The kaersutite diorite consist primarily of andesine, diopside, kaersutite, phlogopite, and minor amounts of magnetite and ilmenite, along with accessory minerals such as apatite, titanite, and zircon. Major and trace element signatures from bulk-rock analyses yield silica under-saturated compositions and light REE enriched patterns (La/Yb_N = 13-14) that are similar to the other rocks from the FNA. Nd isotope analyses yield ε_{Nd} values of +1.7 to +2.2. U-Pb analyses of zircon obtained from the kaersutite diorite provided a crystallization age of 13.69 ± 0.07 Ma, while a combined titanite-apatite U-Pb age record a younger U-Pb age at 9.76 ± 0.94 Ma, reflecting a younger thermal event, probably related to the explosive magmatism that formed the pyroclastic deposit of the basal unit of FNA. These ages also indicate that the FNA magmatism was coeval with onshore continental magmatism found in northeastern Brazil.

KEYWORDS: PLUTONIC ROCKS, APATITE, TITANITE, ZIRCON

LIST OF FIGURES

Figure 1 A) Location of the Fernando de Noronha Ridge and the La Romanche, Chain and Fernando de Noronha (FN) Fracture Zones. B) Details of Fernando de Noronha Ridge. C) Simplified geologic map of Fernando de Noronha Archipelago (after Almeida 1955). The study area is within the square at Enseada da Caieira. Age data in millions of years from Perlingeiro et al. (2013). Abbreviations: W.R. = whole-rock, Or = orthoclase, Ne = nepheline, and Krs = kaersutite..... 19

Figure 2 A-B) Field photos of kaersutite diorite. C-H) Thin section under polarized light. C and D) The relationship between the rock-forming minerals. The opaque minerals (mainly oxides) have an intergranular texture. E) Xenocryst apatite crystal with reabsorbed borders. F) Opaque minerals between amphibole and andesine with intergranular texture. G) Apatite inclusion in diopside. H) Cumulate textures. I-K) Thin sections on backscattering images. C at plane-polarized light; D-H at crossed polarized light. Abbreviations stand for Op: Opaque; Pho: phlogopite; Di: Diopside; Amp: Amphibole; And: Andesine; Apa: Apatite; Ilm: Ilmenite; Mag: Magnetite. 24

Figure 3 Mineral chemistry classification for the kaersutite diorite. A) Classification diagram for feldspar - Orthoclase (Or), Anorthite (An), Albite (Ab) - (MacKenzie, 1989). The plagioclase in the kaersutite diorite is andesine, shaded areas are compiled data from mineral chemistry of subvolcanic xenoliths (Ulbrich and Lopes, 2000). B) The FeO-TiO_2-Fe_2O_3 ternary diagram (Deer et al., 1992; Dunlop, 1990)). The data are plotted as magnetite associated with the titanohematite series. C) Classification diagram for the pyroxenes analyzed - enstatite (En), ferrosilite (Fs), wollastonite (Wo), diopside (Di), and hedenbergite (Hd) (Morimoto et al., 1988). The clinopyroxene in the kaersutite diorite is diopside, shaded areas are compiled data from mineral chemistry of subvolcanic xenoliths (Ulbrich and Lopes, 2000). D) Biotite classification diagram (Rieder et al., 1999). The data is plotted in the phlogopite field. E) Amphibole classification diagram for $Ca_B \geq 1.5$ and $(Na+K)_A \geq 0.5$ and for $Ti < 0.5$ and $Ti \geq 0.5$ apfu (Leake et al., 1997) The amphiboles plotted mainly in the pargasite field, but some amphiboles with higher Ti content plotted in the kaersutite field. Abbreviation stands for apfu.: atom per formula unit. 25

Figure 4 Major elements *versus* MgO (in wt. %). Samples from this study are highlighted in black (n = 3) and compiled samples from Remédios Formations, Quixaba Formation, and São José Formation. Total of compiled samples = 161 (Guimarães et al., 2020; Kay and Gast, 1973; Lopes, 2002, 1997; Maringolo, 1995; Perlingeiro, 2012). 27

Figure 5 Primitive Mantle-normalized REE diagram (McDonough and Sun, 1995). Kaersutite diorite highlighted in black and compiled samples from across the FNA (n = 43; Lopes, 2002). 28

Figure 6 Trace element spider diagram. Kaersutite diorite highlighted in black (n = 3) and compiled samples (n = 122) in gray *(Guimarães et al., 2020; Kay and Gast, 1973; Lopes, 2002, 1997; Maringolo, 1995; Perlingeiro, 2012)*. A) All samples normalized by primitive mantle *(Sun and McDonough, 1989)* B) Samples normative by OIB *(Sun and McDonough, 1989)*. *Cs, Rb and Th were removed due to analytical problems. 29

Figure 7 $^{143}Nd/^{144}Nd$ *versus* SiO_2 (wt. %). The colored areas represent the compiled data *(Lopes, 2002; Perlingeiro, 2012)*..... 30

Figure 8 Pressure versus temperature of the amphibole (Ridolfi, 2021). The amphibole varies between 880.5-1068.2 ºC, and 275 – 775.6 MPa..... 30

Figure 9 Representative zircons from the sample. Scale bar represents 100 μm. Sector zoning occurs in A, D, E and F. Oscillatory zoning is present in A, C, D, E, F, G, and H. Homogeneous crystals also occur, like B or patchy zoning also is common as observed in F. Gray circles represent the spot-analyses location. The $^{206}Pb/^{238}U$ age for each spot is in Ma..... 31

Figure 10 Zircon data for the kaersutite diorite. Concordia diagrams and $^{206}Pb/^{238}U$ Weighted Mean, both using 24 concordant data, from Isoplot R *(Vermeesch, 2018).*..... 32

Figure 11 A) CL images of titanite crystals. The scale bar is 200 μm. B) Titanite U-Pb diagrams. MSWD-mean square of weighted deviations. C) CL images of apatite crystals. The scale bar is 200 μm. D) Apatite-Titanite U-Pb diagrams. MSWD-mean square of weighted deviations. Gray circles represent the spot location. 33

Figure 12 Schematic diagram of the magmatism emplacement with compiled ages, methods, and rock type. The rectangles represent the age (black line) with the error bar. The oldest recorded age is present in this study, followed by an alkali-basalt plug, dated to almost one million years later, followed by a hiatus of 2.5 million years. There is a peak of magmatism registered between 10 and 9 Ma, followed by a hiatus of almost 3 million years, with the beginning of the Quixaba event, where there is intercalation between effusive and explosive volcanism..... 38

LIST OF TABLES

Table 1 Major element geochemistry (in weight percentage – wt. %). [1]Duplicated sample... 26

Table 2 Rare Earth Elements data from the kaersutite diorite (in ppm) 28

Table 3 Trace elements data from the kaersutite diorite. [1]Duplicated sample. (in ppm)..... 29

Table 4 Pyroxenes – Mineral Chemistry..... 52

Table 5 Feldspar – Mineral Chemistry..... 53

Table 6 Amphibole – Mineral Chemistry..... 54

Table 7 Ilmenite – Mineral Chemistry..... 55

Table 8 Phlogopite - Mineral Chemistry..... 56

Table 9 Magnetite - Mineral Chemistry..... 56

Table 10 Apatite - Mineral Chemistry..... 57

TABLE OF CONTENTS

OVERVIEW 13

First U-Pb age constraints from plutonic xenolith preserved in alkaline volcanic rocks of the Brazilian oceanic Fernando de Noronha Archipelago, Southwest Atlantic Ocean 15

1. INTRODUCTION 15

2. GEOLOGICAL SETTING 16

2.1. Stratigraphy and Geochronology 17

2.2. Lithogeochemistry 20

2.3. Isotopic Geochemistry 20

3. ANALYTICAL METHODS 20

3.1. Sampling and petrography 20

3.2. Whole-rock analyses 21

3.3. Mineral chemistry 21

3.4. U-Pb Geochronology 21

3.5. Nd Isotope Analyses 22

4. RESULTS 23

4.1. Petrography and Mineral Chemistry 23

4.2. Geochemistry 26

4.2.1. Whole-rock analysis 26

4.2.2. Rare earth elements 28

4.2.3. Trace Elements 29

4.2.4. Isotope geochemistry 29

4.3. Thermobarometry 30

4.4. U-Pb dating 31

4.4.1. Zircon 31

4.4.2. Titanite and Apatite 32

5. DISCUSSION 33

5.1. Geochemical and petrographic approach to understanding the origin of the plutonic xenoliths 33

5.2. U-Pb Dating and Geodynamic Implications 35

6. CONCLUSIONS 39

REFERENCES 41

APPENDIX A – Mineral Chemistry 52

APPENDIX B – Mineral Chemistry Spot Maps 58

APPENDIX C – U-Pb Methodology – Reference Data for Apatite and Titanite 59

APPENDIX D – U-Pb Methodology – Sample Data for Apatite and Titanite 61

APPENDIX E – U-Pb Methodology – Sample Data for Zircon 62

ANNEX A – The state of the art of low-temperature thermochronometry in Brazil 63

OVERVIEW

This work is part of the Project "Geomorfologia Ambiental das Ilhas Oceânicas Fernando de Noronha e Trindade: compartimentação do relevo, evolução quaternária e interações solo-água", coordinated by Prof. Dr. Fábio Soares de Oliveira (IGC-UFMG).

This master dissertation has the goal of improving and contributing to the geotectonic knowledge about the Fernando de Noronha Archipelago, by analyzing plutonic xenoliths preserved in the pyroclastic deposits of the exposed lowermost Remédios Formation.

To achieve the main aim of this master dissertation, we collected and prepared samples from plutonic xenolith hosted in the pyroclastic rocks from the Remédios Formation.

In **Chapter 2** we present, in article form, new U-Pb ages for zircon, apatite, and titanite as well as Nd isotopic (whole-rock) analyses for plutonic xenolith from Remédios Formation. In addition, new whole-rock geochemical analyses and mineral chemistry for the plutonic xenoliths of the Remédios Formation are provided with the goal of constraining the timing and source of the magma emplacement on the Fernando de Noronha Archipelago.

In addition, fieldwork undertaken in June 2019, identified three other topics of scientific interest for which samples were collected: *i*) isotopic and fossiliferous analysis in biogenic calcarenite; *ii*) analysis in mantle xenolith; *iii*) dikes samples from "Enseada da Caieira" for petrography, mineral chemistry, geochemistry, and isotopic analysis. These topics are in development and are not presented in this volume;

i) isotopic and fossiliferous analysis in biogenic calcarenite: three detailed sections in the Caracas Formation outcrop were done: Rasa Island, Ponta das Caracas and Atalaia Beach. A total of 28 samples were collected and prepared and sent to LABISE-UFPE for stable isotopic analysis (carbon and oxygen). Ten thin sections for petrographic and fossiliferous analysis were also made. These samples will be used to understanding paleoclimatic conditions and constrain the geomorphologic evolution of the oceanic island within the project "Geomorfologia Ambiental das Ilhas Oceânicas Fernando de Noronha e Trindade: compartimentação do relevo, evolução quaternária e interações solo-água".

ii) analysis in mantle xenolith. We collected samples from São José Island, where mantle xenoliths occur in basanite outcrops. These samples will be used in collaboration with UERJ to be part of another Master's project, in order to compare the mantle xenoliths from Fernando de Noronha with the ones from Trindade Island, in collaboration with Prof. Dr. Anderson Costa dos Santos (UERJ/DMPI/Tektos and GeoBioTec Groups).

iii) dikes samples from "Enseada da Caieira". We analysed 16 thin sections from eight dikes of "Enseada da Caieira" (petrography, mineral chemistry LMic – EPMA, geochemistry and isotopic analyses Sm-Nd). A new approach based on machine learning and data-driven process to understand the geochemistry of the multi-zoned pyroxenes phenocrysts and their implications in the magmatic emplacement was done and comprised the second paper in preparation, as well as the geochemistry and isotopic data will be part of a third paper, encompassing a geochemical modeling approach.

I also participated as a collaborator in the research analyzing the offshore magmatism from the Brazilian equatorial margin, with Prof. Dr. Anderson Costa dos Santos (UERJ/DMPI/Tektos and GeoBioTec Groups), analyzing some basalt samples dragged from *guyots*. Another product of this master dissertation was the collaboration in a review paper of the data set and advances of thermochronology in Brazil, which is published in the Journal of the Geological Survey of Brazil (ANNEX I).

In addition, apatite was also separated for thermochronology data at the University of Glasgow, but due to analytical reasons, the thermochronology data was not possible to obtain. Whole-rock isotopic analysis for Hf was also completed, but due to problems at the laboratories, we are awaiting the results, as well as Lu-Hf and REE *in situ* in the zircons.

First U-Pb age constraints from plutonic xenolith preserved in alkaline volcanic rocks of the Brazilian oceanic Fernando de Noronha Archipelago, Southwest Atlantic Ocean

1. INTRODUCTION

Ocean island volcanoes can be unique environments in which to study intraplate magmatism (Pimentel et al., 2020). Although these islands consist almost entirely of volcanic to subvolcanic rocks, rare examples of plutonic rocks brought to the surface by rapidly rising explosive volcanism have been documented on a number of oceanic islands. Plutonic rocks have been described in the Azores, the Canary Islands, Hawaii, Tristan da Cunha, Ascension, the Trindade Island and Fernando de Noronha and others (*e.g.* Le Maitre 1969; Borley et al. 1971; Weis 1983; Mattioli et al. 1997; Marques et al. 1999; Ulbrich and Lopes 2000; Vazquez et al. 2007; Platevoet et al. 2014; Bongiolo et al. 2015; Gao et al. 2016; Pires and Bongiolo 2016). These plutonic rocks preserve evidence of the deeper levels of the magmatic plumbing systems of these islands. Some of them have been interpreted as cognate xenoliths, representing residues from crystallization within the magma chambers (*e.g.* Mattioli et al. 1997; Ulbrich and Lopes 2000). However, a recent U-Pb dating study of zircons from beach sands on the Canary Islands revealed a hidden plutonic history of these islands that is buried underneath younger volcanic activity (Sagan et al., 2020). Thus, these plutonic fragments are a potential source of information about magmatic processes that occur at depth in the feeder zones to volcanoes (Lacroix, 1893). The presence of key accessory minerals, *e.g.* zircon, titanite, and apatite, in the plutonic rocks can provide an extensive history of the timing and evolution of intraplate volcanism (Allibon et al., 2011; Ashwal et al., 2017; Belousova et al., 2002; Sagan et al., 2020; Vazquez et al., 2007).

The Fernando de Noronha Archipelago (FNA) is a highly dissected upper portion of a Miocene-Pleistocene volcanic structure that rises 4 km above the ocean floor and reaches 323 m above sea level. Plutonic xenoliths on the archipelago of Fernando de Noronha have been found within pyroclastic rocks of the basal Remédios Formation and have been classified as clinopyroxenites, clinopyroxene hornblendites, kaersutite gabbros, layered kaersutite diorites, a kaersutite monzogabbros, and monzodiorites (Almeida, 1955; Ulbrich and Lopes, 2000).

A better understanding and analysis of these fragments can provide more information about the earliest magmatic process, emplacement and geochemical evolution of the FNA and other volcanic island settings. In order to constrain the timing and source of the magma

emplacement on Fernando de Noronha Island, we present new U-Pb ages for zircon, apatite, and titanite as well as Nd isotope (whole-rock) analyses for plutonic xenoliths from the Remédios Formation. In addition, new whole-rock geochemical analyses and mineral chemistry for the plutonic xenoliths of the Remédios Formation

2. GEOLOGICAL SETTING

The Fernando de Noronha Archipelago (FNA) consists of the main island of Fernando de Noronha and 20 islets located 370 km east of the northern Brazilian coast between latitudes 3°54'36" and 3°46'48"S and longitudes 32°20'24" and 32°31'48"W in South Atlantic Ocean (Figure 1A). The archipelago trends in the NE-SW direction for 14 km, covering 26 km² and represents the easternmost expression of a line of seamounts referred to as the Fernando de Noronha Ridge (Gorini and Bryan, 1974) near the Fernando de Noronha Fracture Zone (Figure 1A-1B), which extends eastwards from the Brazilian coast into the South Atlantic Ocean. The lineament includes the Rocas Atoll, located between Fernando de Noronha and the continent, as well as a number of volcanic seamounts (*guyots*), *e.g* Guará and Sirius Banks, Touros and Baião *Guyots*, Drina Shoal, and Bentes Seamount. Fernando de Noronha Ridge is located southeastern of the North Brazilian Ridge (Hayes and Ewing, 1970) and, together with some other adjacent *guyots* and volcanic lineament, comprises the Brazilian Equatorial Margin (Santos et al., 2022).

Geological studies of the FNA started in the 19th and early 20th centuries (*e.g*. Branner, 1889; Darwin et al., 1839; Smith and Burri, 1933; Williams, 1889), but systematic geological and petrological studies only began in the middle of the 20th century with work by Almeida (1955). Gorini and Bryan (1976) related the archipelago with the Jean Charcot Fracture Zone, while Bryan et al. (1972) correlated it with the Chain Fracture Zone. Almeida (1983) and Almeida et al. (1988) subsequently proposed that the magmatism of Fernando de Noronha and alkaline magmatism of a similar age in northern Brazil were a product of magmatism associated with the Fernando de Noronha Fracture Zone.

In the following decades, multiple studies suggested that magmatism along the fracture zone was the product of a Pleistocene-aged plume-fed hotspot that formed an alignment of islands and *guyots* due to the South American plate's westward movement over the stationary plume head (Almeida, 2006; Fodor et al., 2002, 1998; Mizusaki et al., 2002; Mohriak, 2020; Morgan, 1983, 1971; Rivalenti et al., 2007, 2000; Steinberger, 2000; Teixeira, 2003; Ulbrich

et al., 2004). This was supported by geochemical and isotopic data from the archipelago (Gerlach et al., 1987; Lopes and Ulbrich, 2006; Schwab and Bloch, 1986; Stormer J. C. and Whitney, 1978) and by comparisons with other oceanic islands in the Atlantic Ocean (Mitchell-Thomé, 1970), including the Cape Verde Islands (Gunn and Watkins, 1976) and Trindade Island (Weaver, 1990).

A number of recent studies have argued against the mantle-plume driven model due to the lack of age progression or geophysical evidence of a deep mantle plume upwelling beneath the archipelago (Montelli et al., 2004). Alternative models included magmatism produced by small-scale plate-driven convection leading to melting of an enriched mantle over a protracted period of time (King, 2007; King and Ritsema, 2000; Knesel et al., 2011; Lopes and Ulbrich, 2015; Perlingeiro et al., 2013). Guimarães et al. (2020) compared the ages from the continental and oceanic alkaline rocks of northeastern Brazil with the onshore/offshore alkaline magmatism associated with the Cameroon line of Africa and subsequently proposed an alternative to the deep-mantle plume origin and the edge-driven convection model. Due to the lack of progressive ages and the longevity of both magmatic settings combined with low $^{3}He/^{4}He$ values for the Cameroon line (Barfod et al., 1999), they proposed that the alkaline magmatism of both locations was the product of the melting of enriched mantle that drained outward from beneath the two continents during the breakup of Gondwana (Guimarães et al., 2020).

2.1. Stratigraphy and Geochronology

Almeida (1955) defined three volcanic formations on the FNA from oldest to youngest: Remédios, Quixaba and São José (Figure 1C). The Remédios Formation mostly occupies the central portion of the main island of Fernando de Noronha. It consists of volcaniclastic deposits (agglomerates, breccias, tuffs) intruded by domes (mainly phonolite), plugs (essexite, trachyte, alkali-basalt), and various dikes of ultrabasic composition (ankaratrites, limburgites, basanites, and tephrites) to basic-intermediate composition (tephrite, phonolitic tephrite, tephritic phonolite, phonolite, alkali basalt, trachyandesite, trachyte, and alkaline lamprophyre), that also cut the earlier intrusions (Almeida, 1955). The pyroclastic unit also contains fragmentary clasts of volcanic, subvolcanic, and plutonic rocks (Ulbrich and Lopes, 2000). The Remédios Formation and Quixaba Formation are separated by an erosional surface (Almeida, 1955). The Quixaba Formation occurs in the northeastern and southwestern edges of the main island, covering ca. 80% of area and consists of melanephelinitic flows intercalated with volcaniclastic

rocks of the same composition. The São José Formation consists of basanites that are notable for the presence of dunite, lherzolite, and harzburgite xenoliths.

The presence of subvolcanic rocks such as clinopyroxenite and clinopyroxene hornblendite, kaersutite gabbro, layered kaersutite diorite, a kaersutite monzogabbro, and monzodiorite with alkali feldspar oikocrysts within pyroclastic rocks of the Remédios Formation as xenoliths were described by Ulbrich and Lopes (2000). These rocks commonly have a layered structure or cumulus and intercumulus textures, suggesting crystal sorting and accumulation within a magma chamber. Ti-magnetite - ilmenite thermometry points to equilibration temperatures of ca. 800 ºC for a clinopyroxene hornblendite (Ulbrich and Lopes, 2000).

The magmatism of Fernando de Noronha has been extensively dated using the $^{40}K/^{40}Ar$ (Cordani, 1970; Kogarko et al., 2007) and $^{40}Ar/^{39}Ar$ methodologies (Buikin et al., 2010; Perlingeiro et al., 2013). Cordani (1970), using the $^{40}K/^{40}Ar$ method, established that the phonolitic rocks from the Remédios Formation yielded ages close to 9 Ma, while alkali basalt resulted in ages up to 12 Ma (Cordani, 1970), both related to the Remédios Formation. This same study also revealed that the São José formation may be synchronous with the Remédios event and that lava flows related to the Quixaba Formation yield ages ranging from 6.3-1.7 Ma (Cordani, 1970). Kogarko et al. (2007) identified the trachytes (11.8–11.7 Ma) of Remédios Formation and basanites (11.7 ± 0.6 Ma) from São José Formation as the oldest rocks in FNA. Buikin et al. (2010) applied the $^{40}Ar/^{39}Ar$ method to the previous analysed rocks $^{40}K/^{40}Ar$ ages (ca. 9-12 Ma, Cordani 1970), and confirmed the age for the Remédios Formations, but obtained an age of 8.57 ± 0.42 Ma for the São José Formation and a much older age of 16.37 ± 1.86 Ma, for Quixaba Formation.

High-resolution laser-heating $^{40}Ar/^{39}Ar$ geochronology (Perlingeiro, 2012; Perlingeiro et al., 2013) defined two magmatic stages separated by a hiatus of 3 Ma in FNA. The earliest potassic series of the Remédios Formation was emplaced from 12.8 ± 0.3 to 12.0 ± 0.1 Ma, followed by a period of sodic and strongly alkaline magma, at 10.9 ± 0.1 and 9.4 ± 0.2 Ma. This sodic series is contemporaneous with the emplacement of the São José Formation between 9.8 ± 0.5 and 9.0 ± 0.1 Ma. The next major magmatic event associated with the Quixaba Formation yields ages of 6.2 ± 0.1 to 1.3 ± 0.1 Ma. The phonolites from Remédios Formations have also been dated using the $^{40}Ar/^{39}Ar$ technique giving ages between 9.4 ± 0.2 and 10.4 ± 0.1 Ma for whole-rock data and mineral samples (feldspar, orthoclase, nepheline, and

kaersutite). Finally, an alkali-basalt pyroclast within the pyroclastic unit of the Remédios Formation was dated at 12.5 ± 0.1 Ma (Cordani, 1970; Perlingeiro, 2012; Perlingeiro et al., 2013).

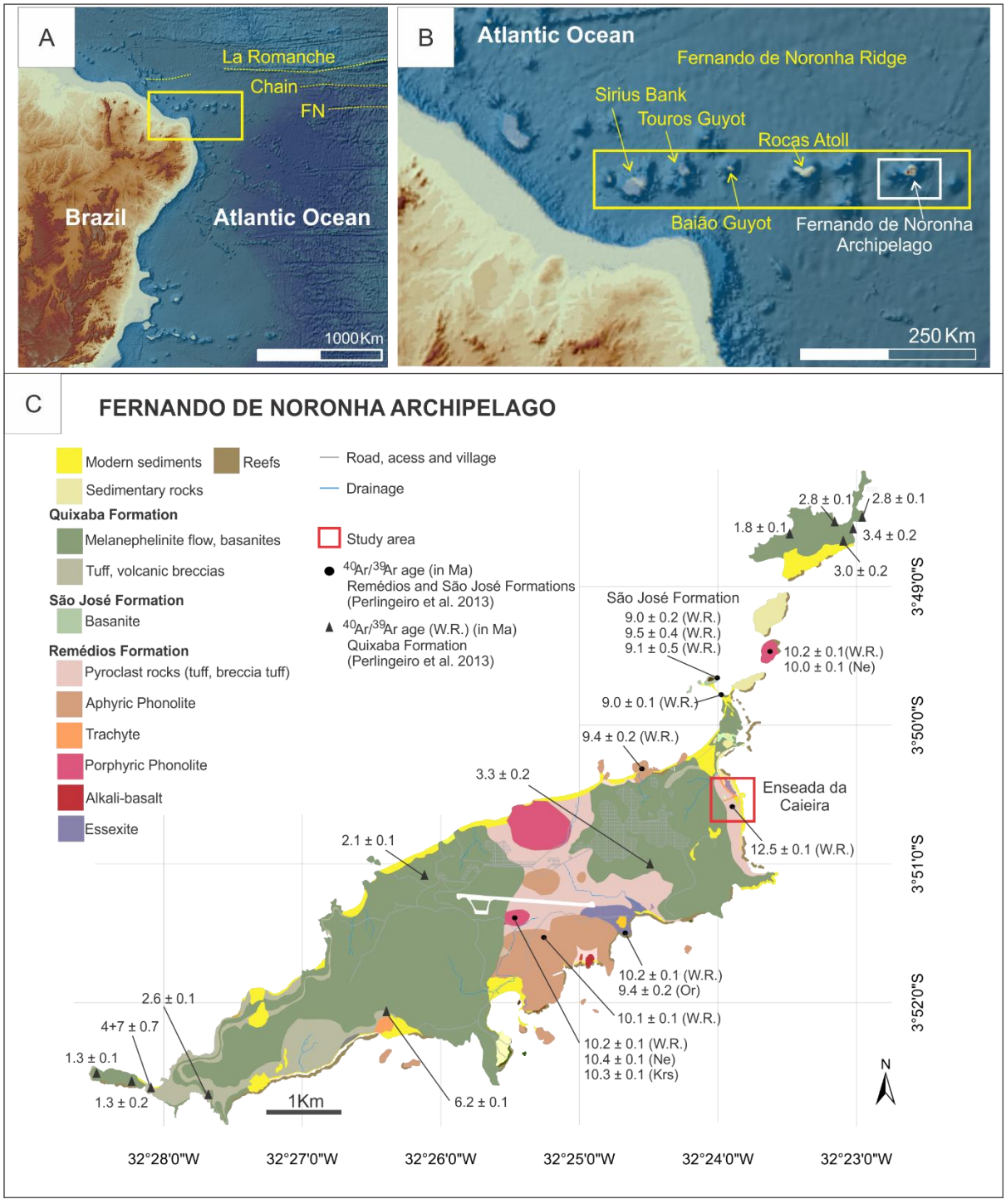

Figure 1 A) Location of the Fernando de Noronha Ridge and the La Romanche, Chain and Fernando de Noronha (FN) Fracture Zones. B) Details of Fernando de Noronha Ridge. C) Simplified geologic map of Fernando de Noronha Archipelago (after Almeida 1955). The study area is within the square at Enseada da Caieira. Age data in millions of years from Perlingeiro et al. (2013). Abbreviations: W.R. = whole-rock, Or = orthoclase, Ne = nepheline, and Krs = kaersutite.

2.2. Lithogeochemistry

In general, Fernando de Noronha magmatism is highly alkaline and strongly silica undersaturated compared with other South Atlantic Ocean islands such as Ascension, Bouvet, Saint Helena, Gough, and Tristan da Cunha (Weaver, 1990; Weaver et al., 1987)

The Remédios Formation is divided into a sodic series (basanite, tephrite, tephri-phonolite, essexite, phonolite) and a moderately potassic sequence (alkali basalt, trachyandesite, trachyte). Both series present continuous trends in major and trace element discrimination diagrams suggesting that they are associated by fractional crystallization. The melanephelinites from Quixaba Formation is mostly composed of strongly silica-undersaturated (SiO_2 37 – 43 wt. %) sodic magmatic rocks, while basanite from Quixaba Formation as well as São José Formation are slightly more enriched (SiO_2 45 – 46 wt. %, Lopes and Ulbrich, 2015).

2.3. Isotopic Geochemistry

Gerlach et al. (1987) characterized the isotopic composition from the rocks from FNA, based into two age-compositional groups in which the older units, mainly formed by alkali basalts and trachytes are characterized by less radiogenic Nd-isotopic compositions ($^{143}Nd/^{144}Nd$ = *0.51271 – 0.51281)* compared to the younger units mainly formed by nephelinites, ankaratrites, and melilitites with $^{143}Nd/^{144}Nd$ = *0.51277 – 0.51290*. Lopes (2002) and Perlingeiro (2012) have also shown that the potassic-series rocks contain the highest $^{87}Sr/^{86}Sr$ and the lowest $^{143}Nd/^{144}Nd$ ratios compared to all of the rocks from the archipelago, while the lamprophyres represent a transitional value between the potassic and sodic series of Remédios Formation. The São José Formation has a similar Nd isotopic composition to the sodic series of the Remédios Formation, and sodic basalts in the Quixaba Formation, while the Quixaba Formation has Nd isotopic ratios ranging from 0.51279 to 0.51286.

3. ANALYTICAL METHODS

3.1. Sampling and petrography

We collected 10 samples of plutonic rocks from the Remédios Formation from a single outcrop at Enseada da Caieira. The petrography was done using optical and scanning electron

microscopes. The rock nomenclature is from Le Maitre et al. (2002) and the mineral abbreviation is derived from Whitney and Evans (2010).

3.2. Whole-rock analyses

Major and trace element analyses for three samples were obtained from SGS Geosol laboratories (Brazil) using Inductively Coupled Plasma Optical Emission Spectrometry (ICP-OES) for the major elements (Al_2O_3, CaO, Cr_2O_3, FE_2O_3, K_2O, M_gO, MnO, Na_2O, P_2O_5, SiO_2, TiO_2) with a detection limit (dl) 0.01% as well as Ba, Sr, Zr (dl = 10 ppm), Zn and V (dl = 5 ppm). Trace element data was obtained via inductively coupled plasma mass spectrometry (ICP-MS) for the following elements Ce, Ga La, Nd Sm Th, W and Yb (dl = 0.1 ppm), Sn (dl = 0.3 ppm), Co, Tl (dl = 0.5 ppm), Cs, Dy, Er, Eu, Gd, Hf, Ho, Lu, Nb, Pr, Ta, Tb, Tm, U and Y (dl = 0.05 ppm), Cu, Ni (dl = 5 ppm), Mo (dl = 2 ppm) and Pb (dl = 0.2 ppm).

3.3. Mineral chemistry

Mineral chemistry analyses were performed on polished and carbon-coated thin sections using a JEOL JXA-8230 electron microprobe micro-analyzer (EPMA), equipped with five wavelength-dispersive spectrometers, at Microscopy and Microanalysis Laboratory (LMic) of Universidade Federal de Ouro Preto – UFOP (Brazil). The analytical conditions were 15 kV accelerating voltage and an electron beam current of 20 nA, with a 1μm beam diameter. Matrix ZAF corrections were applied. Pyroxene analyses with totals <98.5 or >101.5% were rejected. The calibration standards were anorthoclase (Na_2O), calcium fluoride (F), zircon (ZrO_2), quartz (Si), corundum (Al2O3), olivine (MgO), barium sulfate ($BaSO_4$), magnetite (FeO), scapolite (Cl), chromite (Cr_2O_3), glass (V_2O_3), nickel (Ni), fluor-apatite (P_2O_5, CaO), strontianite (SrO), rutile (TiO2), microcline (K_2O) and manganese (MnO). Total iron content was taken as FeO. The calculation of end-member proportions was done using the GabbroSoft spreadsheet using stoichiometry, in which it calculated the FeO and Fe_2O_3 from FeO*, considering the criteria adopted by (Droop, 1987).

3.4. U-Pb Geochronology

One plutonic sample (a kaersutite diorite) was selected for U-Pb geochronology. This sample was crushed using a mill disk, and the minerals were concentrated using mineral separation techniques (gravimetric and magnetic-Frantz isodynamic separator). Zircon, titanite and apatite were handpicked under a binocular microscope, mounted in epoxy, and polished.

Cathodoluminescence and backscattered images of the crystals were obtained. U-Pb isotopic data were obtained from titanite and apatite using a Laser Ablation Inductively Coupled Mass Spectrometer (LA-ICP-MS) at LOPAG - Universidade de Ouro Preto, Brazil. The isotopic data for the zircons were obtained using a NuAttom LA-ICP-MS hosted at the GEOTOP Laboratories at the Université du Québec à Montréal (Canada).

For the zircons, 174 spots were analyzed in 167 crystals. The primary reference material was the 91500 zircon standard (Wiedenbeck et al., 2004, 1995) and the secondary reference materials were Plengai ($^{206}Pb/^{238}U$ age: 4.4 ± 0.1Ma, Li et al. (2010), and Plesovice ($^{206}Pb/^{238}U$ age: 337.13 ± 0.37Ma, Sláma et al. (2008). For the apatite, the secondary reference material was the Madagascar apatite ($^{206}Pb/^{238}U$ age: 474.3 ± 1.1 Ma, Thomson et al. (2009, 2012) and the 401 apatite ($^{206}Pb/^{238}U$ age: 530.3 ± 1.5 Ma, Thompson et al. (2016). For the titanite, the secondary reference material was the MKED1 titanite ($^{06}Pb/^{238}U$ age: 1517.32 ± 0.32 Ma, Spandler et al. (2016) and Khan titanite (522.2 ± 2.2 Ma, Kinny et al. 1994; Heaman 2009). Eight spots were analysed on the apatite and thirteen on the titanite. The primary reference materials are used to monitor and correct mass fractionation and instrumental drift, while the secondary reference materials are used to monitor data accuracy and precision, correct for mass bias and fractionation based on the isotopic ratios of primary reference material that were measured. The data were reduced in Iolite (Paton et al., 2011, 2010; Petrus and Kamber, 2012) and the age calculated in IsoplotR (Vermeesch, 2018).

3.5. Nd Isotope Analyses

Two kaersutite diorites that showed little or no evidence for weathering or secondary alteration were selected for Nd isotope analysis. The powdered samples were weighed out into Teflon vials (~0.08 g) and were digested using a mixture of HF–HNO_3 acids at 90ºC for one week. The resulting solution was evaporated and re-dissolved in concentrated nitric acid overnight. This solution was evaporated and re-dissolved in 6 mol/L HCl at 90ºC. The separation and purification for Nd is based on the technique of Pin and Santos Zalduegui (1997). The method is briefly described as follows: Iron was removed from the sample solution using AG1X8 resin; Rare Earth elements were concentrated using EichromTRU resin and Nd was extracted using Eichrom LN-Spec resin. The Nd isotope analyses were performed in the GEOTOP Laboratories at the Université du Québec à Montréal (Canada), using a NuPlasma II multi-collector inductively coupled plasma mass spectrometer (MC-ICP-MS). The analyses of the JNd1 standard reference materials during the period of this study yielded mean ratios

$^{143}Nd/^{144}Nd$ = 0.512085 ± 0.000006 (2σ) compared to the published value of 0.512115 ± 7 (Tanaka et al., 2000). The samples were corrected by a factor of 0.000024 due to the difference between the reference material values. The standards (BHVO-2) yielded corrected values after the correction was applied between 0.512952 ± 0.000008 and 0.512960 ± 0.000008, while the published value is 0.512957 (Raczek et al., 2003). The results gave a variance (2σ) in the order of 10^{-5} and 10^{-6}.

4. RESULTS

4.1. Petrography and Mineral Chemistry

The kaersutite diorite occur mainly as salt and pepper colored lapilli and block fragments (2 – 10 cm) in the pyroclastic deposit of Remédios Formation. The xenolith range from angular fragments with sharp corners to sub-rounded with variable sphericity, with fine to medium grain size, and occasionally oriented crystals (Figure 2 B). The salt and pepper coloration results from the weathering of plagioclase and mafic minerals on surface exposures (Figure 2 A, B). The kaersutite diorite are composed of pargasite – kaersutite (40%), andesine (35%), phlogopite (20%), and diopside (10%). Apatite, magnetite, ilmenite and titanite occur as minor phases, while zircon occurs as accessory mineral, as well as rare pyrite and ordonezite ($ZnSb_2O_6$) occur as microinclusions (< 25 μm) in the diopside. Diopside, phlogopite, apatite, and ilmenite/magnetite sometimes occur as inclusions in pargasite – kaersutite. The andesine crystals occur as subhedral prisms between the mafic assemblages and show minor alteration to calcite and clay-minerals along cleavage surfaces. Pargasite – kaersutite and phlogopite are subhedral to euhedral. Magnetite associated with ilmenite is anhedral and occurs with interstitial textures, slightly weathered, while euhedral small crystals of magnetite occur as inclusions in pargasite – kaersutite. Titanite occurs as fine-grained crystals in andesine and enveloping ilmenite when included in silicates. Apatite crystals occur as euhedral inclusion in various minerals. Rare apatite xenocrysts with reabsorption textures are observed (Figure 2E).

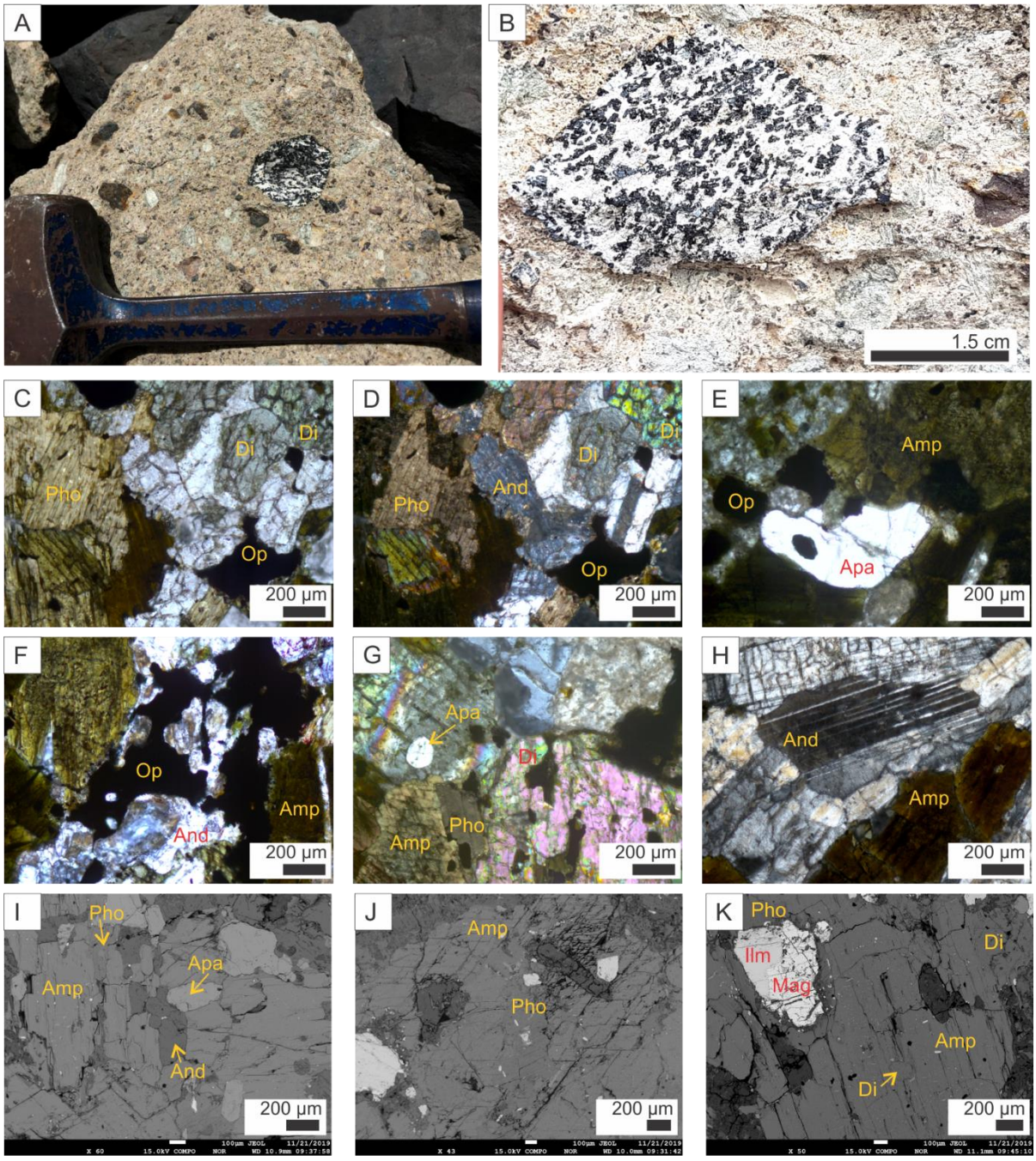

Figure 2 A-B) Field photos of kaersutite diorite. C-H) Thin section under polarized light. C and D) The relationship between the rock-forming minerals. The opaque minerals (mainly oxides) have an intergranular texture. E) Xenocryst apatite crystal with reabsorbed borders. F) Opaque minerals between amphibole and andesine with intergranular texture. G) Apatite inclusion in diopside. H) Cumulate textures. I-K) Thin sections on backscattering images. C at plane-polarized light; D-H at crossed polarized light. Abbreviations stand for Op: Opaque; Pho: phlogopite; Di: Diopside; Amp: Amphibole; And: Andesine; Apa: Apatite; Ilm: Ilmenite; Mag: Magnetite.

Mineral analyses reveal that the plagioclase has a composition in the andesine field - $Ab_{52}An_{47}Or_2$ (Figure 3A) and the clinopyroxenes (Figure 2K, Figure 3C) lie in the diopside field (Morimoto et al., 1988) with Mg# = 77.9 – 88.1. The amphibole compositions range from pargasite to kaersutite (Leake et al., 1997) due to variable Ti content and are enriched in K (0.25-0.31 apfu.) with Mg# between 59.6 – 68.9 (Figure 3E). The phlogopite was classified

based on the relationship between Al^{VI}, and the Fe and Mg content (Deer et al., 1992) with MgO values varying between 15.0 – 16.8%, and TiO_2 varying between 3.5 – 4.5% (Figure 3D).

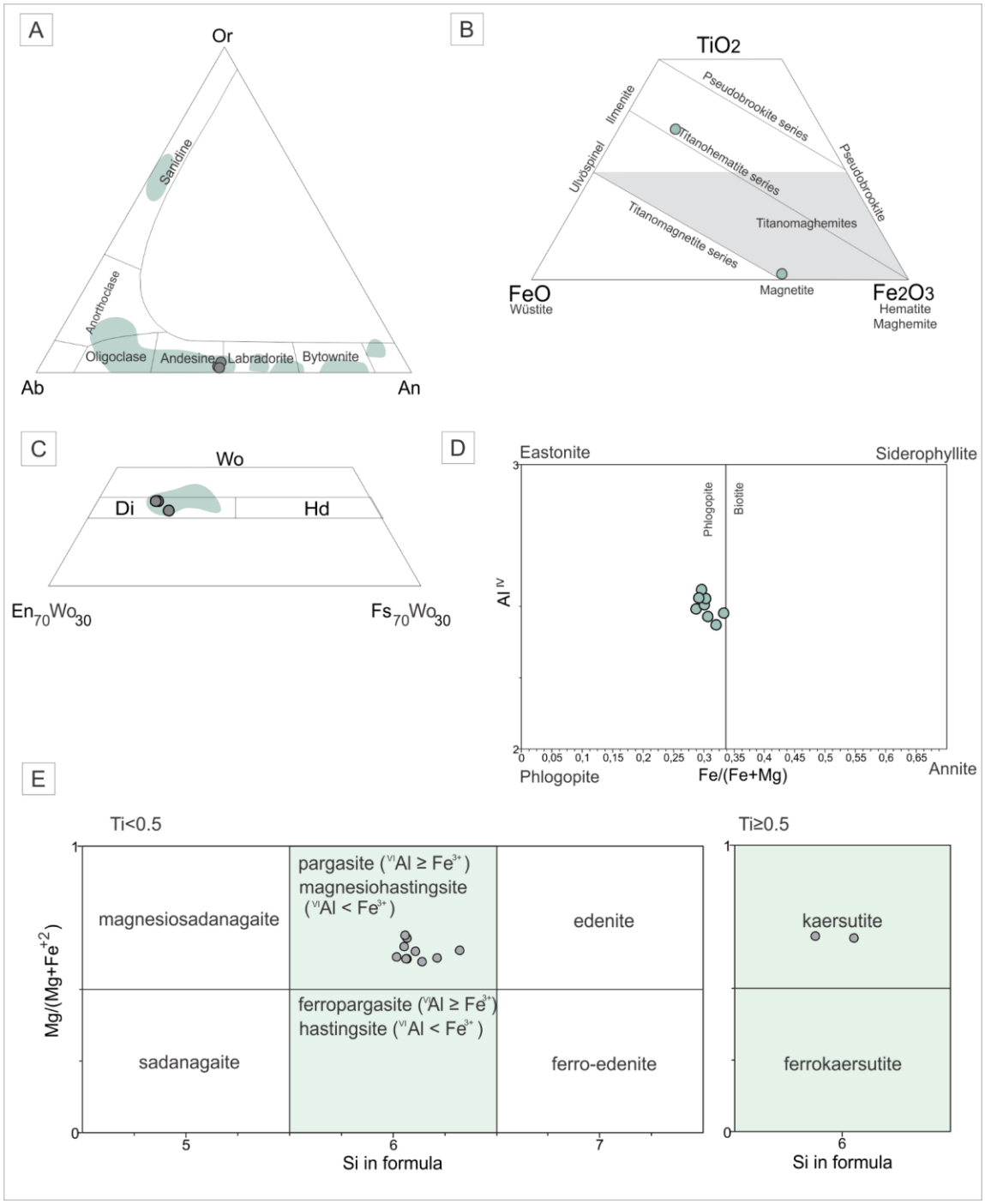

Figure 3 Mineral chemistry classification for the kaersutite diorite. A) Classification diagram for feldspar - Orthoclase (Or), Anorthite (An), Albite (Ab) - (MacKenzie, 1989). The plagioclase in the kaersutite diorite is andesine, shaded areas are compiled data from mineral chemistry of subvolcanic xenoliths (Ulbrich and Lopes, 2000). B) The FeO-TiO_2-Fe_2O_3 ternary diagram (Deer et al., 1992; Dunlop, 1990)). The data are plotted as magnetite associated with the titanohematite series. C) Classification diagram for the pyroxenes analyzed - enstatite (En), ferrosilite (Fs), wollastonite (Wo), diopside (Di), and hedenbergite (Hd) (Morimoto et al., 1988). The clinopyroxene in the kaersutite diorite is diopside, shaded areas are compiled data from mineral chemistry of subvolcanic xenoliths (Ulbrich and Lopes, 2000). D) Biotite classification diagram (Rieder et al., 1999). The data is plotted in the phlogopite field. E) Amphibole classification diagram for $Ca_B \geq 1.5$ and $(Na+K)_A \geq 0.5$

and for Ti < 0.5 and Ti ≥ 0.5 apfu (Leake et al., 1997) The amphiboles plotted mainly in the pargasite field, but some amphiboles with higher Ti content plotted in the kaersutite field. Abbreviation stands for apfu.: atom per formula unit.

4.2. Geochemistry

4.2.1. Whole-rock analysis

Two samples (17F and 17M) and one duplicated were analysed for major and minor elements (Table 1). The relatively low LOI values (2.28 – 1.23%), associated with petrographic analyses are indicative of the low degree of alteration present in the samples. Figure 4 compares the major elements variations of the samples with a compilation of whole-rock geochemistry of the FNA.

Table 1 Major element geochemistry (in weight percentage – wt. %). [1]Duplicated sample.

Sample	SiO_2	TiO_2	Al_2O_3	Fe_2O_3	Cr_2O_3	MnO	MgO	CaO	Na_2O	K_2O	P_2O_5	LOI	∑
17F	38.02	4.52	13.83	12.65	<0.01	0.22	6.99	13.04	2.66	1.87	1.79	2.28	97.87
17M	40.27	4.35	14.7	12.09	<0.01	0.22	6.89	11.46	3.06	1.76	1.82	1.23	98.85
17M[1]	39.74	4.26	14.52	12	<0.01	0.22	6.73	11.29	3.00	1.69	1.81	-	-

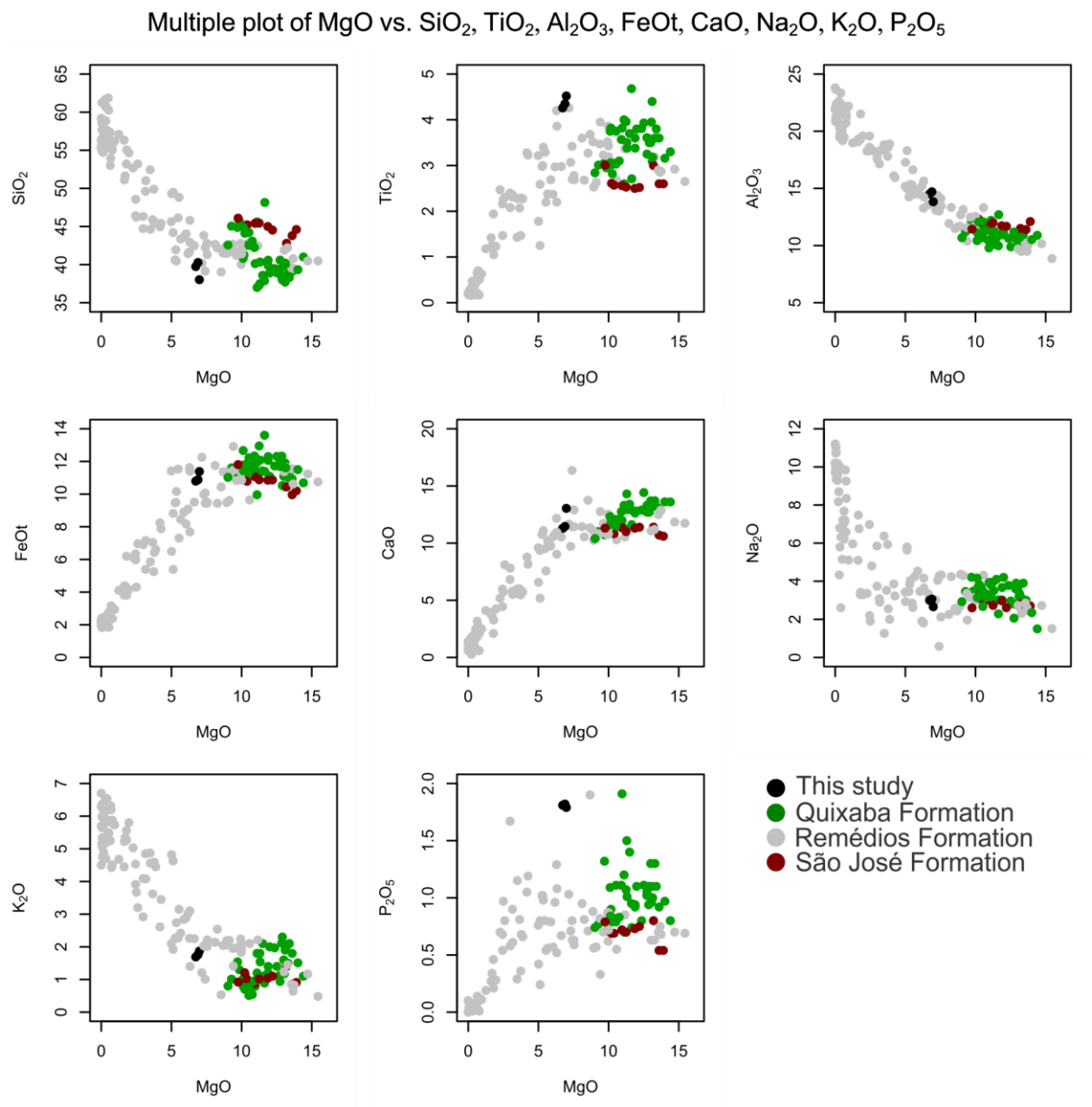

Figure 4 Major elements *versus* MgO (in wt. %). Samples from this study are highlighted in black (n = 3) and compiled samples from Remédios Formations, Quixaba Formation, and São José Formation. Total of compiled samples = 161 (Guimarães et al., 2020; Kay and Gast, 1973; Lopes, 2002, 1997; Maringolo, 1995; Perlingeiro, 2012).

Harker diagrams for the compiled whole-rock FNA data show trends consistent with increasing magmatic differentiation (decreasing MgO content). SiO_2, Al_2O_3 Na_2O, and K_2O increase while FeOt, CaO, TiO_2, and P_2O_5 decrease against decreasing MgO. The Remédios Formation depicts a wide variety of compositions while Quixaba Formation and São José Formations are restricted to the high MgO field (Figure 4).

The kaersutite diorite studied here are under-saturated in silica and fall within the Remédios Formation in the Harker diagrams. The relatively high content of TiO_2 may be

related to titanite and ilmenite accumulation, while the high P_2O_5 most likely reflects apatite accumulation.

4.2.2. Rare earth elements

Chondrite-normalized rare earth elements (REE) patterns for the kaersutite diorite (Table 2) are plotted with compiled data from the surrounding rocks and shown in Figure 5. The kaersutite diorite yield linear light REE enriched patterns (La/Yb_N = 13-14) that are similar to the majority of REE profiles for the Remédios, Quixaba, and São José formations. Although some samples from the Remédios Formation have concave patterns. The sample also tend to be enriched in all REE compared to the other lithologies but are slightly depleted in the light REE.

Table 2 Rare Earth Elements data from the kaersutite diorite (in ppm)

Sample	La	Ce	Pr	Nd	Sm	Eu	Gd	Tb	Dy	Ho	Er	Tm	Yb	Lu
17F	53.0	119	16.69	71.9	15.4	4.56	13.61	1.8	9.67	1.63	4	0.49	2.7	0.36
17M	59.7	144.9	20.65	90.6	18.7	5.45	16.36	2.12	11.08	1.9	4.53	0.54	3	0.39

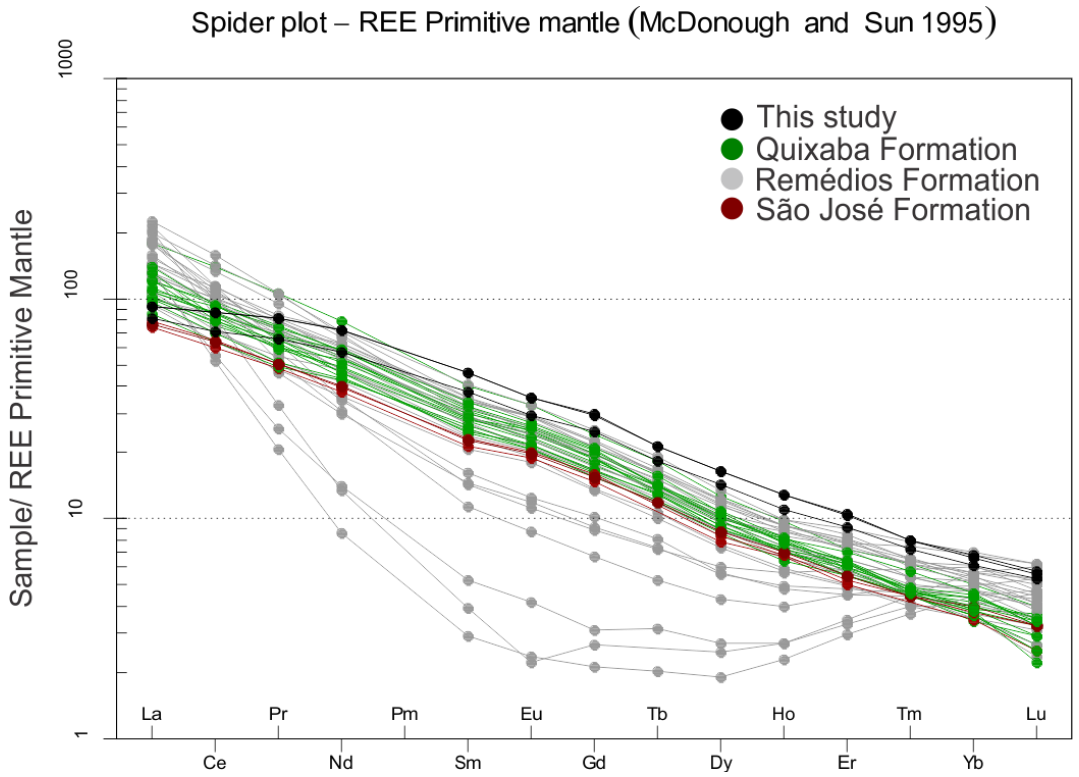

Figure 5 Primitive Mantle-normalized REE diagram (McDonough and Sun, 1995). Kaersutite diorite highlighted in black and compiled samples from across the FNA (n = 43; Lopes, 2002).

4.2.3. Trace Elements

The trace elements (Table 3) are presented in trace element normalized diagrams in Figure 6a (Primitive Mantle) and b (Ocean Island Basalts; OIB) using the normalization values from Sun and McDonough 1989). The samples yield profiles that are similar to those of other rocks from the archipelago. The overall concentrations of the trace elements plot at the lower end of the Remédios Formation and overlap those of the Quixaba and São José Formations. The higher concentrations of Rb and Ba in the sample is consistent with the compatibility of these elements with hydrous K-bearing phases such as kaersutite and phlogopite that are abundant in the rocks.

Table 3 Trace elements data from the kaersutite diorite. [1]Duplicated sample. (in ppm)

Sample	**Ba**	**Rb**	**Sr**	**Y**	**Zr**	**Nb**	**Th**	**Ga**	**Zn**	**Cu**	**Ni**	**V**	**Hf**	**Cs**	**Ta**	**Co**	**U**	**W**	**Tl**	**Sn**	**Mo**
17F	406	58.3	1036	40.1	254	50.86	0.6	21.4	107	23	14	362	5.42	1.66	2.3	28.3	1.18	<0,1	<0.5	0.4	<2
17M	346	342	1106	47.01	238	51.13	<0.1	22.1	119	18	12	351	5.6	46.43	2.45	27	1.05	2.4	<0.5	0.7	<2
17M[1]	342	--	1093	--	243	--	--	--	114	--	--	346	--	--	--	--	--	--	--	--	--

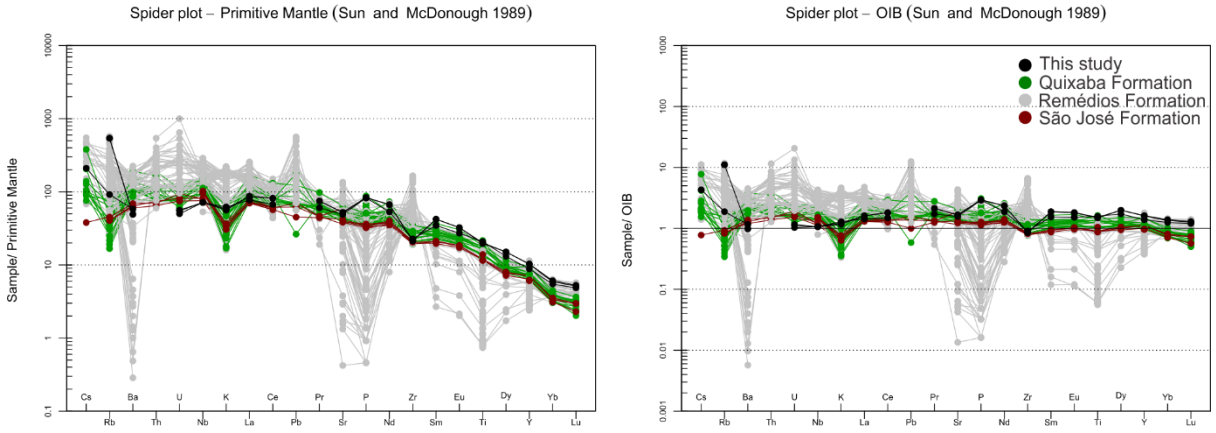

Figure 6 Trace element spider diagram. Kaersutite diorite highlighted in black (n = 3) and compiled samples (n = 122) in gray (Guimarães et al., 2020; Kay and Gast, 1973; Lopes, 2002, 1997; Maringolo, 1995; Perlingeiro, 2012). A) All samples normalized by primitive mantle (Sun and McDonough, 1989) B) Samples normative by OIB (Sun and McDonough, 1989). *Cs, Rb and Th were removed due to analytical problems.

4.2.4. Isotope geochemistry

The Nd isotope ratios of the two kaersutite diorite samples are $^{143}Nd/^{144}Nd = 0.512749$ ($\varepsilon_{Nd} = +2.2$) *and* 0.512726 ($\varepsilon_{Nd} = +1.7$). These isotopic compositions are lower than the majority of Nd isotope compositions for Fernando de Noronha but similar to those of the early

K-series from Remédios (Figure 7, in red). A comparison with previous Nd isotope data is shown in Figure 7.

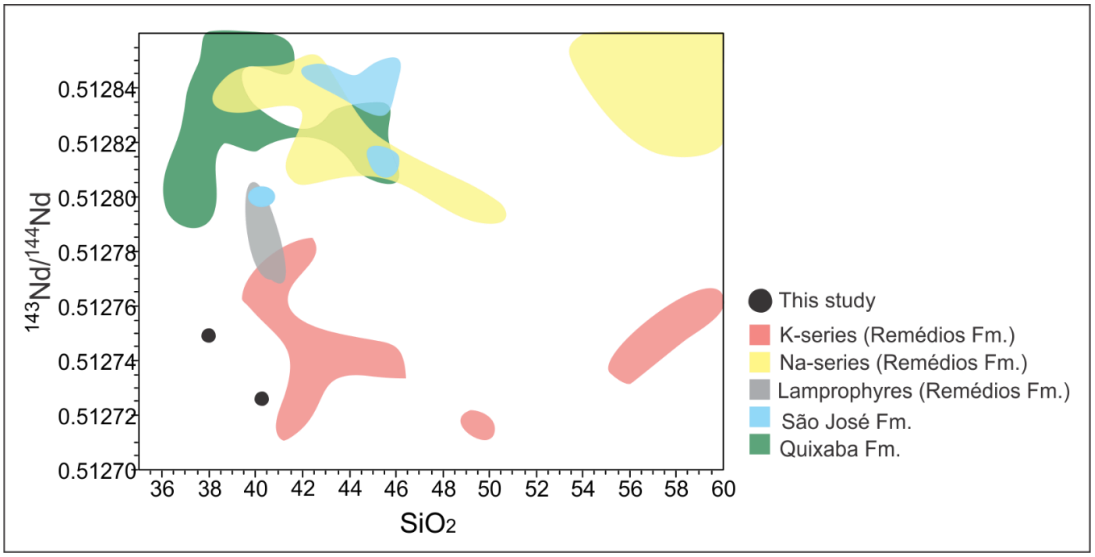

Figure 7 $^{143}Nd/^{144}Nd$ *versus* SiO_2 (wt. %). The colored areas represent the compiled data (Lopes, 2002; Perlingeiro, 2012)

4.3. Thermobarometry

Thermobarometry calculations were performed for calcic amphiboles from their major elements (Ridolfi, 2021; Ridolfi and Renzulli, 2011). The amphiboles from the sample yielded temperatures of 880.5 – 1068.2 ºC, and pressures of 275.0 – 775.6 MPa. These values correspond to calculated depths (White, 2020) of 10 – 29 km consistent with a source in the lithospheric mantle (Figure 8).

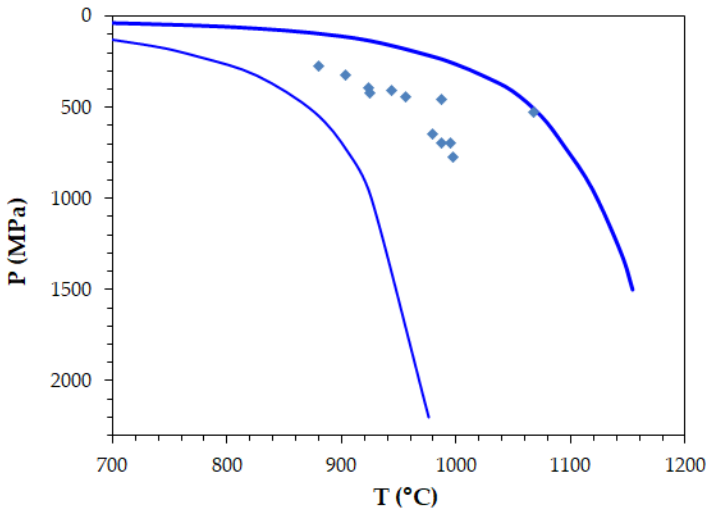

Figure 8 Pressure versus temperature of the amphibole (Ridolfi, 2021). The amphibole varies between 880.5-1068.2 ºC, and 275 – 775.6 MPa.

4.4. U-Pb dating

Zircon, titanite, and apatite grains from one sample of the kaersutite diorite from the Remédios Formation were analyzed for U-Pb isotopes.

4.4.1. Zircon

More than 160 zircons grains were found, described, and dated. A total of 174 laser spot analyses were carried out. The zircon grains are colorless to pinkish-yellowish and range from 50 to 350 μm in size. The zircons are euhedral to subhedral, and some crystals present oscillatory and sector zoning, while others show a homogeneous interior with patchy zoning and dissolution textures (Figure 9). Homogeneous crystals show a low luminescence response to cathodoluminescence. The Th/U ratios of the zircons are variable, ranging from 0.38 to 2.83. Titanite and apatite occur as inclusions in some zircon crystals.

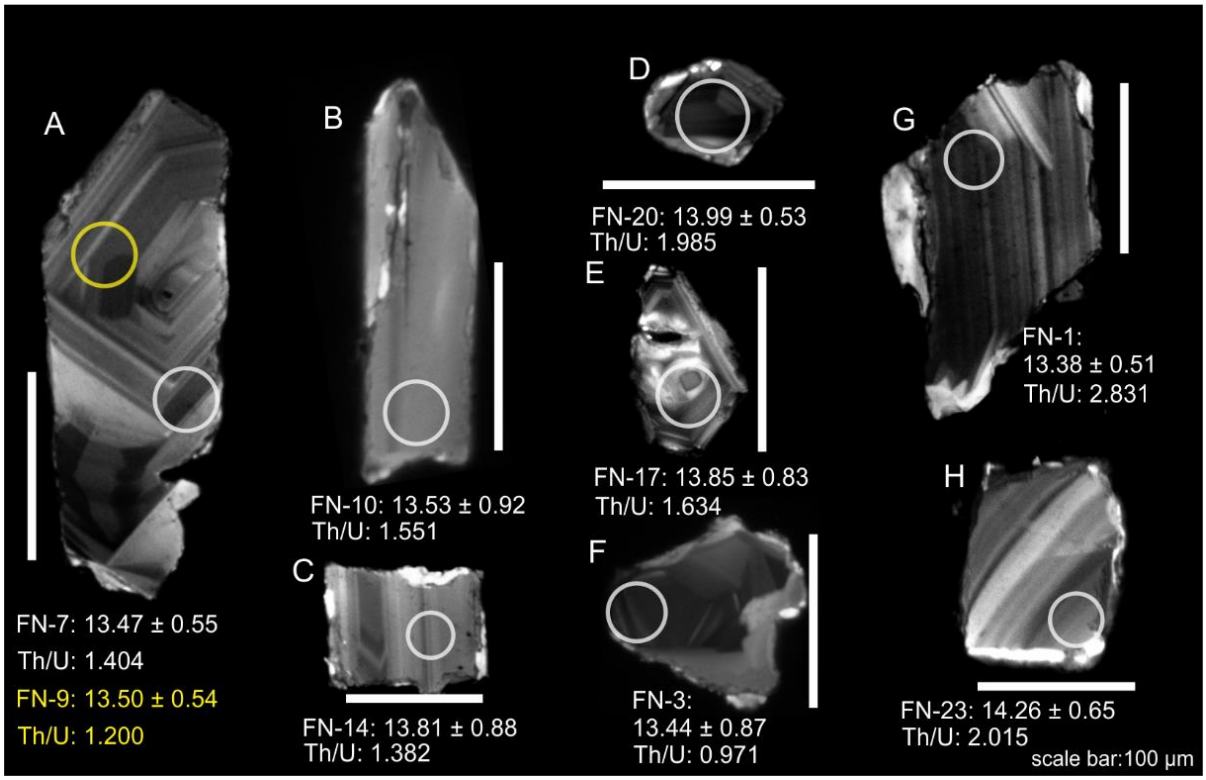

Figure 9 Representative zircons from the sample. Scale bar represents 100 μm. Sector zoning occurs in A, D, E and F. Oscillatory zoning is present in A, C, D, E, F, G, and H. Homogeneous crystals also occur, like B or patchy zoning also is common as observed in F. Gray circles represent the spot-analyses location. The $^{206}Pb/^{238}U$ age for each spot is in Ma.

From 163 grains, 174 U-Pb spot analyses show spreading dates along the Concordia. Aiming to determine the more accurate crystallization age (*i.e.* the beginning of the U-Pb isotopic system stabilization); we took twenty-four oldest spots that outline a continuous

spreading pattern in the Concordia. We calculate a Concordia age of 13.69 ± 0.07 Ma (MSWD = 5.5) with a $^{206}Pb/^{238}U$ weighted mean age of 13.70 ± 0.07 (MSWD = 0.67). This age is interpreted as the beginning of the igneous crystallization of the kaersutite diorite (Figure 10), and it has regional importance as it is the oldest age determined in the FNA.

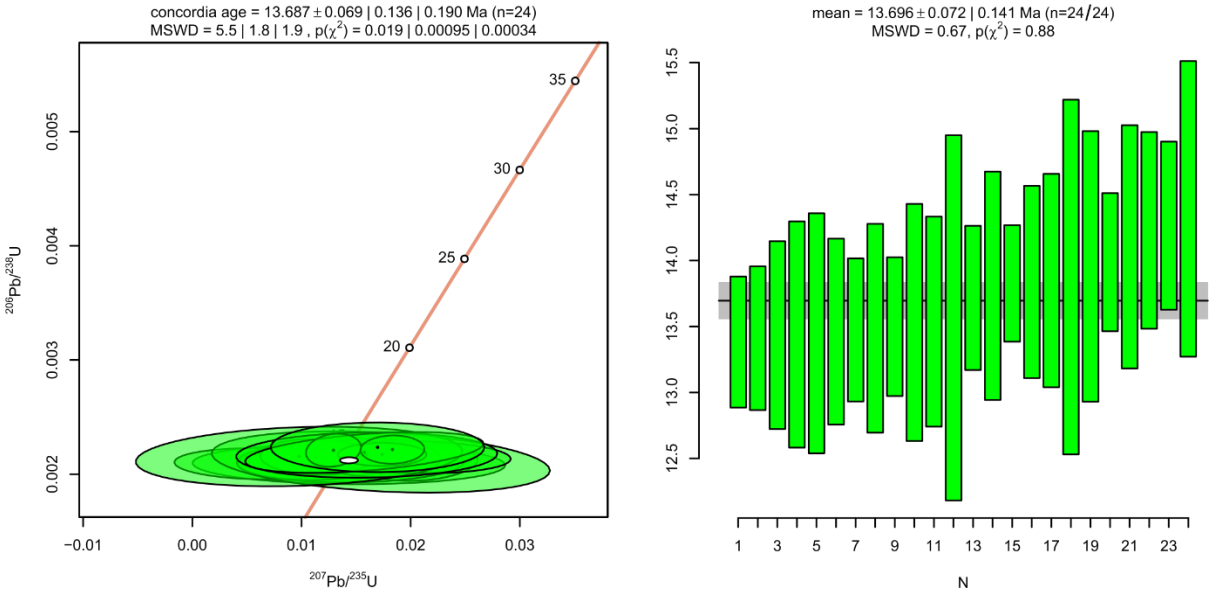

Figure 10 Zircon data for the kaersutite diorite. Concordia diagrams and $^{206}Pb/^{238}U$ Weighted Mean, both using 24 concordant data, from Isoplot R (Vermeesch, 2018).

4.4.2. Titanite and Apatite

Titanite grains vary between 700 and 320µm, are generally euhedral to subhedral, and have homogeneous textures (Figure 11A), with colors ranging from colorless, to brownish or yellowish.The laser ablation data are discordant due to the incorporation of common-Pb, however, the grains contain a range in U/Pb (Figure 11B) and therefore the spread of the data in TeraWasserberg space was enough to obtain a regression line with a lower intercept age of 10.7 ± 2.4 Ma. (MSWD = 0.49, n = 13). Apatite grains vary between 720-200 µm and are normally colorless and predominantly long prismatic euhedral to subhedral homogeneous crystals or fragments of euhedral crystals (Figure 11C). Due to the relatively high content of common lead and the limited spread in U/Pb, it was not possible to calculate an age using the apatite crystals alone. By combining the apatite and titanite data together, a linear regression of the data yielded a lower intercept age with the Concordia of 9.76 ± 0.94 Ma (MSWD = 0.76, n = 21), which is more precise than the titanite age (Figure 11D).

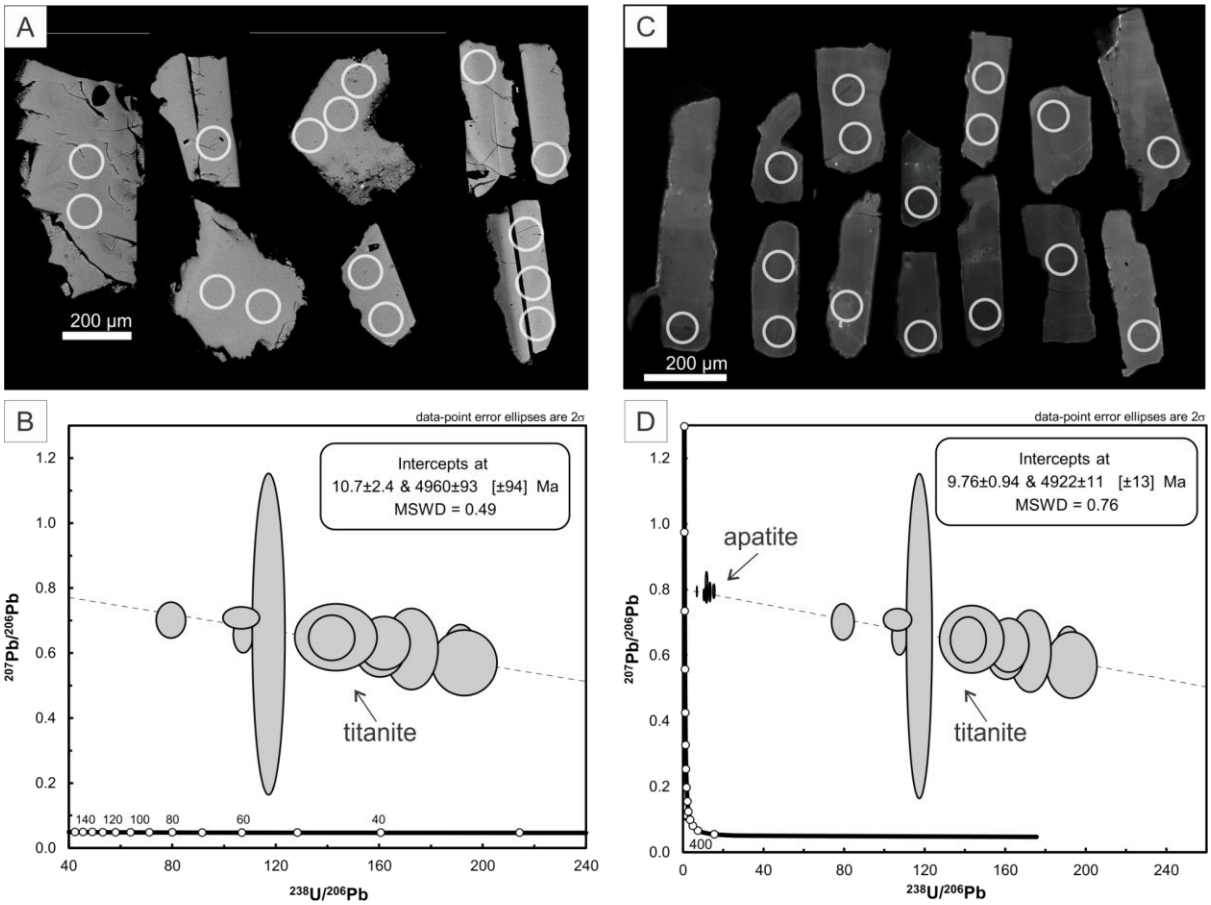

Figure 11 A) CL images of titanite crystals. The scale bar is 200 µm. B) Titanite U-Pb diagrams. MSWD-mean square of weighted deviations. C) CL images of apatite crystals. The scale bar is 200 µm. D) Apatite-Titanite U-Pb diagrams. MSWD-mean square of weighted deviations. Gray circles represent the spot location.

5. DISCUSSION

5.1. Geochemical and petrographic approach to understanding the origin of the plutonic xenoliths

The highly undersaturated magmatism of Fernando de Noronha is interpreted to reflect a lower degree of partial melting compared to the other OIB settings in the South Atlantic Ocean (Weaver et al., 1987). Rocks of the FNA yield spidergram patterns that are generally typical of OIB (Sun and McDonough 1989), but slightly enriched in HFSE and marked by positive Rb anomalies. The relative enrichment of REE in the plutonic xenolith compared with the compiled geochemistry from the FNA (Figure 6) can be explained by the abundance of amphiboles in the samples, which contains significant amounts of these elements (Bottazzi et al., 1999). These plutonic rocks have been interpreted as representing fractionating phases (cognate xenoliths) in the magma chamber or previous intrusions brought to the surface by the eruption related to the Remédios Formation (Ulbrich and Lopes, 2000).

Gerlach et al. (1987) used existing geochronology and new isotope data to divide the geology of the FNA between the older alkali basalts and trachytes and the younger, more alkaline Si-undersaturated (nephelinites, ankaratrites, and melilitites). At least two separate components in the sources of both series were identified on the basis of Pb and Sr isotope: one possibly derived from delaminated subcontinental lithosphere, one similar to the source of St. Helena lavas, and a possible third source related to the younger magmatism that may be derived from the depleted mantle. More recently, Perlingeiro (2012) suggested that the early potassic series of the Remédios Formation, was derived from an enriched-mantle (EM2) source. The later sodic series of the Remédios Formation and the São José Formation, have low Sr isotopic ratios and higher Pb and Nd isotopic ratios that are indicative of a HIMU source (Perlingeiro, 2012).

The relative contributions of the four common mantle end members (HIMU, EM1, EM2, MORB), to the FNA are investigated in a plot of CaO/Al_2O_3 *vs* K_2O/TiO_2 containing the compiled FNA data (with 10%< MgO <16%), plutonic samples and the four mantle end-members (Jackson and Dasgupta, 2008; Zindler and Hart, 1986). The FNA data plot between the EM2 and HIMU end members and the plutonic sample (MgO ca. 7%) is located near the EM2 field. This is in agreement with the interpretation of Perlingeiro (2012) that the early potassic series is derived from an enriched mantle.

Alkaline lavas in oceanic island settings are thought to be derived from the melting of metasomatized lithospheric mantle containing hydrous phases, such as amphibole and phlogopite (Clague and Frey, 1982; Class and Goldstein, 1997; Kesson and Price, 1972; Pilet et al., 2011, 2008; Sun and Hanson, 1975). Neither amphibole, nor phlogopite are stable at the temperatures of upwelling deep mantle plumes or the temperatures of the convecting upper mantle, thus the presence of these K-bearing phases might indicate evidence of melting of metasomatized lithospheric mantle. These minerals thus suggest that, the mantle was infiltrated (metasomatized) by fluids or volatile-rich melts prior to melting resulting in a lowering of the solidus temperature of the lithospheric mantle (Class and Goldstein, 1997). The high Rb and Ba contents of the FNA rocks relative to other incompatible elements due to the melting of K-bearing hydrous phases such as kaersutite and phlogopite are consistent with a small degree of melting of an enriched lithospheric mantle.

Nd isotopic data for the FNA rocks is similar to data from other volcanic occurrences along the east coast of Brazil. This includes the Abrolhos Volcanic Complex (Fodor et al., 1989), Trindade Island (Bongiolo et al., 2015; Halliday et al., 1992; Marques et al., 1999; Siebel

et al., 2000), the Martin Vaz Archipelago (Santos et al., 2018; Siebel et al., 2000), and Columbia Seamount (Fodor and Hanan, 2000). The $^{143}Nd/^{144}Nd$ isotopes composition of the samples (0.512726 - 0.512749) as well those of the early K-series of the Remédios Formation (Figure 7) are the lowest values among the FNA rocks. As a group, these early FNA samples are enriched compared to typical MORB depleted mantle values (Ito et al., 1987) and add further evidence for melting of an enriched source mantle lithosphere.

Lopes and Ulbrich (2015) argue that the plutonic xenoliths with phaneritic cumulus texture from the pyroclastic unit of the Remédios Formation represent samples from different crystallization states of ancient magma chambers beneath FNA. The presence of calcic pyroxene, kaersutite and biotite suggests that the fractionating magma was a silica saturated or undersaturated hydrous alkaline magma. The mineralogy of the samples are consistent with initial fractionation of diopside, phlogopite, and apatite, followed by amphibole and plagioclase, with apatite, magnetite, titanite, and zircon as accessory phases. The crystallization of the main minerals probably controlled the silica-saturation trend of the Remédios Formation.

5.2. U-Pb Dating and Geodynamic Implications

The ages determined by mineral isochron or mineral-whole rock isochron records the time-lapsed since the samples passed below the closure temperature for the specific decay system of the mineral, and are often referred to as cooling ages (Ganguly and Tirone, 2009). Because the closure temperature for Pb diffusion in zircon is extremely high, U-Pb dating of zircon is regarded as recording the time of zircon crystallization (Cherniak and Watson, 2001; Cherniak, 2003). Although apatite and titanite have lower closer temperatures for Pb diffusion than zircon, U-Pb ages of these minerals may be interpreted as either crystallization or cooling ages depending on the geological context (Cherniak and Watson, 2001; Cherniak, 2003; Chew et al., 2014). The combination of these three minerals with different closure temperatures for the Pb diffusion can provide information regarding the time and temperature of the magma evolution and emplacement.

The zircons extracted from the kaersutite diorite show a combination of dissolution, oscillatory, and zoning pattern textures under cathodoluminescence, due to the heterogeneous distribution of trace elements. The dissolution textures may indicate the alternation between periods of zircon under-saturation followed by periods of zircon-saturation in the melt (Hoskin and Schaltegger, 2003; Schaltegger and Davies, 2017).

Zirconium is an incompatible element and therefore its concentration in a melt rises during fractional crystallization. Due to the changing composition of the magma during the crystallization, the zircon saturation conditions also change, and when the system has the conditions favorable for zircon crystallization, it precipitates (Davies et al., 2021). Generally, zircon precipitates in a wide range of rock types, with some exceptions – such as SiO_2-poor magmas and highly alkaline magmas (Burnham, 2018).

Apatite ($Ca_5(PO_4)_3(F, Cl, OH)$) is also a common accessory mineral in most igneous rocks types (Watson, 1980, 1979) and is extensively used as a U-Pb geochronometer (Chew et al., 2014, 2011; Oosthuyzen and Burger, 1973; Pochon et al., 2016; Storey et al., 2007; Thomson et al., 2012; Zhang et al., 2018). Past studies have documented that the diffusion of Pb between apatite and the surrounding magmas occurs at a lower temperature (typically between ca. 350 – 550 °C depending on the grain size) than that of zircon (> 900 ºC, diffusion temperature for Pb) (Chamberlain and Bowring, 2001; Cherniak et al., 1991; Cherniak and Watson, 2001; Chew and Spikings, 2015; Harrison et al., 2002). Unlike zircon, apatite also incorporates common lead in its crystal lattice that leads to anomalous ages without proper correction (Chew et al., 2014; Wohlgemuth-Ueberwasser et al., 2017). Titanite ($CaTiSiO_5$) is also a useful geochronometer (*e.g.* Frost et al. 2001; Storey et al. 2007; Sun et al. 2012; Spencer et al. 2013; Chew et al. 2014) as it can host U in its structures along with limited amounts of common Pb (Kirkland et al., 2017; Kohn, 2017; Spandler et al., 2016). The closure temperature for Pb diffusion in titanite is estimated to be ca. 650 – 700 ºC depending on its grain size (Cherniak, 1993; Pidgeon et al., 1996; Scott and St-Onge, 1995).

A number of the $^{40}K/^{40}Ar$ and $^{40}Ar/^{39}Ar$ ages disagree with the field observations with respect to the stratigraphic order of the formations (Almeida, 1955; Buikin et al., 2010; Cordani, 1970; Kogarko et al., 2007). To avoid this confusion, we discuss only the recent $^{40}Ar/^{39}Ar$ ages produced by laser-heating (Perlingeiro et al., 2013) which are in agreement with the field observations (Figure 1C).

The 13.69 ± 0.07 Ma U-Pb age determined from the zircons from the kaersutite diorite is the oldest age yet determined for magmatism on Fernando de Noronha and in combinations with the apatite and titanite ages provides context to the timing and evolution of the magmatism on the island.

The zircon age indicates that there was magmatism activity related to the FNA occurring prior to the earliest magmatism related to the alkali-basalt samples (Perlingeiro, 2012). The time recorded by the alkali-basalt clast within the pyroclastic deposit was 12.5 ± 0.1 Ma by $^{40}Ar/^{39}Ar$ (Perlingeiro et al., 2013) and an extensive plug of alkali-basalt on Enseada dos Abreus is dated at 12.8 ± 0.3 Ma (Perlingeiro, 2012). The U-Pb zircon age provides evidence of magmatism as early as 13.69 ± 0.07 Ma.

The younger combined apatite and titanite age of 9.76 ± 0.94 Ma from the kaersutite diorite likely reflects the lower closure temperature for these minerals compared to zircon. Thus, the age difference may possibly reflect a resetting of the isotopic clock of the apatite and titanite by another thermal (volcanic) event, while the zircon ages reflect the crystallization age of the kaersutite diorite preserved within the pyroclastic deposit. The heating event may be related to the explosive magmatism that produced the pyroclastic deposits of the Remédios Formations. In this scenario, the titanite age of 10.7 Ma could represent a mixed-age between the crystallization age and the reheating that produced the explosive magmatism, leading to a partial Pb loss.

Previous $^{40}Ar/^{39}Ar$ studies (Perlingeiro et al., 2013) constrained the age of the Remédios Formation between 12.5 ± 0.1 and 9.4 ± 0.2 Ma, and indicate that the São José Formation with ages of 9.2 ± 0.5 to 9.0 ± 0.1 Ma was contemporaneous with the later Remédios volcanism. Based on a geochronological compilation, Perlingeiro et al. (2013) suggested that the peak of magmatism occurred around 10.2 Ma. The $^{40}Ar/^{39}Ar$ age of 12.5 ± 0.1 Ma is derived from a pyroclastic deposit from the Remédios Formation (sample UCFN30, Perlingeiro et al. (2013)). Given that, the major mineral and main source of K in this sample is alkali feldspar, it is entirely plausible that the 12.5 Ma age reflects that of a lithic fragment derived from a previously crystallized alkali-basalt plug or dike. For example, an extensive plug of alkali-basalt on Enseada dos Abreus is dated at 12.8 ± 0.3 Ma (Perlingeiro, 2012).

Therefore, this multiphase U-Pb approach reveals that evidence for a magmatic event record by the 13.69 ± 0.07 Ma zircon age preceded the magmatic event documented by the age of the alkali-basalt plug at 12.8 ± 0.3 Ma (Perlingeiro, 2012) and the alkali-basalt within the pyroclast deposit at 12.5 ± 0.3 Ma (Perlingeiro et al., 2013). With the combined titanite-apatite data from this study, it is possible to constrain the age of the pyroclastic deposit at 9.76 ± 0.94 Ma. With the addition of this new data, the following volcanic chronology is suggested: eruption of the alkali-basalt at 12.8 ± 0.3 Ma (Perlingeiro, 2012) followed by a sequence of

intrusions (phonolite, exessite, basanite; (Perlingeiro et al., 2013) and eruptions (pyroclast deposit) after a 2.4 million year hiatus (Figure 12). It is suggested that the constrained age of the Remédios Formation could be between 10.4 ± 0.1 and 9.4 ± 0.2 Ma (Perlingeiro et al., 2013), and the alkali-basalt dated at 12.8 ± 0.3 Ma (Perlingeiro, 2012), with 2.4 million years of hiatus could be referred as another older formation (Figure 12). Thus, a review of the stratigraphy of FNA, excluding the alkali-basalt as a separated unit is suggested.

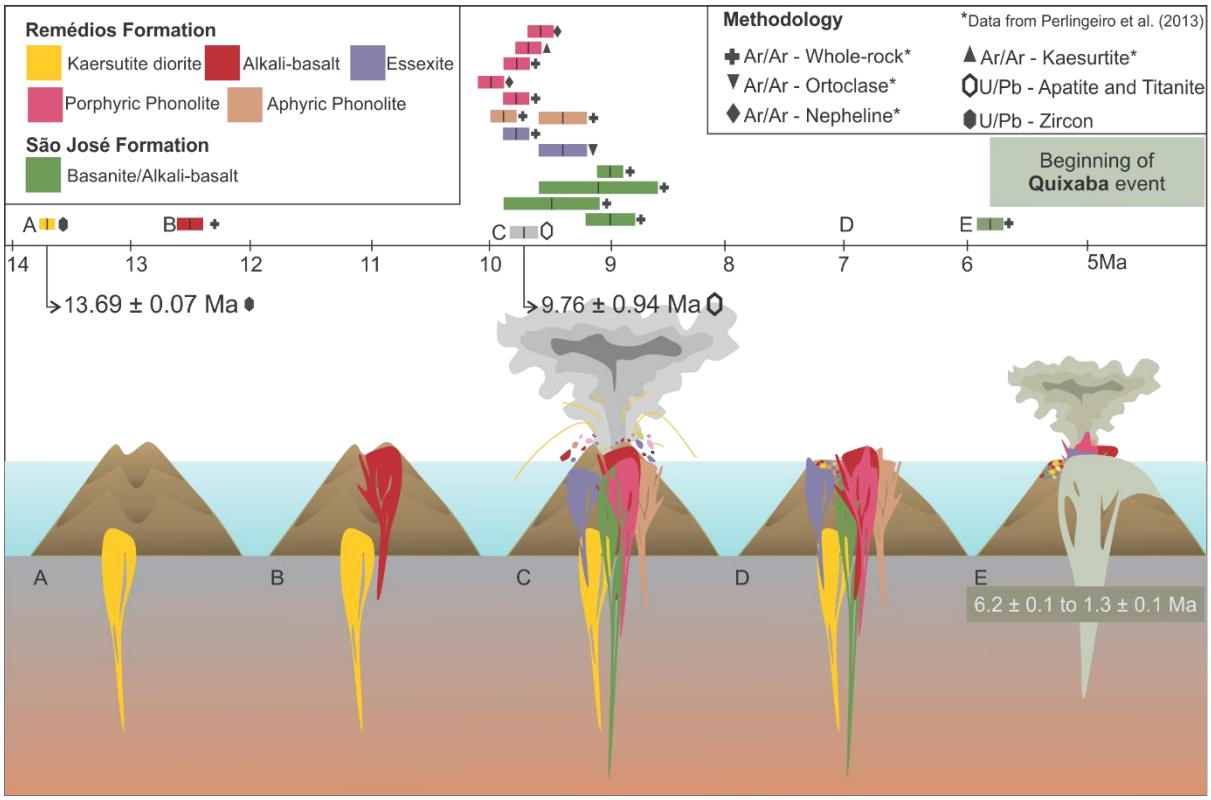

Figure 12 Schematic diagram of the magmatism emplacement with compiled ages, methods, and rock type. The rectangles represent the age (black line) with the error bar. The oldest recorded age is present in this study, followed by an alkali-basalt plug, dated to almost one million years later, followed by a hiatus of 2.5 million years. There is a peak of magmatism registered between 10 and 9 Ma, followed by a hiatus of almost 3 million years, with the beginning of the Quixaba event, where there is intercalation between effusive and explosive volcanism.

Published $^{40}Ar/^{39}Ar$ data from the Cenozoic continental magmatic provinces of Northeast Brazil range between 51.8 ± 0.9 Ma to 7.1 ± 0.3 Ma (Guimarães et al., 2020; Knesel et al., 2011; Silveira, 2006; Souza et al., 2003), showing contemporaneous activity with the Fernando de Noronha Archipelago during the Late Miocene (Cordani, 1970; Perlingeiro et al., 2013). The 13.69 Ma age obtained in this study from the kaersutite diorite suggest that the overlap in contemporaneous volcanic activity is more significant than previously thought. Given that the Fernando de Noronha Archipelago represents only a small highly dissected upper portion of a volcanic body that is 4 km high and 75 km in length (Almeida, 1955; Bryan et al., 1972), it is likely that a significant portion of the geological history of the FNA remains

to be discovered. The ages from the Fernando de Noronha Archipelago also overlap with both oceanic and continental magmatism related to the Cameroon line (Guimarães et al., 2020).

This contemporaneous late Miocene magmatic activity across Northeastern Brazil is not consistent with volcanic activity erupting through lithospheric plates moving over a stationary deep-mantle plume (Fodor et al., 1998; Morgan, 1983; Rivalenti et al., 2007, 2000). The highly alkaline nature of this volcanism generated from a source containing amphibole and phlogopite (Class and Goldstein, 1997), as well as the lithospheric temperatures (880.5 - 1068.2 ºC) and pressures (275-775.6 MPa) obtained from calcic amphibole thermobarometry (Ridolfi, 2021) are more are more consistent with melt derivation from the lithospheric mantle (White, 2020)

A spreading rate of 20 mm/y for the Atlantic Ocean (Müller et al., 2008) over a fixed plume, would give a hotspot track of about 250 km over a period of 13.69 Ma. This track length is four times longer than that of the FNA (60 km) alone and less than half the track length of the FNA ridge (approximately 650 km long). Neither of these scenarios can explain the lack of the progression ages and synchronous magmatic activity (Knesel et al., 2011; Perlingeiro et al., 2013), nor the lack of seismic evidence for a deep mantle upwelling (Montelli et al., 2004). It is unlikely that FNA magmatism can be related to a simple stationary plume model. Alternatively, King and Ritsema (2000) proposed that FNA magmatism might be the product of lithospheric downwelling due to edge-driven convection. This is based on evidence for the contribution of the continental lithospheric mantle (Gerlach et al., 1987; Knesel et al., 2011; Weaver, 1990), and the lack of age progression related to the mantle plume theory (King, 2007; King and Ritsema, 2000; Perlingeiro et al., 2013).

6. CONCLUSIONS

Intraplate magmatism in the South Atlantic Ocean such as is found in the Brazilian, Fernando de Noronha Archipelago provides important insights about the geodynamics of the rupture of Gondwana and the opening of the Atlantic Ocean. Our contribution of new geochemical, isotopic and geochronological data for plutonic rocks sheds new light on the timing and sources of magmatism within the FNA. The xenoliths represent remnants of the early magmatic evolution of the FNA that do not outcrop and were brought to the surface by a younger pyroclastic eruption.

U-Pb zircon dating of a plutonic sample yielded an age of 13.69 ± 0.07 Ma and is interpreted as the crystallization age of the kaersutite diorite. A U-Pb analysis of titanite and apatite from the same sample yielded an age of 9.76 ± 0.94 M that is interpreted as the eruption age of the pyroclastic unit of the Remédios Formation from which the kaersutite diorite was sampled. This represents a reinterpretation of previous studies that suggest that volcanic activity related to the Remédios Formation pyroclast deposit was at 12.5 ± 0.1 Ma due to an alkali basalt dated (Cordani, 1970; Perlingeiro et al., 2013). The 13.69 ± 0.07 Ma age of the sample also indicates that the timing of plutonic magmatic activity of the FNA more significantly overlaps with the period of onshore magmatism present in Northeastern Brazil (Knesel et al., 2011; Perlingeiro et al., 2013) than previously thought. The revised chronology of events also reveals a greater overlap between FNA magmatism and onshore and offshore magmatism present in the Cameroon Line (Guimarães et al., 2020).

Geochemical and isotopic data for the kaersutite diorite are similar to the earliest potassic series from Fernando de Noronha (Lopes and Ulbrich, 2015; Perlingeiro et al., 2013), and are consistent with derivation from enriched mantle source (EM2 component; Jackson and Dasgupta 2008; Perlingeiro 2012)

Future investigation of detrital zircons in either sedimentary rocks or beach sands from the FNA would help further constrain the temporal evolution of the FNA and ocean islands in general. Zircons are chemically inert, resistant to mechanical abrasion, and can provide important information about ages (U-Pb) and geochemistry (Hf and O isotopes) of the magma composition for portions of the island that had been already eroded (Sagan et al., 2020). Future geochronological studies of the *guyots* related to the FNA and the Brazilian continental margin would provide a better understanding of the age and evolution of the Fernando de Noronha Ridge.

REFERENCES

Allibon, J., Ovtcharova, M., Bussy, F., Cosca, M., Schaltegger, U., Bussien, D., Lewin, É., 2011. Lifetime of an ocean island volcano feeder zone: constraints from U–Pb dating on coexisting zircon and baddeleyite, and $^{40}Ar/^{39}Ar$ age determinations, Fuerteventura, Canary Islands. Can. J. Earth Sci. 48, 567–592. https://doi.org/10.1139/E10-032

Almeida, F.F.M. de, 2006. Ilhas oceânicas brasileiras e suas relações com a tectônica atlântica. Terrae Didat. 2, 3. https://doi.org/10.20396/td.v2i1.8637462

Almeida, F.F.M. de, 1955. Geologia e Petrologia do Arquipelago de Fernando de Noronha. SERGRAF do IBGE, Rio de Janeiro.

Almeida, F.F.M. de, Carneiro, Celso Dal Ré; Machado Jr., D. de L., Dehira, L.K., 1988. Magmatismo Pós-Paleozóico no Nordeste Oriental do Brasil. Rev. Bras. Geociências 18, 451–462. https://doi.org/10.25249/0375-7536.1988451462

Almeida, F.F.M., 1983. Relações tectônicas das rochas alcalinas mesozóicas da região meridional da Plataforma Sul-Americana. Rev. Bras. Geociências 13, 139–158.

Ashwal, L.D., Wiedenbeck, M., Torsvik, T.H., 2017. Archaean zircons in Miocene oceanic hotspot rocks establish ancient continental crust beneath Mauritius. Nat. Commun. 8, 14086. https://doi.org/10.1038/ncomms14086

Barfod, D.N., Ballentine, C.J., Halliday, A.N., Fitton, J.G., 1999. Noble gases in the Cameroon line and the He, Ne, and Ar isotopic compositions of high μ (HIMU) mantle. J. Geophys. Res. Solid Earth 104, 29509–29527. https://doi.org/10.1029/1999JB900280

Belousova, E.A., Griffin, W.L., O'Reilly, S.Y., Fisher, N.I., Griffin, A.W.L., O'Reilly, S.Y., Fisher, A.N.I., 2002. Igneous zircon: Trace element composition as an indicator of source rock type. Contrib. to Mineral. Petrol. 143, 602–622. https://doi.org/10.1007/s00410-002-0364-7

Bongiolo, E.M., Pires, G.L.C., Geraldes, M.C., Santos, A.C., Neumann, R., 2015. Geochemical modeling and Nd–Sr data links nephelinite–phonolite successions and xenoliths of Trindade Island (South Atlantic Ocean, Brazil). J. Volcanol. Geotherm. Res. 306, 58–73. https://doi.org/10.1016/j.jvolgeores.2015.10.002

Borley, G.D., Suddaby, P., Scott, P., 1971. Some Xenoliths from the alkalic rocks of Teneriffe, Canary Islands. Contrib. to Mineral. Petrol. 31, 102–114. https://doi.org/10.1007/BF00373453

Bottazzi, P., Tiepolo, M., Vannucci, R., Zanetti, A., Brumm, R., Foley, S.F., Oberti, R., 1999. Distinct site preferences for heavy and light REE in amphibole and the prediction of Amph/LDREE. Contrib. to Mineral. Petrol. 1999 1371 137, 36–45. https://doi.org/10.1007/S004100050580

Branner, J.C., 1889. Geology of Fernando de Noronha; Part I. Am. J. Sci. s3-37, 145–161. https://doi.org/10.2475/ajs.s3-37.218.145

Bryan, G.M., Kumar, N., Castro, P.J.M. de, 1972. The North Brazilian Ridge and the extension of equatorial fracture zones into the continent. Cong. Bras. Geol 41, 133–143.

Buikin, A.I., Kogarko, L.N., Korochantseva, E. V., Hopp, J., Trieloff, M., 2010. $^{40}Ar/^{39}Ar$ dating of volcanic rocks from the Fernando de Noronha Archipelago. Geochemistry Int. 48, 1035–1038. https://doi.org/10.1134/S0016702910100083

Burnham, A.D., 2018. Zircon, in: Reference Module in Earth Systems and Environmental Sciences. Elsevier. https://doi.org/10.1016/B978-0-12-409548-9.10911-X

Chamberlain, K.R., Bowring, S.A., 2001. Apatite–feldspar U–Pb thermochronometer: a reliable, mid-range (~450°C), diffusion-controlled system. Chem. Geol. 172, 173–200. https://doi.org/https://doi.org/10.1016/S0009-2541(00)00242-4

Cherniak, D.., Lanford, W.., Ryerson, F.., 1991. Lead diffusion in apatite and zircon using ion implantation and Rutherford Backscattering techniques. Geochim. Cosmochim. Acta 55, 1663–1673. https://doi.org/10.1016/0016-7037(91)90137-T

Cherniak, D.., Watson, E.., 2001. Pb diffusion in zircon. Chem. Geol. 172, 5–24. https://doi.org/10.1016/S0009-2541(00)00233-3

Cherniak, D.J., 2003. Diffusion in Zircon. Rev. Mineral. Geochemistry 53, 113–143. https://doi.org/10.2113/0530113

Cherniak, D.J., 1993. Lead diffusion in titanite and preliminary results on the effects of radiation damage on Pb transport. Chem. Geol. 110, 177–194. https://doi.org/https://doi.org/10.1016/0009-2541(93)90253-F

Chew, D.M., Petrus, J.A., Kamber, B.S., 2014. U-Pb LA-ICPMS dating using accessory mineral standards with variable common Pb. Chem. Geol. 363, 185–199. https://doi.org/10.1016/j.chemgeo.2013.11.006

Chew, D.M., Spikings, R.A., 2015. Geochronology and Thermochronology Using Apatite: Time and Temperature, Lower Crust to Surface. Elements 11, 189–194. https://doi.org/10.2113/gselements.11.3.189

Chew, D.M., Sylvester, P.J., Tubrett, M.N., 2011. U-Pb and Th-Pb dating of apatite by LA-ICPMS. Chem. Geol. 280, 200–216. https://doi.org/10.1016/j.chemgeo.2010.11.010

Clague, D.A., Frey, F.A., 1982. Petrology and Trace Element Geochemistry of the Honolulu Volcanics, Oahu: Implications for the Oceanic Mantle below Hawaii. J. Petrol. 23, 447–504. https://doi.org/10.1093/petrology/23.3.447

Class, C., Goldstein, S.L., 1997. Plume-lithosphere interactions in the ocean basins: constraints from the source mineralogy. Earth Planet. Sci. Lett. 150, 245–260. https://doi.org/https://doi.org/10.1016/S0012-821X(97)00089-7

Cordani, U.G., 1970. Idade do vulcanismo do Oceano Atlântico Sul. Bol. do Inst. Geol. e Astron. 1, 9–75.

Darwin, C., King Philip, P., Fitzroy, R., 1839. Narrative of the surveying voyages of His Majesty's Ships Adventure and Beagle between the years 1826 and 1836, describing their examination of the southern shores of South America, and the Beagle's circumnavigation of the globe. London :Henry Colburn,.

Davies, J.H.F.L., Marzoli, A., Bertrand, H., Youbi, N., Ernesto, M., Greber, N.D., Ackerson, M., Simpson, G., Bouvier, A.S., Baumgartner, L., Pettke, T., Farina, F., Ahrenstedt, H. V.,

Schaltegger, U., 2021. Zircon petrochronology in large igneous provinces reveals upper crustal contamination processes: new U–Pb ages, Hf and O isotopes, and trace elements from the Central Atlantic magmatic province (CAMP). Contrib. to Mineral. Petrol. 2021 1761 176, 1–24. https://doi.org/10.1007/S00410-020-01765-2

Deer, W.A., Howie, R.A., Zussman, J., 1992. An introduction to the rock-forming minerals: Essex. Engl. Longman Sci. Technol.

Droop, G.T.R., 1987. A general equation for estimating Fe3+ concentrations in ferromagnesian silicates and oxides from microprobe analyses, using stoichiometric criteria. Mineral. Mag. 51, 431–435. https://doi.org/10.1180/minmag.1987.051.361.10

Dunlop, D.J., 1990. Developments in rock magnetism. Reports Prog. Phys. 53, 707–792. https://doi.org/10.1088/0034-4885/53/6/002

Fodor, R.., Sial, A.., Gandhok, G., 2002. Petrology of spinel peridotite xenoliths from northeastern Brazil: lithosphere with a high geothermal gradient imparted by Fernando de Noronha plume. J. South Am. Earth Sci. 15, 199–214. https://doi.org/10.1016/S0895-9811(02)00032-9

Fodor, R. V., Hanan, B.B., 2000. Geochemical evidence for the Trindade hotspot trace: Columbia seamount ankaramite. Lithos 51. https://doi.org/10.1016/S0024-4937(00)00002-5

Fodor, R. V., Mukasa, S.B., Gomes, C.B., Cordani, U.G., 1989. Ti-rich eocene basaltic rocks, abrolhos platform, Offshore Brazil, 18°S: Petrology with respect to South Atlantic magmatism. J. Petrol. 30. https://doi.org/10.1093/petrology/30.3.763

Fodor, R. V., Mukasa, S.B., Sial, A.N., 1998. Isotopic and trace-element indications of lithospheric and asthenospheric components in Tertiary alkalic basalts, northeastern Brazil. Lithos 43, 197–217. https://doi.org/10.1016/S0024-4937(98)00012-7

Frost, B.R., Chamberlain, K.R., Schumacher, J.C., 2001. Sphene (titanite): phase relations and role as a geochronometer. Chem. Geol. 172, 131–148. https://doi.org/10.1016/S0009-2541(00)00240-0

Ganguly, J., Tirone, M., 2009. Closure Temperature, Cooling Age and High Temperature Thermochronology, in: Physics and Chemistry of the Earth's Interior. https://doi.org/10.1007/978-1-4419-0346-4_5

Gao, R., Lassiter, J.C., Barnes, J.D., Clague, D.A., Bohrson, W.A., 2016. Geochemical investigation of Gabbroic Xenoliths from Hualalai Volcano: Implications for lower oceanic crust accretion and Hualalai Volcano magma storage system. Earth Planet. Sci. Lett. 442, 162–172. https://doi.org/10.1016/j.epsl.2016.02.043

Gerlach, D.C., Stormer, J.C., Mueller, P.A., 1987. Isotopic geochemistry of Fernando de Noronha. Earth Planet. Sci. Lett. 85, 129–144. https://doi.org/10.1016/0012-821X(87)90027-6

Gorini, M., Bryan, G., 1976. The tectonic fabric of the Equatorial Atlantic and adjoining continental margins: Gulf of Guinea to the northeastern Brazil. An. Acad. Bras. Ciênc 48, 101-119.

Gorini, M.A., Bryan, G.M., 1974. Semi-isolated basin off northeast brazilian margin, in: Transactions-American Geophysical Union. pp. 278–279.

Guimarães, A.R., Fitton, J.G., Kirstein, L.A., Barfod, D.N., 2020. Contemporaneous intraplate magmatism on conjugate South Atlantic margins: A hotspot conundrum. Earth Planet. Sci.

Lett. 536, 116147. https://doi.org/10.1016/j.epsl.2020.116147

Gunn, B.M., Watkins, N.D., 1976. Geochemistry of the Cape Verde Islands and Fernando de Noroñha. Geol. Soc. Am. Bull. 87, 1089. https://doi.org/10.1130/0016-7606(1976)87<1089:GOTCVI>2.0.CO;2

Halliday, A.N., Davies, G.R., Lee, D.C., Tommasini, S., Paslick, C.R., Fitton, J.G., James, D.E., 1992. Lead isotope evidence for young trace element enrichment in the oceanic upper mantle. Nat. 1992 3596396 359, 623–627. https://doi.org/10.1038/359623a0

Harrison, T.M., Catlos, E.J., Montel, J.-M., 2002. U-Th-Pb Dating of Phosphate Minerals. Rev. Mineral. Geochemistry 48, 524–558. https://doi.org/10.2138/rmg.2002.48.14

Hayes, D.E., Ewing, M., 1970. North Brazilian Ridge and Adjacent Continental Margin. Am. Assoc. Pet. Geol. Bull. 54, 2120–2150. https://doi.org/10.1306/5d25cc75-16c1-11d7-8645000102c1865d

Heaman, L.M., 2009. The application of U–Pb geochronology to mafic, ultramafic and alkaline rocks: An evaluation of three mineral standards. Chem. Geol. 261, 43–52. https://doi.org/10.1016/J.CHEMGEO.2008.10.021

Hoskin, P.W.O., Schaltegger, U., 2003. The Composition of Zircon and Igneous and Metamorphic Petrogenesis. Rev. Mineral. Geochemistry 53, 27–62. https://doi.org/10.2113/0530027

Ito, E., White, W.M., Göpel, C., 1987. The O, Sr, Nd and Pb isotope geochemistry of MORB. Chem. Geol. 62, 157–176. https://doi.org/10.1016/0009-2541(87)90083-0

Jackson, M.G., Dasgupta, R., 2008. Compositions of HIMU, EM1, and EM2 from global trends between radiogenic isotopes and major elements in ocean island basalts. Earth Planet. Sci. Lett. 276, 175–186.

Kay, R.W., Gast, P.W., 1973. The Rare Earth Content and Origin of Alkali-Rich Basalts. J. Geol. 81, 653–682.

Kesson, S., Price, R.C., 1972. The major and trace element chemistry of kaersutite and its bearing on the petrogenesis of alkaline rocks. Contrib. to Mineral. Petrol. 35, 119–124. https://doi.org/10.1007/BF00370923

King, S.D., 2007. Hotspots and edge-driven convection. Geology 35, 223. https://doi.org/10.1130/G23291A.1

King, S.D., Ritsema, J., 2000. African hot spot volcanism: Small-scale convection in the upper mantle beneath cratons. Science (80-.). 290, 1137–1140. https://doi.org/10.1126/science.290.5494.1137

Kinny, P., Mcnaughton, N., Fanning, C., Maas, R., 1994. 518 Ma sphene (titanite) from the Khan Pegmatite, Namibia, Southwest Africa: a potential ionmicroprobe standard.

Kirkland, C.L., Hollis, J., Danišík, M., Petersen, J., Evans, N.J., McDonald, B.J., 2017. Apatite and titanite from the Karrat Group, Greenland; implications for charting the thermal evolution of crust from the U-Pb geochronology of common Pb bearing phases. Precambrian Res. 300, 107–120. https://doi.org/10.1016/j.precamres.2017.07.033

Knesel, K.M., Souza, Z.S., Vasconcelos, P.M., Cohen, B.E., Silveira, F. V, 2011. Young volcanism

in the Borborema Province, NE Brazil, shows no evidence for a trace of the Fernando de Noronha plume on the continent. Earth Planet. Sci. Lett. 302, 38–50. https://doi.org/10.1016/j.epsl.2010.11.036

Kogarko, L.N., Lebedev, V.A., Levskii, L.K., 2007. Heterogeneity of isotope sources of alkaline magmatism in the hot spot of the southwestern Atlantic: Fernando de Noronha Islands. Dokl. Earth Sci. 412, 85–88. https://doi.org/10.1134/S1028334X07010199

Kohn, M.J., 2017. Titanite Petrochronology. Rev. Mineral. Geochemistry 83. https://doi.org/10.2138/rmg.2017.83.13

Lacroix, A., 1893. Les enclaves des roches volcaniques. Protat Freres.

Le Maitre, R.W., 1969. Kaersutite-bearing plutonic xenoliths from Tristan da Cunha, South Atlantic. Mineral. Mag. 37, 185–197. https://doi.org/10.1180/minmag.1969.037.286.05

Le Maitre, R.W., Streckeisen, A., Zanettin, B., Le Bas, M.J., Bonin, B., Bateman, P., Bellieni, G., Dudek, A., Efremvoa, S., Keller, J.., Lameyre, J.., Sabine, P.A., Schmid, R., Sorensen, H., Woolley, A.R., 2002. Igneous Rocks: a Classification and Glossary of Terms, 2nd ed. Cambridge University Press, New York.

Leake, B.E., Woolley, A.R., Arps, C.E.S., Birch, W.D., Gilbert, M.C., Grice, J.D., Hawthorne, F.C., Kato, A., Kisch, H.J., Krivovichev, V.G., Linthout, K., Laird, J., Mandarino, J.A., Maresch, W. V., Nickel, E.H., Rock, N.M.S., Schumacher, J.C., Smith, D.C., Stephenson, N.C.N., Ungaretti, L., Whittaker, E.J.W., Youzhi, G., 1997. Nomenclature of amphiboles: Report of the subcommittee on amphiboles of the international mineralogical association, commission on new minerals and mineral names. Can. Mineral. 35, 219–246.

Li, X.-H., Long, W.-G., Li, Q.-L., Liu, Y., Zheng, Y.-F., Yang, Y.-H., Chamberlain, K.R., Wan, D.-F., Guo, C.-H., Wang, X.-C., Tao, H., 2010. Penglai Zircon Megacrysts: A Potential New Working Reference Material for Microbeam Determination of Hf-O Isotopes and U-Pb Age. Geostand. Geoanalytical Res. 34, 117–134. https://doi.org/10.1111/j.1751-908X.2010.00036.x

Lopes, R.P., 2002. O vulcanismo do Arquipélago de Fernando de Noronha, PE: química mineral e geoquímica. Universidade de São Paulo, São Paulo. https://doi.org/10.11606/T.44.2002.tde-17092013-095935

Lopes, R.P., 1997. Petrologia dos Fonólitos do Arquipélago de de Fernando de Noronha, PE.

Lopes, R.P., Ulbrich, M.N.C., 2015. Geochemistry of the alkaline volcanicsubvolcanic rocks of the Fernando de Noronha Archipelago, southern Atlantic Ocean. Brazilian J. Geol. 45, 307–333. https://doi.org/10.1590/23174889201500020009

Lopes, R.P., Ulbrich, M.N.C., 2006. Rochas vulcânicas alcalinas da formação quixaba de fernando de noronha, pe: química mineral e litogeoquímica. Rev. Bras. Geociências 36, 35–48.

MacKenzie, W.S., 1989. J. V. Smith and W. L. Brown. Feldspar Minerals: 1. Crystal Structures, Physical, Chemical, and Microtextural Properties. 2nd Edition. Berlin, Heidelberg and New York (Springer-Verlag), 1988. xviii + 828 pp., 352 figs. Price DM360.00. Mineral. Mag. 53, 655–656. https://doi.org/10.1180/minmag.1989.053.373.21

Maringolo, V., 1995. Estudo Petrográfico e Químico de Diques Ultramáficos e Máficos do

Arquipélago de Fernando de Noronha, PE.

Marques, L.S., Ulbrich, M.N.C., Ruberti, E., Tassinari, C.G., 1999. Petrology, geochemistry and Sr–Nd isotopes of the Trindade and Martin Vaz volcanic rocks (Southern Atlantic Ocean). J. Volcanol. Geotherm. Res. 93, 191–216. https://doi.org/10.1016/S0377-0273(99)00111-0

Mattioli, M., Upton, B.G.J., Renzulli, A., 1997. Sub-volcanic crystallization at Sete Cidades volcano, São Miguel, Azores, inferred from mafic and ultramafic plutonic nodules. Mineral. Petrol. 60, 1–26. https://doi.org/10.1007/BF01163132

McDonough, W.F., Sun, S. s., 1995. The composition of the Earth. Chem. Geol. 120, 223–253. https://doi.org/10.1016/0009-2541(94)00140-4

Mitchell-Thomé, R.C., 1970. Geology of the South Atlantic Islands. Schweizerbart Science Publishers, Stuttgart, Germany.

Mizusaki, A.M.P., Thomaz-Filho, A., Milani, E.J., De Césero, P., 2002. Mesozoic and Cenozoic igneous activity and its tectonic control in northeastern Brazil. J. South Am. Earth Sci. 15, 183–198. https://doi.org/10.1016/S0895-9811(02)00014-7

Mohriak, W., 2020. Genesis and evolution of the South Atlantic volcanic islands offshore Brazil. Geo-Marine Lett. 40, 1–33. https://doi.org/10.1007/s00367-019-00631-w

Montelli, R., Nolet, G., Dahlen, F.A., Masters, G., Engdahl, E.R., Hung, S.H., 2004. Finite-Frequency Tomography Reveals a Variety of Plumes in the Mantle. Science (80-.). 303. https://doi.org/10.1126/science.1092485

Morgan, W.J., 1983. Hotspot Tracks and the Early Rifting of the Atlantic. Dev. Geotecton. 19, 123–139. https://doi.org/10.1016/B978-0-444-42198-2.50015-8

Morgan, W.J., 1971. Convection plumes in the lower mantle. Nature 230. https://doi.org/10.1038/230042a0

Morimoto, N., Fabries, J., Ferguson, A.K., Ginzburg, I. V., Ross, M., Seifert, F.A., Zussman, J., Aoki, K., Gottardi, G., 1988. Nomenclature of Pyroxenes. Mineral. Petrol. 39, 55–76. https://doi.org/10.1007/BF01226262

Müller, R.D., Sdrolias, M., Gaina, C., Roest, W.R., 2008. Age, spreading rates, and spreading asymmetry of the world's ocean crust. Geochemistry, Geophys. Geosystems 9, n/a-n/a. https://doi.org/10.1029/2007GC001743

Oosthuyzen, E.J., Burger, A.J., 1973. The suitability of apatite as an age indicator by the uranium-lead isotope method. Earth Planet. Sci. Lett. 18, 29–36. https://doi.org/https://doi.org/10.1016/0012-821X(73)90030-7

Paton, C., Hellstrom, J., Paul, B., Woodhead, J., Hergt, J., 2011. Iolite: Freeware for the visualisation and processing of mass spectrometric data. J. Anal. At. Spectrom. 26, 2508. https://doi.org/10.1039/c1ja10172b

Paton, Chad, Woodhead, Jon D, Hellstrom, John C, Hergt, Janet M, Greig, Alan, Maas, Roland, Paton, C, Woodhead, J D, Hellstrom, J C, Hergt, J M, Greig, A, Maas, R, 2010. Improved laser ablation U-Pb zircon geochronology through robust downhole fractionation correction. Geochem. Geophys. Geosyst 11, 0–06. https://doi.org/10.1029/2009GC002618

Perlingeiro, G., 2012. Geochronology, geochemistry and petrogenesis of alkalic magmas at Fernando de Noronha, Brazil.

Perlingeiro, G., Vasconcelos, P.M., Knesel, K.M., Thiede, D.S., Cordani, U.G., 2013. $^{40}Ar/^{39}Ar$ geochronology of the Fernando de Noronha Archipelago and implications for the origin of alkaline volcanism in the NE Brazil. J. Volcanol. Geotherm. Res. 249, 140–154. https://doi.org/10.1016/j.jvolgeores.2012.08.017

Petrus, J.A., Kamber, B.S., 2012. VizualAge: A Novel Approach to Laser Ablation ICP-MS U-Pb Geochronology Data Reduction. Geostand. Geoanalytical Res. 36, 247–270. https://doi.org/10.1111/j.1751-908X.2012.00158.x

Pidgeon, R.T., Bosch, D., Bruguier, O., 1996. Inherited zircon and titanite U-Pb systems in an Archaean syenite from southwestern Australia: Implications for U-Pb stability of titanite. Earth Planet. Sci. Lett. 141. https://doi.org/10.1016/0012-821x(96)00068-4

Pilet, S., Baker, M.B., Müntener, O., Stolper, E.M., 2011. Monte Carlo Simulations of Metasomatic Enrichment in the Lithosphere and Implications for the Source of Alkaline Basalts. J. Petrol. 52, 1415–1442. https://doi.org/10.1093/PETROLOGY/EGR007

Pilet, S., Baker, M.B., Stolper, E.M., 2008. Metasomatized lithosphere and the origin of alkaline lavas. Science (80-.). 320. https://doi.org/10.1126/science.1156563

Pimentel, A., Ramalho, R.S., Becerril, L., Larrea, P., Brown, R.J., 2020. Editorial: Ocean Island Volcanoes: Genesis, Evolution and Impact, Frontiers in Earth Science. https://doi.org/10.3389/feart.2020.00082

Pin, C., Santos Zalduegui, J.F., 1997. Sequential separation of light rare-earth elements, thorium and uranium by miniaturized extraction chromatography: Application to isotopic analyses of silicate rocks. Anal. Chim. Acta 339. https://doi.org/10.1016/S0003-2670(96)00499-0

Pires, G.L.C., Bongiolo, E.M., 2016. The nephelinitic–phonolitic volcanism of the Trindade Island (South Atlantic Ocean): Review of the stratigraphy, and inferences on the volcanic styles and sources of nephelinites. J. South Am. Earth Sci. 72, 49–62. https://doi.org/10.1016/j.jsames.2016.07.008

Platevoet, B., Elitok, Ö., Guillou, H., Bardintzeff, J.-M., Yagmurlu, F., Nomade, S., Poisson, A., Deniel, C., Özgür, N., 2014. Petrology of Quaternary volcanic rocks and related plutonic xenoliths from Gölcük volcano, Isparta Angle, Turkey: Origin and evolution of the high-K alkaline series. J. Asian Earth Sci. 92, 53–76. https://doi.org/10.1016/j.jseaes.2014.06.012

Pochon, A., Poujol, M., Gloaguen, E., Branquet, Y., Cagnard, F., Gumiaux, C., Gapais, D., 2016. U-Pb LA-ICP-MS dating of apatite in mafic rocks: Evidence for a major magmatic event at the Devonian-Carboniferous boundary in the Armorican Massif (France). Am. Mineral. 101, 2430–2442. https://doi.org/10.2138/am-2016-5736

Raczek, I., Jochum, K.P., Hofmann, A.W., 2003. Neodymium and Strontium Isotope Data for USGS Reference Materials BCR-1, BCR-2, BHVO-1, BHVO-2, AGV-1, AGV-2, GSP-1, GSP-2 and Eight MPI-DING Reference Glasses 27, 173–179.

Ridolfi, F., 2021. Amp-TB2: An Updated Model for Calcic Amphibole Thermobarometry. Minerals 11, 324. https://doi.org/10.3390/min11030324

Ridolfi, F., Renzulli, A., 2011. Calcic amphiboles in calc-alkaline and alkaline magmas: thermobarometric and chemometric empirical equations valid up to 1,130°C and 2.2 GPa. Contrib. to Mineral. Petrol. 2011 1635 163, 877–895. https://doi.org/10.1007/S00410-011-0704-6

Rieder, M., Cavazzini, G., D'yakonov, Y.S., Frank-Kamenetskii, V.A., Gottardi, G., Guggenheim, S., Koval', P. V., Müller, G., Neiva, A.M.R., Radoslovich, E.W., Robert, J.-L., Sassi, F.P., Takeda, H., Weiss, Z., Wones, D.R., 1999. Nomenclature of the micas. Mineral. Mag. 63, 267–279. https://doi.org/10.1180/minmag.1999.063.2.13

Rivalenti, G., Mazzucchelli, M., Girardi, V.A.V., Vannucci, R., Barbieri, M.A., Zanetti, A., Goldstein, S.L., 2000. Composition and processes of the mantle lithosphere in northeastern Brazil and Fernando de Noronha: evidence from mantle xenoliths. Contrib. to Mineral. Petrol. 138, 308–325. https://doi.org/10.1007/s004100050565

Rivalenti, G., Zanetti, A., Girardi, V.A.V., Mazzucchelli, M., Tassinari, C.C.G., Bertotto, G.W., 2007. The effect of the Fernando de Noronha plume on the mantle lithosphere in north-eastern Brazil. Lithos 94, 111–131. https://doi.org/10.1016/j.lithos.2006.06.012

Sagan, M., Heaman, L.M., Pearson, D.G., Luo, Y., Stern, R.A., 2020. Removal of continental lithosphere beneath the Canary archipelago revealed from a U Pb Age and Hf/O isotope study of modern sand detrital zircons. Lithos 362–363, 105448. https://doi.org/10.1016/j.lithos.2020.105448

Santos, A.C., Geraldes, M.C., Siebel, W., Mendes, J., Bongiolo, E., Santos, W.H., Garrido, T.C. V., Rodrigues, S.W.O., 2018. Pleistocene alkaline rocks of Martin Vaz volcano, South Atlantic: low-degree partial melts of a CO_2 -metasomatized mantle plume. Int. Geol. Rev. 61, 296–313. https://doi.org/10.1080/00206814.2018.1425921

Santos, A.C. dos, Bonifácio, J.F., Guimarães Pereira Monteiro, L., Rocha-Júnior, E.R.V., Guerra, L.S. de C., Heilbron, M., Magini, C., Jeck, I.K., Bruno, H., 2022. Brazilian Equatorial Margin: magmatic genesis and evolution. Meso-Cenozoic Brazilian Offshore Magmat. 433–472. https://doi.org/10.1016/B978-0-12-823988-9.00016-2

Schaltegger, U., Davies, J.H.F.L., 2017. Petrochronology of Zircon and Baddeleyite in Igneous Rocks: Reconstructing Magmatic Processes at High Temporal Resolution. Rev. Mineral. Geochemistry 83, 297–328. https://doi.org/10.2138/RMG.2017.83.10

Schwab, R.G., Bloch, W., 1986. Geochemical Distribution Patterns of Magmatites from the Archipelago of Fernando de Noronha. Zentralblatt für Geol. und Paläontologie, Tl. I 1985, 1477–1483. https://doi.org/10.1127/zbl_geol_pal_1/1985/1986/1477

Scott, D.J., St-Onge, M.R., 1995. Constraints on Pb closure temperature in titanite based on rocks from the Ungava orogen, Canada: Implications for U-Pb geochronology and P-T-t path determinations. Geology 23, 1123. https://doi.org/10.1130/0091-7613(1995)023<1123:COPCTI>2.3.CO;2

Siebel, W., Becchio, R., Volker, F., Hansen, M.A.F., Viramonte, J., Trumbull, R.B., Haase, G., Zimmer, M., 2000. Trindade and Martín Vaz Islands, South Atlantic: Isotopic (Sr, Nd, Pb) and trace element constraints on plume related magmatism. J. South Am. Earth Sci. 13, 79–103. https://doi.org/10.1016/S0895-9811(00)00015-8

Silveira, F.V., 2006. Magmatismo cenozóico da porção central do Rio Grande do Norte, NE do

Brasil. Universidade Federal do Rio Grande do Norte.

Sláma, J., Košler, J., Condon, D.J., Crowley, J.L., Gerdes, A., Hanchar, J.M., Horstwood, M.S.A., Morris, G.A., Nasdala, L., Norberg, N., Schaltegger, U., Schoene, B., Tubrett, M.N., Whitehouse, M.J., 2008. Plešovice zircon — A new natural reference material for U-Pb and Hf isotopic microanalysis. Chem. Geol. 249, 1–35. https://doi.org/10.1016/J.CHEMGEO.2007.11.005

Smith, W.C., Burri, C., 1933. The igneous rocks of Fernando Noronha. Schweiz Miner. Petrogr Mitt 13, 405–434.

Souza, Z.S., Vasconcelos, P.M., Nascimento, M.A.L., Silveira, F. V, Paiva, H.S., Dias, L.G.S., Thiede, D., Carmo, I.O., 2003. $^{40}Ar/^{39}Ar$ geochronology of Mesozoic and Cenozoic magmatism in NE Brazil, in: Short Papers of the IV South American Symposium on Isotope Geology.

Spandler, C., Hammerli, J., Sha, P., Hilbert-Wolf, H., Hu, Y., Roberts, E., Schmitz, M., 2016. MKED1: A new titanite standard for in situ analysis of Sm-Nd isotopes and U-Pb geochronology. Chem. Geol. 425. https://doi.org/10.1016/j.chemgeo.2016.01.002

Spencer, K.J., Hacker, B.R., Kylander-Clark, A.R.C., Andersen, T.B., Cottle, J.M., Stearns, M.A., Poletti, J.E., Seward, G.G.E., 2013. Campaign-style titanite U-Pb dating by laser-ablation ICP: Implications for crustal flow, phase transformations and titanite closure. Chem. Geol. 341, 84–101. https://doi.org/10.1016/j.chemgeo.2012.11.012

Steinberger, B., 2000. Plumes in a convecting mantle: Models and observations for individual hotspots. J. Geophys. Res. Solid Earth 105, 11127–11152. https://doi.org/10.1029/1999JB900398

Storey, C.D., Smith, M.P., Jeffries, T.E., 2007. In situ LA-ICP-MS U–Pb dating of metavolcanics of Norrbotten, Sweden: Records of extended geological histories in complex titanite grains. Chem. Geol. 240, 163–181. https://doi.org/10.1016/J.CHEMGEO.2007.02.004

Stormer J. C., J., Whitney, S.E., 1978. Fourchite to phonolite: the origin of phonolite on Fernando de Noronha. Trans. Amer. Geophys. Union 59, 140.

Sun, J.F., Yang, J.H., Wu, F.Y., Xie, L.W., Yang, Y.H., Liu, Z.C., Li, X.H., 2012. In situ U-Pb dating of titanite by LA-ICPMS. Chinese Sci. Bull. 57. https://doi.org/10.1007/s11434-012-5177-0

Sun, S.S., Hanson, G.N., 1975. Evolution of the mantle: Geochemical evidence from alkali basalt. Geology 3. https://doi.org/10.1130/0091-7613(1975)3<297:EOTMGE>2.0.CO;2

Sun, S.S., McDonough, W.F., 1989. Chemical and isotopic systematics of oceanic basalts: implications for mantle composition and processes. Geol. Soc. London, Spec. Publ. 42, 313–345. https://doi.org/10.1144/GSL.SP.1989.042.01.19

Tanaka, T., Togashi, S., Kamioka, H., Amakawa, H., Kagami, H., Hamamoto, T., Yuhara, M., Orihashi, Y., Yoneda, S., Shimizu, H., Kunimaru, T., Takahashi, K., Yanagi, T., Nakano, T., Fujimaki, H., Shinjo, R., Asahara, Y., Tanimizu, M., Dragusanu, C., 2000. JNdi-1: a neodymium isotopic reference in consistency with LaJolla neodymium. Chem. Geol. 168, 279–281. https://doi.org/10.1016/S0009-2541(00)00198-4

Teixeira, W., 2003. Arquipélago Fernando de Noronha: o paraíso do vulcão. Terra Virgem Editora.

Thompson, J., Meffre, S., Maas, R., Kamenetsky, V., Kamenetsky, M., Goemann, K., Ehrig, K., Danyushevsky, L., 2016. Matrix effects in Pb/U measurements during LA-ICP-MS analysis of the mineral apatite. J. Anal. At. Spectrom. 31, 1206–1215. https://doi.org/10.1039/C6JA00048G

Thomson, S.N., Gehrels, G.E., Cecil, R., Ruiz, J., 2009. Exploring Routine Laser Ablation Multicollector ICPMS U-Pb Dating of Apatite, in: AGU Fall Meeting Abstracts. pp. V33B-2043.

Thomson, S.N., Gehrels, G.E., Ruiz, J., Buchwaldt, R., 2012. Routine low-damage apatite U-Pb dating using laser ablation–multicollector–ICPMS. Geochemistry, Geophys. Geosystems 13. https://doi.org/10.1029/2011GC003928

Ulbrich, M.N.C., Lopes, R.P., 2000. Xenólitos de origem subvulcânica na Formação Remédios, arquipélago de Fernando de Noronha: petrografia, textura e química mineral. Geochim. Bras. https://doi.org/10.21715/gb.v14i1.170

Ulbrich, M.N.C., Marques, L.S., Lopes, R.P., 2004. As ilhas vulcânicas brasileiras: fernando de noronha e trindade. Geol. do Cont. Sul-Americano Evolução da Obra Fernando Flávio Marques Almeida 555–573.

Vazquez, J.A., Shamberger, P.J., Hammer, J.E., 2007. Plutonic xenoliths reveal the timing of magma evolution at Hualalai and Mauna Kea, Hawaii. Geology 35, 695–698. https://doi.org/10.1130/G23495A.1

Vermeesch, P., 2018. IsoplotR: A free and open toolbox for geochronology. Geosci. Front. 9, 1479–1493. https://doi.org/10.1016/j.gsf.2018.04.001

Watson, E.B., 1980. Apatite and phosphorus in mantle source regions: An experimental study of apatite/melt equilibria at pressures to 25 kbar. Earth Planet. Sci. Lett. 51, 322–335. https://doi.org/https://doi.org/10.1016/0012-821X(80)90214-9

Watson, E.B., 1979. Apatite saturation in basic to intermediate magmas. Geophys. Res. Lett. 6, 937–940. https://doi.org/https://doi.org/10.1029/GL006i012p00937

Weaver, B.L., 1990. Contributions to Geochemistry of highly-undersaturated ocean island basalt suites from the South Atlantic Ocean: Fernando de Noronha and Trindade islands, Contrib Mineral Petrol.

Weaver, B.L., Wood, D.A., Tarney, J., Joron, J.L., 1987. Geochemistry of ocean island basalts from the South Atlantic: Ascension, Bouvet, St. Helena, Gough and Tristan da Cunha. Geol. Soc. London, Spec. Publ. 30, 253–267.

Weis, D., 1983. Pb isotopes in Ascension Island rocks: oceanic origin for the gabbroic to granitic plutonic xenoliths. Earth Planet. Sci. Lett. 62, 273–282. https://doi.org/10.1016/0012-821X(83)90090-0

White, W.M., 2020. Geochemistry. John Wiley & Sons.

Whitney, D.L., Evans, B.W., 2010. Abbreviations for names of rock-forming minerals. Am. Mineral. 95, 185–187. https://doi.org/10.2138/am.2010.3371

Wiedenbeck, M., Allé, P., Corfu, F., Griffin, W.L., Meier, M., Oberli, F., Quadt, A. Von, Roddick, J.C., Spiegel, W., 1995. Three Natural Zircon Standarts for U-Th-Pb, Lu-Hf, Trace Elements and REE Analyses. Geostand. Geoanalytical Res. 19, 1–23. https://doi.org/10.1111/j.1751-908X.1995.tb00147.x

Wiedenbeck, M., Hanchar, J.M., Peck, W.H., Sylvester, P., Valley, J., Whitehouse, M., Kronz, A., Morishita, Y., Nasdala, L., Fiebig, J., Franchi, I., Girard, J.-P., Greenwood, R.C.C., Hinton, R., Kita, N., Mason, P.R.D.R.D., Norman, M., Ogasawara, M., Piccoli, P.M.M., Rhede, D., Satoh, H., Schulz-Dobrick, B., Skår, O., Spicuzza, M.J., Terada, K., Tindle, A., Togashi, S., Vennemann, T., Xie, Q., Zheng, Y.-F., 2004. Further Characterisation of the 91500 Zircon Crystal. Geostand. Geoanalytical Res. 28, 9–39.

Williams, G.H., 1889. Geology of Fernando de Noronha; Part II, Petrography. Am. J. Sci. s3-37, 178–188. https://doi.org/10.2475/ajs.s3-37.219.178

Wohlgemuth-Ueberwasser, C.C., Tegner, C., Pease, V., 2017. LA-Q-ICP-MS apatite U/Pb geochronology using common Pb in plagioclase: Examples from layered mafic intrusions. Am. Mineral. 102, 571–579. https://doi.org/doi:10.2138/am-2017-5903

Zhang, F.-F., Wang, X.-L., Sun, Z.-M., Chen, X., Zhou, X.-H., Yang, T., 2018. Geochemistry and zircon-apatite U-Pb geochronology of mafic dykes in the Shuangxiwu area: Constraints on the initiation of Neoproterozoic rifting in South China. Precambrian Res. 309, 138–151. https://doi.org/https://doi.org/10.1016/j.precamres.2017.04.008

Zindler, A., Hart, S., 1986. Chemical Geodynamics. Annu. Rev. Earth Planet. Sci. 14, 493–571. https://doi.org/10.1146/annurev.ea.14.050186.002425

APPENDIX A – Mineral Chemistry

Table 4 Pyroxenes – Mineral Chemistry

Spot	31	32	33
SiO_2	48.548	49.421	48.55
TiO_2	2.089	2.182	3.357
Al_2O_3	5.683	5.822	4.24
FeOt	6.68	6.494	8.631
Cr_2O_3	0.01	0.04	0.039
MnO	0.28	0.196	0.275
NiO	0.029	0.004	0.006
MgO	13.171	13.221	12.822
CaO	23.094	22.921	22.05
Na_2O	0.706	0.705	0.668
K_2O	0.032	0.048	0.029
ZrO_2	0	0.096	0
Si	1.807	1.819	1.814
Al^{IV}	0.193	0.181	0.186
Al^{VI}	0.056	0.071	0.001
Ti	0.058	0.060	0.094
Fe^{+3}	0.107	0.061	0.066
Fe^{+2}	0.099	0.138	0.202
Cr	0.000	0.001	0.001
Mn	0.009	0.006	0.009
Mg	0.731	0.725	0.714
Ca	0.921	0.904	0.883
Na	0.051	0.050	0.048
K	0.002	0.002	0.001
Mg#	88.1	84.0	77.9
Wo	49.335	49.275	47.106
En	39.154	39.551	38.117
Fs	11.512	11.174	14.777

Table 5 Feldspar – Mineral Chemistry

Spot	15	16	17
SiO_2	56.651	56.636	56.588
TiO_2	0.010	0.008	0.035
Al_2O_3	27.742	27.496	27.836
FeO	0.253	0.280	0.342
CaO	9.535	9.625	9.643
Na_2O	5.725	5.882	6.029
K_2O	0.445	0.189	0.231
Total	100.361	100.116	100.704
Si	10.149	10.167	10.114
Ti	0.001	0.001	0.005
Al	5.857	5.817	5.863
Fe^{2+}	0.038	0.042	0.051
Ca	1.830	1.851	1.846
Na	1.988	2.047	2.089
K	0.102	0.043	0.053
An	46.683	46.965	46.298
Ab	50.723	51.937	52.382
Or	2.594	1.098	1.321

Table 6 Amphibole – Mineral Chemistry

Spot	1	2	3	4	9	10	11	12	25	26	27	28
Type	Pargasite	Pargasite	Kaersutite	Pargasite	Pargasite	Pargasite	Pargasite	Pargasite	Pargasite	Pargasite	Kaersutite	Pargasite
SiO_2	40.706	40.895	41.130	40.457	41.282	42.279	40.424	40.224	41.186	40.745	39.851	40.075
TiO_2	3.538	4.022	4.835	3.962	3.372	2.918	3.835	3.529	3.673	3.969	7.173	4.265
Al_2O_3	11.936	12.173	12.640	12.864	11.666	11.018	12.657	12.470	13.061	12.901	12.436	12.668
Cr_2O_3	0.045	0.000	0.031	0.024	0.057	0.000	0.020	0.000	0.000	0.000	0.007	0.000
FeOt	13.707	12.613	11.031	11.576	13.236	13.020	13.136	13.783	11.484	10.566	10.615	12.989
MnO	0.221	0.187	0.160	0.161	0.194	0.191	0.278	0.183	0.228	0.142	0.162	0.192
MgO	11.332	12.053	12.829	12.039	11.509	12.317	11.253	11.349	12.801	13.079	12.748	11.514
CaO	11.967	11.944	11.964	12.183	12.006	11.889	12.213	11.923	11.999	11.988	11.692	12.041
Na_2O	2.180	2.196	2.280	2.293	2.232	2.136	2.302	2.153	2.305	2.241	2.199	2.202
K_2O	1.631	1.568	1.348	1.367	1.511	1.440	1.339	1.552	1.388	1.355	1.395	1.437
ZrO_2	0.025	0.000	0.000	0.106	0.000	0.000	0.000	0.000	0.000	0.000	0.000	0.000
F	0.215	0.147	0.354	0.110	0.029	0.068	0.189	0.219	0.173	0.053	0.138	0.200
Cl	0.095	0.051	0.026	0.030	0.093	0.098	0.053	0.077	0.020	0.022	0.024	0.036
Total F-Cl	0.310	0.198	0.380	0.140	0.122	0.166	0.242	0.296	0.193	0.075	0.162	0.236
Total Oxides	97.288	97.651	98.248	97.032	97.065	97.208	97.457	97.166	98.125	96.986	98.278	97.383
Total	97.598	97.849	98.628	97.172	97.187	97.374	97.699	97.462	98.318	97.061	98.440	97.619
Si	6.142	6.109	6.053	6.056	6.218	6.327	6.070	6.068	6.069	6.061	5.874	6.020
Al ^{IV}	1.858	1.891	1.947	1.944	1.782	1.673	1.930	1.932	1.931	1.939	2.126	1.980
Al ^{VI}	0.265	0.253	0.245	0.325	0.288	0.270	0.309	0.285	0.337	0.323	0.034	0.263
Fe^{3+}	0.000	0.000	0.000	0.000	0.000	0.039	0.000	0.064	0.072	0.003	0.000	0.000
Cr	0.005	0.000	0.004	0.003	0.007	0.000	0.002	0.000	0.000	0.000	0.001	0.000
Ti	0.402	0.452	0.535	0.446	0.382	0.328	0.433	0.400	0.407	0.444	0.795	0.482
Fe^{2+}	1.729	1.576	1.357	1.449	1.667	1.590	1.649	1.675	1.343	1.311	1.308	1.632
Mn	0.028	0.024	0.020	0.020	0.025	0.024	0.035	0.023	0.028	0.018	0.020	0.024
Mg	2.549	2.684	2.815	2.687	2.584	2.748	2.519	2.552	2.812	2.901	2.801	2.579
Ca	1.935	1.912	1.886	1.954	1.937	1.906	1.965	1.927	1.894	1.911	1.846	1.938
Na	0.638	0.636	0.651	0.665	0.652	0.620	0.670	0.630	0.658	0.646	0.628	0.641
K	0.314	0.299	0.253	0.261	0.290	0.275	0.256	0.299	0.261	0.257	0.262	0.275
Mg#	59.579	63.014	67.464	64.964	60.788	63.345	60.432	60.377	67.672	68.865	68.164	61.247

Table 7 Ilmenite – Mineral Chemistry

Spot	20	21	22
TiO_2	45.139	45.403	45.068
Al_2O_3	0.051	0.047	0.088
Cr_2O_3	0.018	0.009	0.000
FeOt	51.092	51.283	51.191
MnO	0.992	1.095	1.047
MgO	0.987	1.041	0.939
CaO	0.019	0.001	0.010
Total	98.298	98.879	98.343
Ti	1.717	1.717	1.714
Al	0.003	0.003	0.005
Fe^{2+}	2.161	2.156	2.164
Mn	0.042	0.047	0.045
Mg	0.074	0.078	0.071
Ca	0.001	0.000	0.001
Fe/Fe+Mg	0.967	0.965	0.968
Fe^{2+}	1.600	1.592	1.598
Fe^{3+}	0.561	0.564	0.566
SiO_2	0.015	0.000	0.010
TiO_2	45.139	45.403	45.068
Al_2O_3	0.051	0.047	0.088
Fe_2O_3	14.737	14.903	14.879
FeO	37.831	37.873	37.802
MnO	0.992	1.095	1.047
MgO	0.987	1.041	0.939
CaO	0.019	0.001	0.010
TOTAL	99.771	100.363	99.843

Table 8 Phlogopite - Mineral Chemistry

Spot	5	6	7	8	13	14	36	37
SiO_2	37.109	36.854	37.044	36.827	36.804	37.546	37.196	36.85
TiO_2	3.686	3.889	3.76	4.511	4.43	4.261	3.851	3.517
Al_2O_3	14.933	14.827	14.808	14.954	14.758	14.521	15.751	15.451
FeO	12.767	11.947	12.893	12.431	13.414	13.443	12.634	12.351
MnO	0.103	0.171	0.109	0.089	0.096	0.133	0.109	0.089
MgO	16.180	16.603	16.715	15.997	15.027	15.926	16.764	16.791
CaO	0.069	0.14	0.172	0.13	0.134	0.14	0.015	0.058
Na_2O	0.636	0.787	0.636	0.7	0.543	0.613	0.782	0.698
K_2O	8.855	8.634	9.015	9.416	9.09	8.423	9.279	8.932
Cl	0.116	0.101	0.091	0.045	0.1	0.102	0.066	0.056
F	0.247	0.31	0.273	0.331	0.211	0.134	0.266	0.161
Total	94.701	94.263	95.516	95.431	94.607	95.242	96.713	94.954
Si	5.536	5.510	5.494	5.472	5.523	5.563	5.440	5.469
Al^{IV}	2.464	2.490	2.506	2.528	2.477	2.437	2.560	2.531
Al^{VI}	0.161	0.122	0.082	0.091	0.132	0.099	0.155	0.172
Ti	0.414	0.437	0.419	0.504	0.500	0.475	0.424	0.393
Fe^{2+}	1.592	1.493	1.599	1.545	1.683	1.666	1.545	1.533
Mn	0.013	0.022	0.014	0.011	0.012	0.017	0.014	0.011
Mg	3.598	3.700	3.696	3.544	3.362	3.518	3.655	3.715
Ca	0.011	0.022	0.027	0.021	0.022	0.022	0.002	0.009
Na	0.184	0.228	0.183	0.202	0.158	0.176	0.222	0.201
K	1.685	1.646	1.705	1.785	1.740	1.592	1.731	1.691
Cl	0.029	0.026	0.023	0.011	0.025	0.026	0.016	0.014
F	0.117	0.147	0.128	0.156	0.100	0.063	0.123	0.076
Total	15.658	15.672	15.725	15.702	15.609	15.565	15.747	15.725

Table 9 Magnetite - Mineral Chemistry

Spots	23	24
SiO_2	0.43	0.343
TiO_2	0.566	0.322
Al_2O_3	0.932	1.92
Cr_2O_3	0.306	0.265
FeO	85.34	85.234
MnO	0.165	0.126
MgO	0.177	0.299
CaO	0.049	0.048
Total	87.965*	88.557*

*altered magnetite.

Table 10 Apatite - Mineral Chemistry

Spots	18	19
CaO	54.428	54.351
Na_2O	0.129	0.153
MnO	0.095	0.012
FeO	0.084	0.116
P_2O_5	40.772	41.263
SiO_2	0.229	0.273
Cl	0.819	0.807
F	2.777	2.857
Total	99.333	99.832

APPENDIX B – Mineral Chemistry Spot Maps

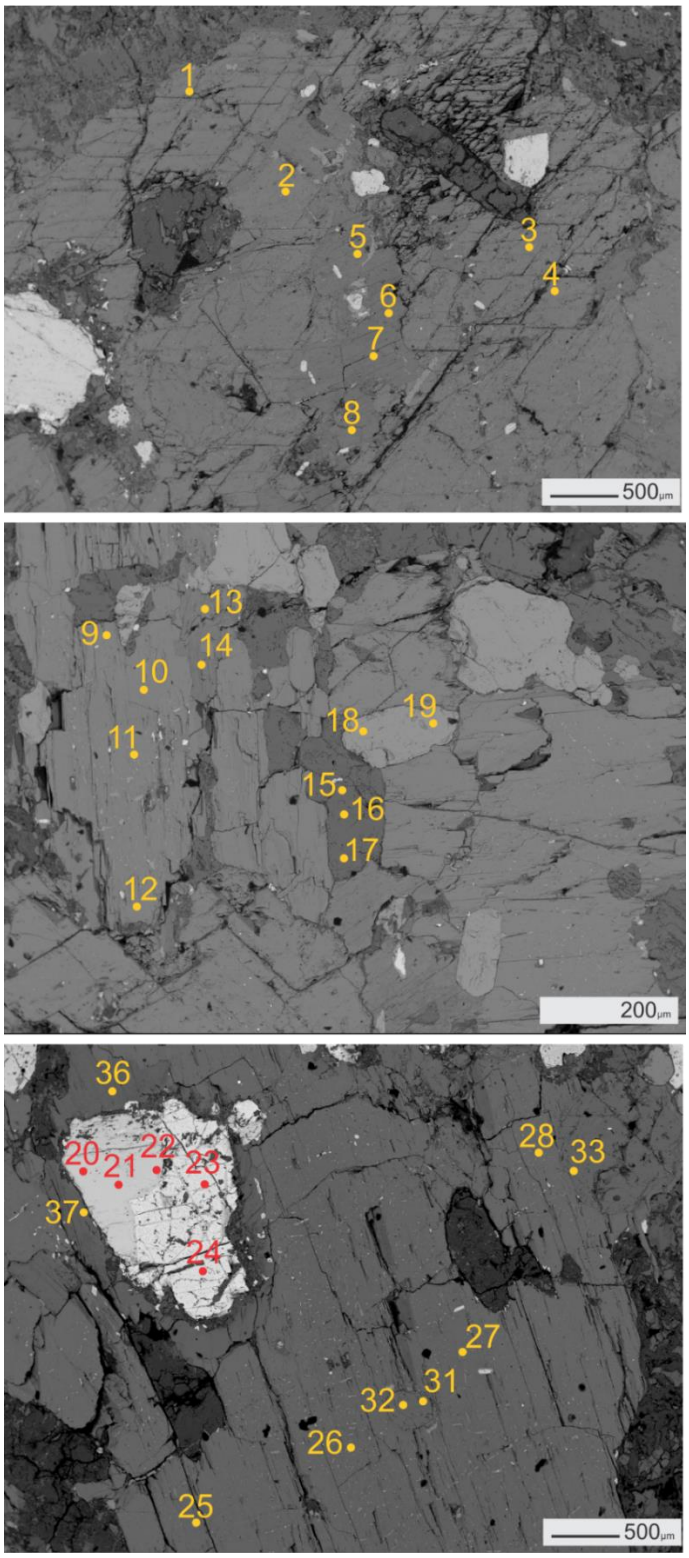

APPENDIX C – U-Pb Methodology – Reference Data for Apatite and Titanite

SPOT	$U_{(ppm)}$	Th/U	$^{202}Hg_{(cps)}$	$^{204}Pb_{(cps)}$	$^{207}Pb_{(cps)}$	$^{206}Pb_{(cps)}$	$^{208}Pb_{(cps)}$	$^{207}Pb/^{206}Pb$	2σ(%)	$^{207}Pb/^{235}U$	2σ(%)	$^{206}Pb/^{238}U$	2σ(%)	ρ	$^{206}Pb/^{238}U$	2σ(s)	$^{207}Pb/^{235}U$	2σ(s)	$^{207}Pb/^{206}Pb$	2σ(s)
TANZ PRIMARY STD 600 Ma																				
001	0.00	1.554	3154.824	2888.282	16930.83	284922.20	0.00	0.061	1.2	0.800	2.4	0.096	2.1	0.9	589	12	597	11	627	26
002	0.00	1.370	3175.997	3006.067	12945.63	222257.28	0.00	0.059	2.8	0.819	4.6	0.100	3.6	0.8	613	21	607	21	585	61
011	0.00	1.469	3670.527	3228.555	15965.06	269409.29	0.00	0.060	1.2	0.814	2.4	0.098	2.1	0.9	602	12	605	11	617	26
012	0.00	1.455	3710.306	3248.450	15792.34	268762.11	0.00	0.060	1.2	0.806	2.4	0.098	2.1	0.9	602	12	600	11	593	25
021	0.00	1.331	4217.617	3468.668	10998.60	185403.62	0.00	0.060	1.2	0.811	2.4	0.098	2.1	0.9	601	12	603	11	610	27
001	0.00	1.459	3770.896	3316.361	16258.61	270802.02	0.00	0.061	0.9	0.815	1.3	0.098	0.9	0.7	601	5	605	6	622	20
002	0.00	1.511	3797.676	3313.095	15609.92	264591.77	0.00	0.060	1.0	0.802	1.3	0.098	0.9	0.7	601	5	598	6	589	21
011	0.00	1.487	3822.008	3257.621	15608.58	264819.17	0.00	0.060	1.0	0.803	1.3	0.097	0.9	0.7	599	5	598	6	597	21
012	0.00	1.490	3787.144	3243.777	15708.45	264825.11	0.00	0.060	1.3	0.809	1.7	0.097	1.0	0.6	599	6	602	8	610	29
021	0.00	1.361	3752.441	3261.505	13295.58	226144.02	0.00	0.060	1.0	0.812	1.3	0.098	0.8	0.7	604	5	604	6	603	21
022	0.00	1.485	3725.423	3256.111	15503.99	262867.28	0.00	0.060	1.0	0.807	1.3	0.097	0.8	0.6	599	5	601	6	609	21

SPOT	$U_{(ppm)}$	Th/U	$^{202}Hg_{(cps)}$	$^{204}Pb_{(cps)}$	$^{207}Pb_{(cps)}$	$^{206}Pb_{(cps)}$	$^{208}Pb_{(cps)}$	$^{207}Pb/^{206}Pb$	2σ(%)	$^{207}Pb/^{235}U$	2σ(%)	$^{206}Pb/^{238}U$	2σ(%)	ρ	$^{206}Pb/^{238}U$	2σ(s)	$^{207}Pb/^{235}U$	2σ(s)	$^{207}Pb/^{206}Pb$	2σ(s)
SECONDARY APATITE REF MATERIAL - 401 apatite 508 Ma																				
003	13.62	12.717	3226.385	2978.577	6473.86	92151.22	0.00	0.072	2.4	0.838	3.2	0.084	2.1	0.7	522	11	618	15	990	49
004	13.47	12.582	3289.239	3002.677	6120.25	89417.97	0.00	0.070	1.8	0.803	2.8	0.083	2.1	0.8	514	11	599	13	933	37
005	13.17	12.211	3382.501	3040.562	5932.90	87316.07	0.00	0.070	2.0	0.796	2.9	0.083	2.1	0.7	513	11	595	13	919	41
~~006~~	~~13.09~~	~~12.107~~	~~3420.049~~	~~3533.936~~	~~13189.31~~	~~100951.29~~	~~0.00~~	~~0.133~~	~~6.6~~	~~1.772~~	~~7.6~~	~~0.096~~	~~3.7~~	~~0.5~~	~~593~~	~~21~~	~~1035~~	~~51~~	~~2143~~	~~116~~
SECONDARY APATITE REF MATERIAL - MADAGASCAR apatite 470 Ma																				
007	15.75	44.734	3445.567	3344.096	9489.70	100458.76	0.00	0.097	1.4	1.062	2.5	0.080	2.1	0.8	495	10	735	13	1559	26
008	16.07	45.507	3523.206	3372.031	9577.34	102718.67	0.00	0.095	1.4	1.046	2.6	0.080	2.1	0.8	495	10	727	13	1527	27
009	15.95	45.074	3554.922	3437.632	9737.83	102062.22	0.00	0.097	1.3	1.073	2.5	0.080	2.1	0.8	496	10	740	13	1574	25
010	16.10	44.704	3619.646	3452.589	9764.07	103181.18	0.00	0.096	1.5	1.068	2.6	0.080	2.1	0.8	498	10	738	14	1556	28
SECONDARY TITANITE REF MATERIAL - MKED apatite 1518 Ma																				

003	104.56	3.942	3827.148	3833.102	227027.61	2408736.20	0.00	0.095	2.5	3.482	2.5	0.265	0.5	0.2	1517	6	1523	20	1532	46
004	102.93	3.966	3821.873	3370.546	217768.10	2367087.65	0.00	0.094	2.5	3.445	2.6	0.265	0.6	0.2	1513	8	1515	21	1517	48
005	99.47	3.970	3833.757	3389.718	208707.11	2269263.18	0.00	0.096	2.7	3.471	2.9	0.262	0.9	0.3	1501	12	1521	23	1547	51
006	104.01	3.868	3818.812	3369.739	220783.92	2401986.31	0.00	0.098	2.4	3.567	2.4	0.265	0.3	0.1	1516	4	1542	19	1578	45
023	105.33	3.769	3770.876	4021.289	227067.25	2360558.86	0.00	0.096	1.5	3.512	1.8	0.265	1.0	0.6	1516	14	1530	15	1549	29
024	104.32	3.846	3790.514	3367.352	216478.69	2341350.49	0.00	0.092	1.1	3.382	1.5	0.266	1.0	0.6	1518	13	1500	12	1475	22
025	109.08	4.044	3783.565	3583.466	229641.30	2458901.32	0.00	0.093	0.9	3.430	1.3	0.266	0.8	0.7	1522	11	1511	10	1496	18
026	108.76	3.947	3808.655	3292.225	225950.03	2459271.34	0.00	0.092	0.9	3.385	1.2	0.267	0.8	0.7	1526	11	1501	10	1466	18
SECONDARY TITANITE REF MATERIAL - KAHN apatite 518 Ma																				
007	597.77	0.861	3817.824	17548.862	238796.95	4208050.92	0.00	0.059	1.2	0.674	1.6	0.083	1.0	0.6	513	5	523	7	567	26
008	586.09	0.845	3861.104	17504.850	240667.04	4179723.83	0.00	0.060	1.0	0.693	1.4	0.084	0.9	0.7	519	5	535	6	601	22
009	570.22	1.051	3865.762	17485.135	230750.95	4057497.11	0.00	0.059	1.1	0.683	1.4	0.084	0.9	0.6	518	4	529	6	575	24
010	564.99	1.092	3840.584	17197.096	226285.13	3982837.10	0.00	0.059	1.2	0.676	1.6	0.083	1.1	0.7	513	5	524	7	574	27

APPENDIX D – U-Pb Methodology – Sample Data for Apatite and Titanite

SPOT	$U_{(ppm)}$	Th/U	$^{202}Hg_{(cps)}$	$^{204}Pb_{(cps)}$	$^{207}Pb_{(cps)}$	$^{206}Pb_{(cps)}$	$^{208}Pb_{(cps)}$	$^{207}Pb/^{206}Pb$	2σ(%)	$^{207}Pb/^{235}U$	2σ(%)	$^{206}Pb/^{238}U$	2σ(%)	ρ	$^{206}Pb/^{238}U$	2σ(s)	$^{207}Pb/^{235}U$	2σ(s)	$^{207}Pb/^{206}Pb$	2σ(s)
SAMPLE APATITE																				
013	4.39	7.100	3722.350	4934.457	24213.58	29996.11	0.00	0.819	3.3	9.765	5.1	0.087	3.8	0.8	535	20	2413	48	4955	47
014	4.40	6.494	3720.941	4439.990	17738.52	22691.49	0.00	0.793	2.2	7.200	3.3	0.066	2.5	0.8	411	10	2137	30	4910	31
015	3.83	5.270	3738.322	5494.074	34924.44	44658.42	0.00	0.792	1.6	16.232	2.8	0.149	2.3	0.8	893	19	2891	27	4908	22
016	3.79	5.234	3728.029	4612.330	20785.90	26839.57	0.00	0.785	2.1	9.761	3.5	0.090	2.8	0.8	557	15	2413	33	4894	30
017	4.50	4.997	3719.273	4980.492	27001.81	34959.02	0.00	0.782	1.8	10.588	3.0	0.098	2.4	0.8	604	14	2488	28	4889	25
018	2.98	6.731	3739.664	4366.310	13652.60	17514.90	0.00	0.790	3.0	8.210	4.1	0.075	2.8	0.7	468	13	2254	38	4904	43
019	2.67	6.366	3813.098	4160.841	13928.85	17993.54	0.00	0.784	2.8	9.325	4.1	0.086	3.1	0.7	533	16	2370	39	4893	39
020	5.19	5.188	3758.086	6810.337	27341.68	35222.37	0.00	0.785	1.7	9.321	2.9	0.086	2.4	0.8	533	12	2370	27	4894	24
SAMPLE TITANITE																				
013	17.74	10.792	3654.547	4251.037	13119.72	18721.21	0.00	0.699	6.5	1.214	8.7	0.013	5.9	0.7	81	5	807	50	4729	93
014	16.45	11.407	3677.250	3851.432	8335.41	12831.83	0.00	0.654	7.0	0.839	7.6	0.009	2.9	0.4	60	2	619	36	4632	101
015	16.49	10.907	3667.927	3834.041	7663.07	11772.20	0.00	0.656	61.6	0.772	61.7	0.009	4.4	0.1	55	2	581	318	4638	889
016	24.75	4.952	3697.912	3752.367	6444.07	11255.33	0.00	0.578	5.6	0.431	6.4	0.005	3.1	0.5	35	1	364	20	4453	82
017	23.77	5.335	3699.273	3675.401	6039.61	10417.12	0.00	0.583	14.5	0.420	14.8	0.005	3.1	0.2	34	1	356	45	4467	211
018	26.23	4.861	3722.698	3686.488	6459.67	11428.29	0.00	0.568	14.4	0.406	15.4	0.005	5.3	0.3	33	2	346	46	4429	211
019	19.13	4.614	3721.698	3674.461	5639.67	9328.08	0.00	0.610	16.7	0.488	17.4	0.006	4.9	0.3	37	2	403	60	4532	243
020	20.78	5.337	3668.861	3771.458	6977.11	11359.56	0.00	0.620	8.2	0.555	9.0	0.006	3.6	0.4	42	1	448	33	4556	119
029	19.58	4.996	3670.101	3642.389	6213.29	10354.72	0.00	0.607	11.0	0.522	12.1	0.006	4.9	0.4	40	2	426	43	4525	160
030	19.85	5.474	3674.356	3656.629	6454.06	10393.61	0.00	0.628	10.6	0.535	11.8	0.006	5.1	0.4	40	2	435	42	4575	153
031	23.04	4.278	3643.486	3761.837	8669.23	13604.38	0.00	0.646	13.0	0.621	15.9	0.007	9.1	0.6	45	4	491	64	4615	188
032	20.47	5.579	3656.406	3741.114	7826.65	12259.47	0.00	0.645	8.9	0.628	10.2	0.007	5.1	0.5	45	2	495	41	4612	128
033	21.34	4.737	3652.448	3957.860	11900.50	16989.35	0.00	0.706	3.9	0.914	6.7	0.009	5.4	0.8	60	3	659	33	4744	56

APPENDIX E – U-Pb Methodology – Sample Data for Zircon

Sample	U pmm (mean)	Pb ppm (mean)	Th ppm (mean)	Th/U	$^{207}Pb/^{235}U$	2σ (abs)	$^{238}U/^{206}Pb$	2σ (abs)	$^{207}Pb/^{206}Pb$	2σ (abs)	ρ	Age $^{207}Pb/^{235}U$	SE	Age $^{206}Pb/^{238}U$	SE	Concordia Age	SE
FN-1	628.332	18.661	1778.945	2.831	0.015	0.003	481.2347	18.244	0.047345	0.00914	0.28001	13.67	1.3	13.38	0.3	13.4	0.2
FN-2	389.090	2.868	425.060	1.092	0.016	0.004	480.181	19.91638	0.056574	0.0142	-0.19908	16.35	2.1	13.41	0.3	13.32	0.3
FN-3	513.384	3.330	498.724	0.971	0.013	0.003	479.1701	31.22443	0.042406	0.01004	0.34131	12.31	1.4	13.44	0.4	13.32	0.4
FN-4	236.249	0.510	91.059	0.385	0.014	0.004	479.3208	25.94319	0.050889	0.01542	0.04677	14.75	2.2	13.44	0.4	13.44	0.4
FN-5	152.752	0.852	74.098	0.485	0.015	0.012	478.8345	33.09753	0.049836	0.041	0.13775	14.46	5.9	13.45	0.5	13.46	0.5
FN-6	248.032	1.447	232.216	0.936	0.005	0.006	478.3759	25.566	0.021166	0.02209	0.14874	6.17	3.2	13.46	0.4	13.29	0.4
FN-7	407.743	2.357	572.494	1.404	0.013	0.003	477.9218	19.66479	0.043152	0.01113	0.53016	12.56	1.5	13.47	0.3	13.39	0.2
FN-8	393.188	7.026	750.647	1.909	0.023	0.005	477.486	28.63612	0.072666	0.01433	0.08402	21.08	2.1	13.49	0.4	13.45	0.4
FN-9	514.305	5.327	616.920	1.200	0.019	0.003	477.0511	19.00803	0.061484	0.01139	0.25106	17.88	1.6	13.5	0.3	13.64	0.3
FN-10	156.072	1.787	242.080	1.551	0.015	0.008	475.9393	32.29138	0.050219	0.02931	0.05348	14.66	4.3	13.53	0.5	13.54	0.5
FN-11	243.592	1.811	340.476	1.398	0.010	0.006	475.704	28.58868	0.037133	0.01899	0.11577	10.87	2.7	13.54	0.4	13.48	0.4
FN-12	88.349	0.500	65.236	0.738	0.022	0.014	474.7024	49.47501	0.059472	0.04573	0.40343	17.38	6.3	13.57	0.7	13.72	0.7
FN-13	672.169	12.867	1517.666	2.258	0.017	0.003	469.476	19.11277	0.058924	0.00922	-0.00342	17.41	1.4	13.72	0.3	13.67	0.3
FN-14	252.299	2.373	348.753	1.382	0.017	0.005	466.3357	29.84956	0.056605	0.01716	0.27458	16.85	2.4	13.81	0.4	13.94	0.4
FN-15	2089.722	12.862	2527.944	1.210	0.012	0.001	465.7148	15.19907	0.04355	0.00456	0.25571	13	0.7	13.83	0.2	13.75	0.2
FN-16	134.909	1.320	124.122	0.920	0.022	0.008	465.3369	25.04096	0.068908	0.02483	0.25336	20.51	3.6	13.84	0.4	13.98	0.4
FN-17	304.634	4.249	497.653	1.634	0.012	0.005	465.0063	27.75872	0.038193	0.01442	0.22538	11.43	2.1	13.85	0.4	13.73	0.4
FN-18	85.346	0.482	72.933	0.855	0.011	0.012	464.1126	45.95781	0.032933	0.0407	-0.09896	9.88	6.1	13.87	0.7	13.9	0.7
FN-19	160.376	1.130	134.370	0.838	0.015	0.009	461.437	34.64561	0.053496	0.03269	0.05408	16.1	4.9	13.96	0.5	13.96	0.5
FN-20	616.033	8.949	1222.745	1.985	0.017	0.003	460.3528	17.60216	0.058096	0.01128	0.19784	17.51	1.7	13.99	0.3	14.08	0.3
FN-21	191.008	1.744	187.093	0.980	0.019	0.009	456.5731	30.495	0.052205	0.0282	-0.33406	15.88	4.5	14.1	0.5	14.04	0.4
FN-22	785.656	8.096	1175.947	1.497	0.013	0.002	452.5488	24.2255	0.04246	0.00678	0.17265	13.05	1	14.23	0.4	14.14	0.4
FN-23	568.091	8.670	1144.481	2.015	0.018	0.003	451.4178	20.59872	0.060032	0.00819	0.29654	18.44	1.2	14.26	0.3	14.52	0.3
FN-24	135.701	0.979	68.615	0.506	0.019	0.009	447.435	35.59161	0.055088	0.02631	0.16572	17.08	4	14.39	0.6	14.45	0.6

ANNEX A – The state of the art of low-temperature thermochronometry in Brazil

Journal of the Geological Survey of Brazil vol 4, nº 3, 239 - 256, December 2021

Journal of the Geological Survey of Brazil

The state of the art of low-temperature thermochronometry in Brazil

Tiago Amâncio Novo[1*], Tobias Maia Rabelo Fonte-Boa[1], Júlia Mattioli Rolim[1], Ana Carolina Fonseca[2]

[1]UFMG - Universidade Federal de Minas Gerais, Programa de Pós-Graduação em Geologia, CPMTC-IGC, Campus Pampulha, Belo Horizonte, MG, Brazil. CEP: 31270-901
[2]Department of Geology, Ghent University, Ghent, Belgium

Abstract

Low-temperature thermochronology focuses on the comprehension of the upper crust's thermal history, where morphotectonic processes take place. We present a robust compilation (1120 data in almost 30 years of research) of fission-track and (U-Th)/He studies and their implications to the understanding of Brazilian geomorphology development. Brazil has a complex geological evolution, involving multiple orogenic and taphrogenic episodes that shaped cratons, orogens, and basins together through time. The thermochronology data set is inconsistently distributed, most of it is concentrated in coastal regions, mainly in the southeastern region; while the intracontinental portions lack studies. The available data set suggests a complex reactivation scenario near the coast to a more stable situation inland. The Mantiqueira and Borborema provinces show a great Early Cretaceous denudation event and a less important Permian to Jurassic, and Paleogene denudation events. The cratonic areas show different patterns, with denudation related to the Devonian to the Jurassic. The data suggest that elastic thickness, structural network, and drainage system play an important role in the morphotectonic control of Brazilian landscape evolution.

Article Information

Publication type: Review Articles
Received 9 June 2021
Accepted 30 November 2021
Online pub. 28 December 2021
Editor: J.M. Lafon

Keywords:
Thermochronology
Thermochronometry
Apatite
Fission-track
(U-Th)/He

**Corresponding author
Tiago Amâncio Novo
tiagoanovo@gmail.com

1 - Introduction

Low-temperature thermochronology is a branch of isotope geology that focuses on the comprehension of the upper crust thermal history, which can be used to reconstruct the timing and rate of heating and cooling at temperatures ~50ºC to ~320ºC (Chew and Spikings 2015; Tagami 2005). It includes a set of thermochronometric systems, being fission track analysis and (U-Th)/He thermochronometry (both in apatite and zircon crystals), the most consolidated and employed methods for investigating the cooling and unearthing processes. Such systems can reveal the temporal and thermal of geological aspects, and give insights into the duration and rates of denudation processes. As fission-track and (U-Th)/He thermochronometry have different closure temperature (Fig.1), the combination of those methods leads to the comprehension and interpretation of the upper crust thermal evolution allowing connections between superficial processes (that acted in erosion and denudation) and tectonic processes (that act in epeirogenic movements).

The thermochronology approach is used to clarify several geological problems such as exhumation rates in orogenic systems, provenance studies of sedimentary basins, understanding of mineral deposits for mineral exploration, maturation of kerogen petroleum for hydrocarbon exploration, and continental margin development. In this paper, we bring the state of the art of low-temperature thermochronology in Brazil, aiming to help future research on the topic. Based on a robust data compilation we show the contributions of fission-track and (U-Th)/He studies to the understanding of the morphotectonic processes that shaped the Brazilian territory. Therefore, we will not propose new interpretations in this work, but bring a compilation of the data and interpretations that already exist. Due to the specificity of the subject, we initiate with a brief introduction to the low-temperature thermochronology methods. Complete reviews can be found in Reiners et al. (2017), Braun et al. (2006), and Reiners and Ehlers (2005). The compiled data is available in Appendix 1 (electronic supplementary material).

1.1. Fission-track thermochronometry

The fission-track thermochronometry is based on the U^{238} fission decay, in which the parent isotope splits into two

ISSN: 2595-1939
https://doi.org/10.29396/jgsb.2021.v4.n3.4
Open access at jgsb.cprm.gov.br

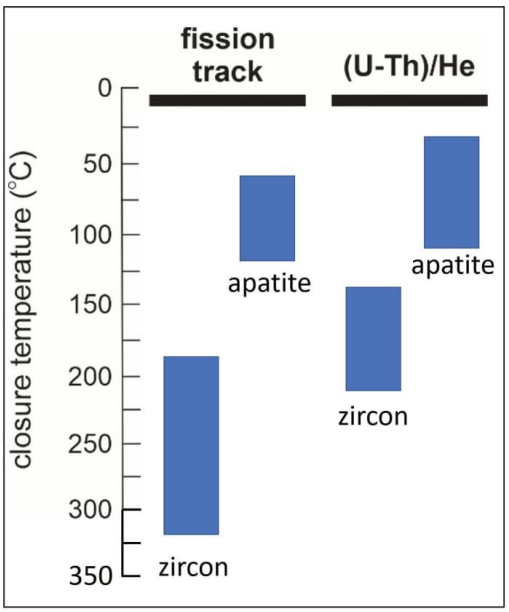

FIGURE 1. Closure temperature for fission-track and (U-Th)/He methods applied in apatite and zircon (modified from Ault et al. 2019).

positively charged high-energy nuclei (Price and Walker 1963, Fleischer et al. 1975). The heavy ionized particles travel at high velocity through the insulating solid (detector) and shape an amorphous damaged channel. These defects in the crystal lattice are the fission tracks, and each one represents a fission-decay event. In uranium-rich mineral grains (e.g., apatite, zircon, titanite), it is possible to determine the density of accumulated track under an optical microscope after polishing and acid etching procedures. For dating, parent isotope concentration is acquired through direct (i.e., laser ablation inductively coupled plasma mass spectrometry - LA-ICP-MS method, Hasebe et al. 2004) or indirect methods (i.e., external detector method, Gleadow and Duddy 1981).

In the fission-track thermochronometry, the heat diffusion can gradually shorten the fission tracks (annealing) until the total disappearance (e.g. Ketcham 2005). Therefore, just below a certain temperature the tracks can accumulate. This temperature highly impacts the closure temperature (CT) (Dodson 1973) which also varies according to the mineral, the cooling rate, and the crystal chemistry (Carlson et al. 1999; Green et al. 1986; Ketcham et al. 2007; Ketcham et al. 1999; Tagami et al. 1998). For example, if the fission-track thermochronometry is applied in apatite (AFT) or zircon (ZFT), the CT will be different. To the AFT, the CT ranges approximately between 120°C to 80°C and in ZFT between ~50°C to ~320°C (Fig. 1). Thus, apatite is a lower temperature thermochronometer than zircon, and its analysis deals with shallower portions in the crust.

Over the years, knowledge about track annealing has become a powerful tool to interpret rock cooling. The track-length analysis added to dating provides a better constraint in the time-temperature path (Gleadow et al. 1986).

1.2. (U-Th)/He thermochronometry

This method is based on the production of an alpha particle (4He) from U^{238}, U^{235}, Th^{232} and Sm^{147} (limited contribution) isotopes decay and the loss of He due to thermal diffusion (e.g., Farley 2000; Strutt 1909; Wolf et al. 1996; Zeitler et al. 1987). In the conventional analysis, the daughter's content is determined by extracting He from samples by laser heating, fusion, and resistance furnace. The measurement is performed by a noble gas quadrupole or magnetic sector mass spectrometer. The parent content (U, Th, and Sm) are mainly measured using LA-ICP-MS in acid dissolved samples.

The understanding of He heat diffusion has been evolving in recent years (e.g., Farley 2000; Flowers et al. 2009; Gautheron et al. 2009; Guenthner et al. 2013; Shuster et al. 2006), and it is not well understood as the annealing in the fission-track thermochronometry. As in the fission-track thermochronometry, the CT in (U-Th)/He thermochronometry is dependent on several factors, including the mineral, grain size, rate of cooling, and radiation damage. In apatite (AHe), it is suggested that CT is approximately between 70°C to 40°C (Farley 2000). In this case, AHe thermochronometry would be the lowest temperature technique and better to constrain changes in the uppermost crust than other approaches. However, a robust published AHe data set shows an excess of dispersion and/or AHe ages older than AFT ages. Thus, the first calculations of CT in the AHe system probably overestimate the diffusion process; as an approximation, the CT is considered to be between 120°C to 30°C (Ault et al. 2019; Fig. 1). The diffusion processes in (U-Th)/He thermochronometry in zircon (ZHe) is even less understood. In general, zircon appears to be more retentive than apatite to He (Reiners et al. 2002; 2004) and then its CT can range from 220°C to 140°C (Guenthner et al. 2013, Fig.1). Despite uncertainties, the carefully applied AHe and ZHe method, combined with other thermochronological techniques, form an ideal device to reconstruct time-temperature (t-T) paths through inverse modeling in the shallow crust (Ketcham et al. 2007; Gallagher 2012).

2 - Brazil thermochronology data set

Brazil is a country with continental proportions and complex geological evolution, involving multiple orogenic and taphrogenic episodes that shaped cratons, orogens, and basins together through time. The data set is distributed in a heterogeneous way, mainly spread in coastal regions, while the inland portions lack studies. We choose to exhibit the dataset divided according to geotectonic domains (Figure 2). That is because the tectonic evolution of a given area directly reflects its properties, such as flexural strength (response to tectonic stress) and structural framework, thus characterizing large areas with reasonably similar thermochronological patterns, i.e., the Archean to Proterozoic São Francisco and Amazonian craton, the Proterozoic Mantiqueira, Tocantins and Borborema provinces, and the Phanerozoic Syneclises, Marginal Basins, and alkaline intrusions.

2.1. São Francisco craton

The São Francisco craton (SFC) is located in central-eastern Brazil, limited by orogenic systems, being Borborema at northbound, Tocantins at westbound, and Mantiqueira in the

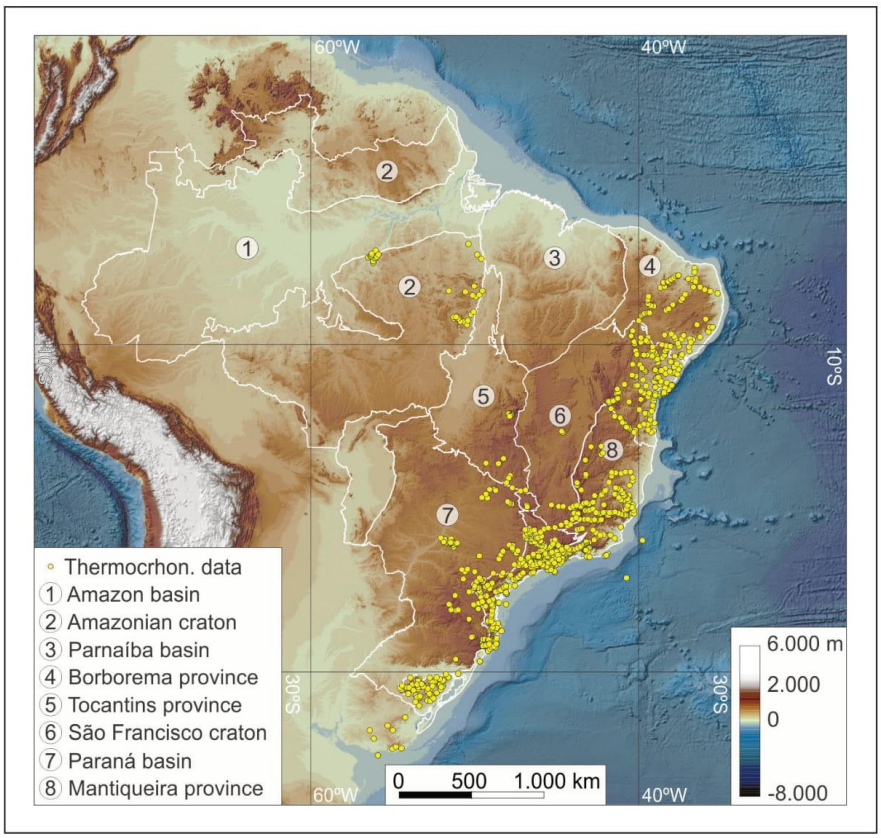

FIGURE 2. Thermochronological data set available for Brazil. The white lines divide the different geotectonic domains (1 to 8).

eastern portion (Fig. 2 and 3). It represents the paleocontinent São Francisco-Congo formed during Rhyacian times through the amalgamation of Archean and Paleoproterozoic blocks. The SFC stayed together with the Congo craton (its African counterpart) from the Paleoproterozoic to the late Cretaceous, when it broke apart to form the South Atlantic Ocean (Porada 1989). As a cratonic entity, the SFC has a cold, stronger, and relatively less dense lithosphere, as well as deeper and cold lithospheric roots (Jordan 1978; Assumpção et al. 2017; Alkmim 2004). The SFC basement is formed mainly by TTG and greenstone terrains (Heilbron et al. 2017; Alkmim 2004), partially covered by intracratonic and passive-margin sedimentation (Martins-Neto et al. 2001; Reis et al. 2017). The Meso-Cenozoic marginal basins developed in the cratonic extended area were controlled by the rift-resistant crystalline basement (Mohriak et al. 2008). That prompted the formation of a relatively narrow platform with sparse magmatism and the inland Recôncavo-Tucano-Jatobá Basin.

Thermochronological data in SFC are intensely concentrated in its northeastern portion which corresponds to a segment of the Brazilian passive margin (Amaral et al. 1997; Harman et al. 1998; Japsen et al. 2012; Jelinek et al. 2014; Jelinek et al. 2020; Turner et al. 2008; Fig. 3). Amaral et al. (1997) reported a few pioneering data showing Permo-Triassic AFT ages. Near the border with Borborema province, Harman et al. (1998) and later Turner et al. (2008) introduce a more robust set of analyzed samples. The data adjacent to the passive margin shows younger AFT ages (Upper Cretaceous) with long mean track lengths (MTL). In contrast, the samples from the countryside exhibit older (Lower Cretaceous to Permian) ages with decreasing MTL. The results indicate two phases of denudational cooling. According to Harman et al. (1998), the first cooling event (c.a. 130 to 95 Ma) was related to the generation of local relief and change in the base level due to the rifting process, which is mainly recorded by coastal samples. Turner et al. (2008) also highlight the possible influence of the relaxing geothermal gradient in this phase. The second cooling event (c.a. 70 to 55 Ma) is interpreted as a denudation response to a post-rift tectonic reactivation. The inversion of intracontinental rift basins close to the area (Harman et al. 1998) is pointed as geological evidence to the inferred event. This phase seems to be widespread, affecting the craton interior. In the central African shear zone system, a late Cretaceous tectonic event is synchronous with the discussed uplift, which suggests major changes in the relative plate motions as the driving force.

Japsen et al. (2012) and Jelinek et al. (2014; 2020) explore the craton coastal margin spanning their sampling to the borders with the Mantiqueira and Borborema provinces, the central portion, and also the interior of the craton (~ 500 km to the continental hinterland). The large AFT data set published by these authors is consistent with the previous works. Japsen et al. (2012) infer a complex thermal history with four post-rift stages, evolving cycles of burial, and erosion phases. Like the previous works (Harman et al. 1998; Turner et al. 2008), the widespread effects of plate motion (mainly due to lateral resistance; Japsen et al. 2012) are evoked as post-rift uplifts cause. On the other hand, Jelinek et al. (2014) cast doubt on the intervening periods of widespread sedimentation proposed by Japsen et al. (2012). Even though periods of reheating can be a solution for the inversion model based on their thermochronological data, it is not unique. Jelinek et al. (2014) points to the lack of evidence in the existence of the sedimentary cover and advocate the erosion of the crystalline basement rather than sedimentary rocks. The several uplifts episodes are also challenged as the exhumation origin and the effects of isostasy aided by magmatic underplating are taken as an alternative hypothesis (Jelinek et al. 2014; 2020). The pre-rift history of SFC was not the scope of these papers, despite a late Paleozoic to Early Mesozoic cooling phase is reported (Japsen et al. 2012; Turner et al. 2008; Jelinek et al., 2014). The inverse models inferred from these samples indicate a limited effect of the thermal and tectonic processes related to the rifting processes. Jelinek et al. (2014) correlate this cooling phase to the final stages of the Gondwanides orogeny, which settled in the south in the paleocontinent during that time. Jelinek et al. (2020) show data focused on the Recôncavo-Tucano-Jatobá Rift and detail cooling stages in the Permian-Triassic, Cretaceous and Cenozoic. The authors point out that the regional warming that began in the Cretaceous resulted in the uplift and erosion of the current continental margin.

Fonseca et al. (2021) present AFT dating results from the continental interior segment of SFC, mainly in its southern portion far from the Atlantic Ocean. The authors discuss two cooling phases revealed by the data: (i) firstly during the Paleozoic, and (ii) then between Late Cretaceous to Paleocene. The Paleozoic cooling phase seems to have affected several West Gondwana basement areas besides the SFC (e.g. Brasília Orogen, Fonseca et al. 2020), thus the authors argue for a far-field mechanism responsible for inducing widespread erosion during this time. The Gondwana geodynamic cycles are probably connected with high Paleozoic subsidence rates of adjacent depocenters (e.g. Paraná basin) and other intracontinental sags basins in the West Gondwana interior. These geodynamic cycles probably triggered basement tectonic readjustments leading to the erosion and cooling events of the paleohighs, such as SFC. This hypothesis is also suggested by Jelinek et al. (2014) for the late Paleozoic to Early Mesozoic cooling phase in the marginal portion of SFC. The second cooling phase is revealed between the Late Cretaceous to Paleocene and it affected the narrow weak zones (e.g. Recôncavo-Tucano-Jatobá rift) and at the cratonic borders. The proposed driving mechanism for the post-rift erosional event is reactivations prompted by far-field stress transmitted from the plate boundaries.

2.2. Amazonian craton

This province is located in the northwest Brazilian territory extent and is limited by Parnaíba Basin and Tocantins provinces at its eastern border (Fig. 2). It contains the Amazonas basin which separates this cratonic area into two provinces, the Rio Branco province in the northern extent and the Rio Tapajós province in the south. Although it covers almost half of the Brazilian territory, the Amazonian craton is the less geologically-known area (Hasui 2012). It comprises multiple terrains elongated according to NW direction with a complex Archean-Proterozoic tectonic history (Santos et al. 2000; Tassinari and Macambira 1999). During Neoproterozoic Era, the region of the Amazonian province participated in the Brasiliano/Pan African orogenic cycle with other paleocontinents, such as São Francisco-Congo and Paranapanema, was amalgamated to compose the West Gondwana paleocontinent. The Phanerozoic history of the Amazonian craton and nearby regions is well registered by the sedimentary record of the Phanerozoic intracontinental basins.

Despite the small amount of thermochronological data, locally scattered in the southeastern portion of the craton (Figs. 2 and 4), they corroborate with the sedimentary evidence. The Amazonian craton passed through a substantial amount of denudation assigned by the main pulses of exhumation and cooling. ATF in Paleoproterozoic crystalline rocks showed three cooling stages (Pina 2010): i) a mid to late-Paleozoic cooling episode (between 392 and 270 Ma); ii) followed by Triassic heating event (between 260 and 180 Ma); iii) and then another cooling process in the Cretaceous (100 Ma). Furthermore, in the eastern border of the Amazonian craton, Harman et al. (1998) identified ages from Upper Carboniferous (309 Ma) to Lower Cretaceous (137 Ma). Both works relate the Paleozoic ages to a substantial amount of denudation in the craton interiors, apparently, uncorrelated with the tectonic process. The Cretaceous ages are consonant with the convergent movement of the Andean subduction zone and the opening of the eastern equatorial Atlantic. The models point to a young denudational cooling in the Late Cretaceous interpreted as a result of differences in the relative plate motions between South American and African plates implying reactivation of the Proterozoic shear zones resulting in intracontinental deformation over the cratonic area by this time.

2.3. Mantiqueira province

The Mantiqueira province configures a strip along the Brazilian coastal region between southern Bahia and Rio Grande do Sul states, with an extension to Uruguay. It is about 3,000 km long, 200 km wide in the south, and 600 km in the north (Figs. 2 and 5). To the west, it borders the São Francisco craton, the southern end of the Brasília belt (Tocantins province) and the coverage of the Paraná basin (Almeida et al. 1981). To the east, it borders the Atlantic coast. The Mantiqueira province is a Neoproterozoic orogenic system developed during Western Gondwana amalgamation. The orogeny starts with the consumption of the Adamastor ocean when subduction processes generate arc-related rocks. Diachronic collisional episodes put together terrains formed by basement rocks (older than 1.7 Ga), arc-related rocks, and sedimentary successions. During the Cambrian to Ordovician, a regional orogenic collapse occurs (Trouw et

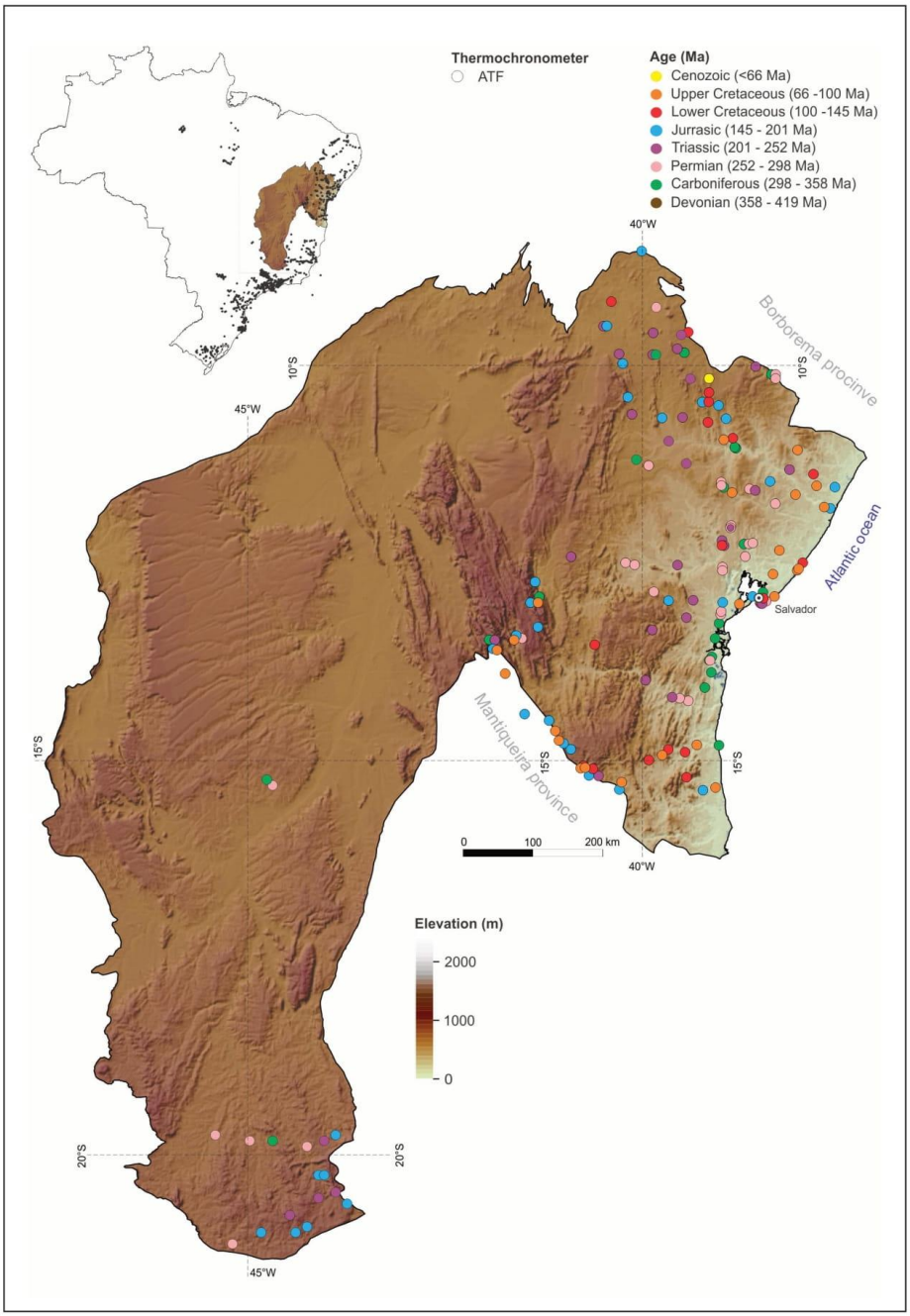

FIGURE 3. Thermochronological data set published in the São Francisco craton. The detailed map highlights the northeast portion of the craton where thermochronological data are concentrated.

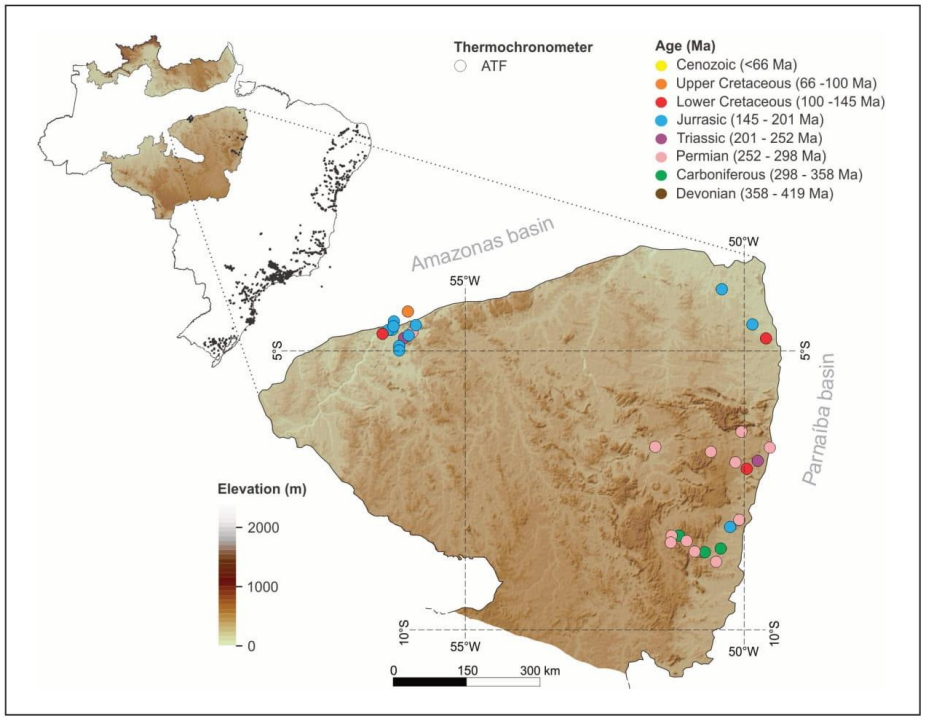

FIGURE 4. Thermochronological data set published in the Amazonian craton.

al. 2000; Pedrosa-Soares and Wiedemann 2000; Pimentel et al. 2000). In the late Cretaceous, the Atlantic opening marks the Gondwana break-up; apparently, this is the last regional tectonic event that affects Mantiqueira province.

Thermochronological studies in the Mantiqueira province started in the early '90s, with the pioneering work of Ariadne Fonseca (Fonseca 1994), nowadays it is the best-studied area in Brazilian territory, highlighting the Serra do Mar range region, that concentrates the most fission-track and (U-Th)/He data set (Fig. 5). During the '90s, few studies were made in Brazil, but they already bring great contributions to thermochronology. Gallagher et al. (1994) and Gallagher et al. (1995) already made aware that a lato sensu passive margin rift does not explain the present-day topography, suggesting control by basement structures. In the late '90s Jelinek et al. (1999) applied for the first time AFT in mineral prospecting. The authors dated hydrothermal fluids in fluorite ore veins in the southernmost portion of Mantiqueira province.

In the '2000s and '2010s, many thermochronological studies were made in the Mantiqueira province, mainly in the Serra do Mar and Mantiqueira mountain ranges aiming to quantify its thermal histories and timing of epeirogenic and tectonic processes (e.g. Oliveira et al. 2000; Tello Saenz et al. 2003; Borba et al. 2003; Tello Saenz et al. 2005; Hackspacher et al. 2004; Cogné et al. 2012; Karl et al. 2013; Hueck et al. 2018; Van Ranst et al. 2019; Fonseca et al. 2021). The studies describe a long stabilization from Cambrian to Mesozoic times. Locally it described a Carboniferous cooling event (Oliveira et al. 2016b; Krob et al. 2019) recorded mainly by zircon fission-track and associated with the final stages of the Gondwanides orogeny. From Permian to Jurassic a major cooling phase is registered in the Southern portion of the Mantiqueira province, probably related to pre-rift lithosphere thinning (Machado et al. 2019). An early Cretaceous uplift is widely registered associated with the south Atlantic opening. Paleogene denudation is also described, related to reactivation in the coastline and plate adjustment. Due to the variability of the structural network, drainage system, and lithosphere elastic thickness across the Mantiqueira province, spatial variations of the denudation rate are expected.

The Serra do Mar mountain range recorded a Late Cretaceous uplift, probably linked to its genesis, but Tello Saenz et al. (2005) and Hackspacher et al. (2004) highlight that Serra do Mar thermal history probably is much more complex. Oliveira et al. (2000) already alert that the Serra do Mar region went through several vertical and horizontal movements from the Cretaceous to nowadays. Hiruma et al. (2010) made one of the greatest contributions to thermochronology in the Brazilian scenario during the 2010s. Studying the highest part of the Serra do Mar, they model the exhumation of the Bocaina plateau. Agreeing with other authors (e.g. Genaro 2008; Hiruma et al. 2010) Cogné et al. (2011) point out that the late Cretaceous uplift could be related to the alkaline magmatism. There is an agreement that denudation and uplift rates have been intensified during the Cretaceous, and the alkaline

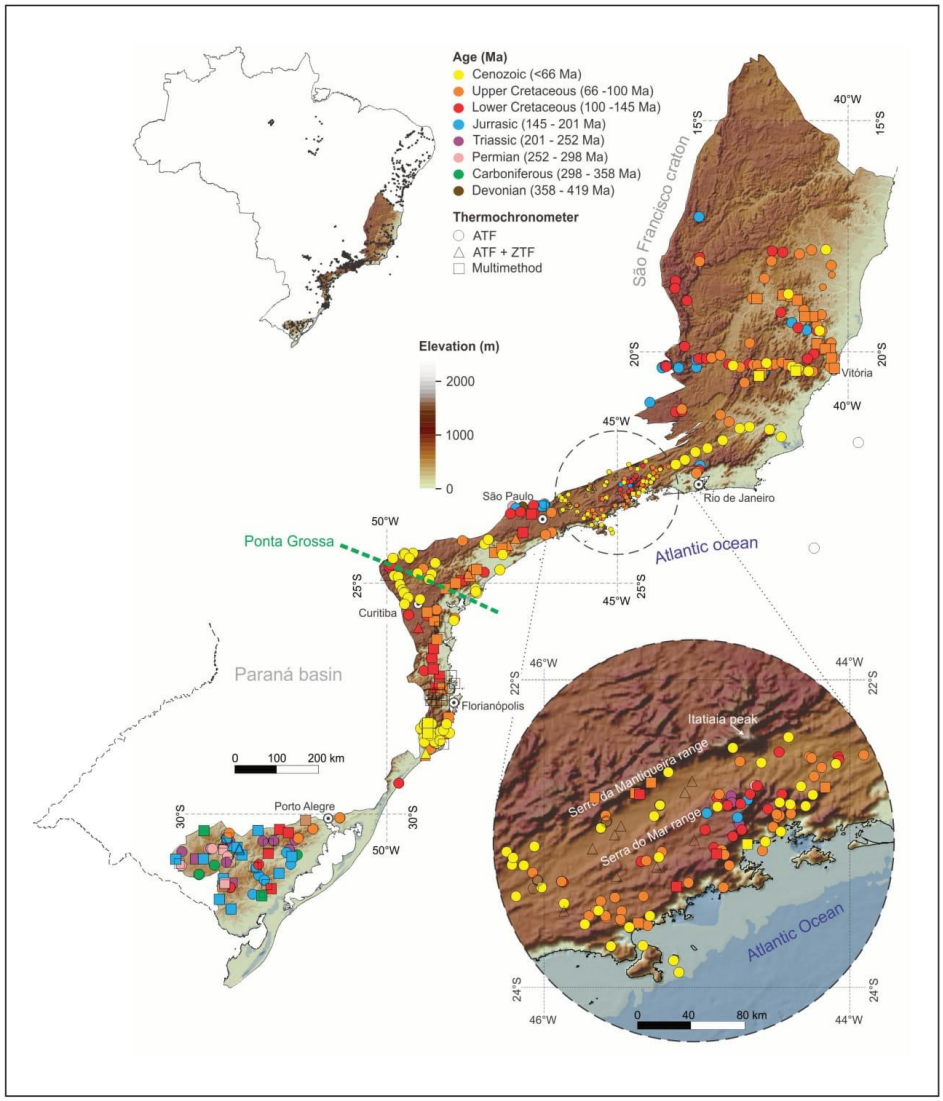

FIGURE 5. Thermochronological data set available for the Mantiqueira province, the circle below is a zoom highlighting the Serra do Mar range region.

magmatism could generate thermal weakening of the lower crust improving those rates.

Hueck et al. (2018; 2019) and Gomes and Almeida (2019) draw attention that besides the thermal weakening, LIPs could overprint thermochronology systems; e.g. Z(He) overprinting due to the Serra Geral magmatism in southern Mantiqueira Province, or the alkaline magmatism associated with the post-rift stage.

Godoy et al. (2006) studied the Pitanga dome, emphasizing the importance of reactivation of basement structures in the Meso-Cenozoic tectonics. Ribeiro et al. (2005a), Ribeiro et al. (2005b), and Ribeiro et al. (2011) also pointed out the importance of the recognition of brittle deformation (pseudotachylytes, cataclasites, and fault gouges) to correlate with the AFT and (U-Th)/He data. Besides the above mention events, Ribeiro et al. (2005b) and Hiruma et al. (2010) recognize a late Triassic uplift, suggesting that Serra do Mar mountain range was a long-lived source of sediments for the Paraná, Bauru, and Santos basins. Oliveira et al. (2016a) studying boreholes of the Santos basin basement, suggest that Serra do Mar mountain range denudation is related to late Cretaceous uplift.

In the last decade, several studies using multi-method thermochronology were made aiming to model the pre-, syn- and post-rift exhumation events in the Mantiqueira province (Cogné et al. 2011; Cogné et al. 2012; Karl et al. 2013; Franco-Magalhães 2014; Oliveira et al. 2016b; Hueck et al. 2017; 2018; 2019; Krob et al. 2019; Van Ranst et al. 2019; Machado et al. 2019, 2021; Gomes and Almeida 2019; Curvo et al. 2013; Souza et al. 2020; Gezatt et al. 2021; Fonseca et al. 2021). Karl et al. (2013) bring for the first time zircon and apatite fission-track and (U– Th–Sm)/He data in a regional view across the Mantiqueira province. The exhumation history varies in the Mantiqueira province due to the variability in the elastic thickness, structural network, and drainage system; being the Serra do Mar and Serra Geral regions the places with the most intense reworking from the Cretaceous to the Paleogene. Souza et al. (2020) performed thermal modeling based on ^{10}Be-derived erosion rates and topographic and climatic parameters. The authors highlight that modern erosion is focused on the escarpments and the incised rivers, pointing out that reactivations of the inherited Precambrian shear zone and transfer zone are the biggest controllers of the relief. According to Karl et al. (2013), three events can be registered in the whole Mantiqueira province: the Paraná– Etendekka event; the alkaline intrusions event; and the evolution of the continental rift basins.

Japsen et al. (2012) suggest a different approach for denudation history on the Brazilian northeast coast. As mentioned in the “São Francisco craton” section, the authors suggest a series of burial and uplift stages taking into account the variability of base level and the lateral resistance to plate motion. Alternatively, other authors assign the exhumation events to far-field stress (related to Gondwanides orogeny), a rift to post-rift tectonism, climate, and underplating (Jelinek et al. 2014; Bicca et al. 2013). According to Jelinek et al. (2014), the idea of burial and uplift cannot be sustained with the thermochronological data set; besides, the material accommodation and surface preservation are hard to explain by a simple burial and uplift model.

Cogné et al. (2011; 2012) using apatite and Franco-Magalhães et al. (2014) and Curvo et al. (2013) using zircon and apatite, present an inverse thermal history modeling based on FT and (U-Th)/He data, providing more detail on the rift to post-rift cooling history. The (U–Th)/He data suggests a Neogene compression event in the South American plate, between the Andean subduction zone (Peruvian phase) and the mid-Atlantic ridge, reactivating Precambrian shear zones. The authors highlight that this reactivation was concentrated in specific places where the reheating seems to be robust (e.g. Taubaté Basin).

The countryside portion of Mantiqueira province lacks studies. Hackspacher et al. (2004) argue that three main stages of denudation control the region, one during the Jurassic, another in Early Cretaceous, and the last one from the Late Cretaceous to the Miocene, involving several reactivations of brittle basement structures. Amaral-Santos et al. (2019) show evidence of a cooling episode starting in the late Devonian to early Permian in the boundary between São Francisco craton and Mantiqueira province. Van Ranst et al. (2019) and Fonseca et al. (2021) bring a great contribution to countryside studies, the authors describe a major phase of uplift and accelerated denudation during the late Cretaceous to early Paleogene. The authors agree that sensu strictu rifting process could not be the only one responsible for the configuration of the relief on the coast. Van Ranst et al. (2019) highlight that the basement structural framework of the northern Mantiqueira province controlled the differential denudation rates, and it directly affects its drainage network. Also, this framework shows a major influence on the small-scale denudation, which has led to the formation of the inselberg landscape, and the persisted role of the Mantiqueira range as a watershed.

It is a fact that the landscape evolution of the Brazilian continental margin cannot be explained by the predicted simple models of continental-margin development. Besides tectonics, the climate directly affects the denudation history of the Mantiqueira province, from the glaciation during a long-term stabilization in Paleozoic times to its breakdown in Early Mesozoic creating variable denudation due to block rearrangement. In the Late Cretaceous, the uplift of the Serra do Mar and Mantiqueira mountain ranges generated a climate barrier in the Brazilian southeast coastline, causing progressive denudation towards the continent related to scarp retraction.

2.4. Tocantins province

Tocantins province (Almeida et al. 1981) is located between the Amazonian and São Francisco cratons and is bounded to the north and south by Parnaíba and Paraná basins, respectively (Fig. 2). It comprises the remnants of a Neoproterozoic orogenic system, generated due to a convergence between Amazonian, São Francisco, and Paranapanema paleocontinents during the Brasiliano/ Pan African cycle (Pimentel et al. 2004). The continental collision was preceded by the consumption of a large ocean crust between ca. 900 and 600 Ma and attachment of minor continental fragments and magmatic arcs. Three large fold belts compose the province: the Brasília belt, situated on the western margin along with the São Francisco craton; and the Araguaia and Paraguay belts, established on the eastern and southeastern margin of the Amazonian craton. The end of the orogeny and then the transition through a relatively stable area inside the West Gondwana was followed by the development of large Paleozoic syneclises (Brito Neves 2002; Milani and Thomas 2000). Widespread post-Paleozoic alkaline magmatism intruded the province’s basement mainly in areas surrounding the Paraná basin. The Brasília belt hosted several alkaline magmatic pulses in the late Cretaceous (Riccomini et al. 2005); more information about the alkaline intrusions in the topic “Alkaline provinces”. Evidence of the Phanerozoic sedimentation is limited to sedimentary beds in Água Bonita graben and Cretaceous and Cenozoic continental covers, standing out the Pantanal (with thickness up to 500 m) and Araguaia plain (Almeida et al. 1981).

Thermochronological studies in the Tocantins province are strongly concentrated in the southern portion of Brasília belt (Cogné et al. 2011; Doranti et al. 2008; Doranti-Tiritan et al. 2014; Gallagher et al. 1994; Hackspacher et al. 2004; 2007; Oliveira 2000; Ribeiro et al. 2005a; 2005b; Tello Saenz et al. 2003; 2005; Fonseca et al. 2020; Fig. 6). Only one study, applying ZFT analysis, was made in the Araguaia belt (Dias et al. 2017; Fig. 6). In this work, based on four bedrock samples, three distinct ZTF age populations are recorded. The older one (498 ± 8 to 489 ± 15 Ma) was interpreted as the orogenic collapse. The intermediate population (345 ± 13 to 331 ± 8 Ma) was related to a reactivation event due to the Gondwanides

orogeny and then erosion of Parnaíba sedimentary deposits that could cover the area. Finally, the younger age population (208 ± 10 to 197 ± 3 Ma) was associated with a possible reheating linked with the Lower Jurassic Mosquito magmatism.

In the Brasilia belt region, the Poços de Caldas plateau is an elevated region that was cut by Cretaceous alkaline intrusions and investigated by thermochronometers. Doranti-Tiritan et al. (2014) using new and previous (Doranti et al. 2008; Cogné et al. 2011; Gallagher et al. 1994) AFT data verified that the thermal effect of the magmatism emplacement was not strong enough to affect the close basement portions and leave any impression on AFT data. Thus, the pre-Cambrian rocks could keep registered its ancient thermal history. The authors associated the oldest cooling phase with the glacial erosional process during the Carboniferous. Afterward, several collisions in the south of Gondwana during the Triassic may have generated widespread uplift, decreasing the cooling rate. The erosion of this raised terrain may have resulted in the Gondwana pediplanation surface (King 1956) generating another cooling cycle. Fonseca et al. (2020) reveal a Devonian to Permian cooling period and correlate it to the final exhumation of the Brasília Belt, associated with the orogenic collapse and sediment influx to Paraná basin.

In a transect starting from Poços de Caldas plateau towards the border with Mantiqueira province, Gallagher et al. (1994) analyzed basement rocks through the AFT method. Years later, Cogné et al. (2011) reanalyzed the same samples through the (U-Th)/He approach. Using both methods was possible to greatly improve the data set and understand in more detail the post-rift cooling history. Only a few samples record an early cooling episode related to the South Atlantic opening (~120 Ma). Most of the results implied two main phases of cooling. The first one during the late Cretaceous with higher rates and regional extent, and subsequently the second one during Cenozoic with lower rates and concentrated along pre-existing shear zones. Together, the cooling events imply exhumation from depths between 2 and 5 km. Cogné et al. (2011) attribute the post-rift cooling history to the compression of the South America plate between the Andean subduction zone and the mid-Atlantic ridge.

In the convergence zone between Tocantins and Mantiqueira provinces, which encompasses the Ituverava shear zone, several analyses investigated the Jundiaí plain and High Mantiqueira mountain range domains (Hackspacher et al. 2004; 2007; Oliveira 2000; Ribeiro et al. 2005b; Tello Saenz et al. 2003). According to Ribeiro et al. (2005b), the Jundiaí plain AFT data are related to the Late Triassic formation of the Gondwana surface (King 1956) and can also be associated with the Paraná basin subsidence. On the other hand, the High Mantiqueira mountain range domain records the Early Cretaceous cooling, which was linked to the Mantiqueira mountain range uplift due to the opening of the South Atlantic Ocean (Hackspacher et al. 2004; 2007; Oliveira 2000; Tello Saenz et al. 2003; 2005). During Late Cretaceous until Oligocene some samples from the region record a heating period that Hackspacher et al. (2007) associate with a thermal anomaly resulted from the mantle plume passage and crustal thinning. The ensuing cooling period was related by the same author with the Japi/Sul-American pediplanation surface (King 1956; Almeida 1964). Ribeiro et al. (2005a), also studying in the southern portion of the Brasília belt, found ATF ages ranging from Ordovician, right next to Paraná basin, to Cenozoic, next to the High Mantiqueira mountain range. The authors suggest that the differential cooling stories are probably connected to basement reactivation during the tectonic subsidence periods of the Paraná Basin.

Martins-Ferreira et al. (2020) show the first fission-track data in zircon and apatite detrital grains in the northern Brasilia belt. ZFT age range from Neoproterozoic to Triassic. The authors suggest that the older ages are related to the West Gondwana assembly exhumation, while the younger ages are linked to the Gondwanide orogeny. The apatite data are Cretaceous to Paleogene age; the authors related it to Pangea breakup.

2.5. Borborema province

The Borborema province in northeast Brazil is limited to the west by the Parnaiba basin and the south by the São Francisco craton. It comprises a long system of strike-slip shear zones, that juxtaposed Archean/Proterozoic blocks and Neoproterozoic metasedimentary rocks during the Brasiliano/Pan African orogenic cycle (Dantas et al. 1998; Neves et al. 2000). These structures represent the main crustal discontinuities which played an important role during the Gondwana fragmentation and later Phanerozoic tectonic events. From Cretaceous times onwards, the Borborema province underwent significant uplift. The main topographic expression is the Borborema plateau which elevates a sequence of continental sediments up to 1200 m above sea level. It has been an intriguing point of discussion in the past four decades. Another point of discussion that needs more analytical data to evaluate is the onshore and offshore evolution of the hydrocarbons deposits.

Morais Neto et al. (2009) made the greatest contribution to thermochronology in the Borborema Province (Fig. 7). Based on AFT and ZFT the authors pointed to two main Phanerozoic denudational/cooling events. One between 100 and 90 Ma, related to post extension lithospheric processes. And further, a 20-0 Ma event probably due to climate change rather than a tectonic source. According to the authors, the late Cretaceous event seemed to be a generalized uplift instead of the denudation slope retreat classic style observed on the Brazilian southeast continental margin.

2.6. Phanerozoic syneclises and Marginal basins

The Phanerozoic syneclises developed during Gondwana stabilization to its break up, passing from a stable to an activated platform in syn to post-rift stages, when the marginal basins formed. It lacks thermochronology studies, being the Paraná basin the only studied Phanerozoic syneclise, and the Campos and Santos basins the marginal basins with thermochronology data. The Campos and Santos basins host large, world-class oil reservoirs. The data set related to the basement of the basins is described in the “São Francisco craton”, “Mantiqueira Province” and “Borborema Province” sections.

2.6.1. Paraná basin - Bauru basin

Bauru basin is the top succession of the Parana basin, located in south-central Brazil (Fig. 8). It is formed by thermal subsidence after an Early Cretaceous volcanic event, and it is mainly composed of sandstones, mudstones, and

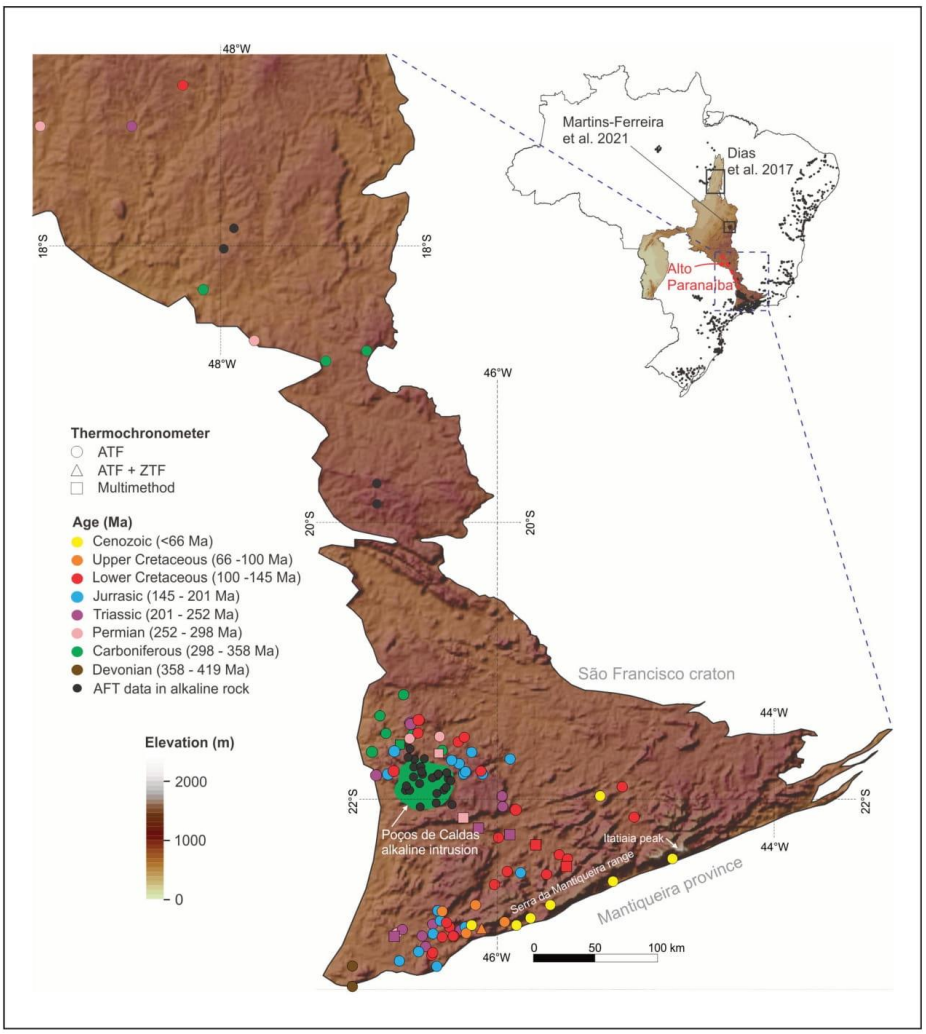

FIGURE 6. Thermochronological data set published in the Tocantins province. In the Brazil map, the study of Dias et al. 2017 is highlighted. In the bottom, the southern portion of the Brasília belt where thermochronological data are concentrated. Poços de Caldas alkaline intrusion is drawn in green and the analyses from its rocks in black; The data of the Poços de Caldas alkaline intrusion is shown in the "Alkaline provinces" section.

conglomerates (Batezelli and Ladeira 2016). Dias et al. (2011) analyzed detrital zircons from Vale do Rio do Peixe Formation, in the Bauru Basin, and obtained ZFT ages varying from 239 Ma to 825 Ma, reflecting the main denudation processes of the South American Plate from Neoproterozoic to Early Triassic, like those related to orogenic cycles of early Brasiliano, Famatinian/Cuyanian and Gondwanides. Dias et al. (2018; 2021a) analyzed detrital zircons from the Bauru basin and the fission-track data record ages from the Neoproterozoic to Late Cretaceous, which were interpreted as uplift and exhumation due to tectonic events along the western margin of the South American platform; like the denudation of Brazilian and Gondwanides and the Serra Geral magmatism.

2.6.2. Campos and Santos basins

In the Campo basin, Oliveira et al. (2018) analyzed the thermotectonic history of the Maastrichtian oil reservoir and obtained a minimum AFT age of 45.9 ± 5.5 Ma. Two phases of heating were distinguished, one after the deposition of Carapebus Formation until 65 Ma, and one during the late Eocene, reflecting subsidence. The phases are separated by a cooling event (65-37 Ma), which is correlated to subaerial

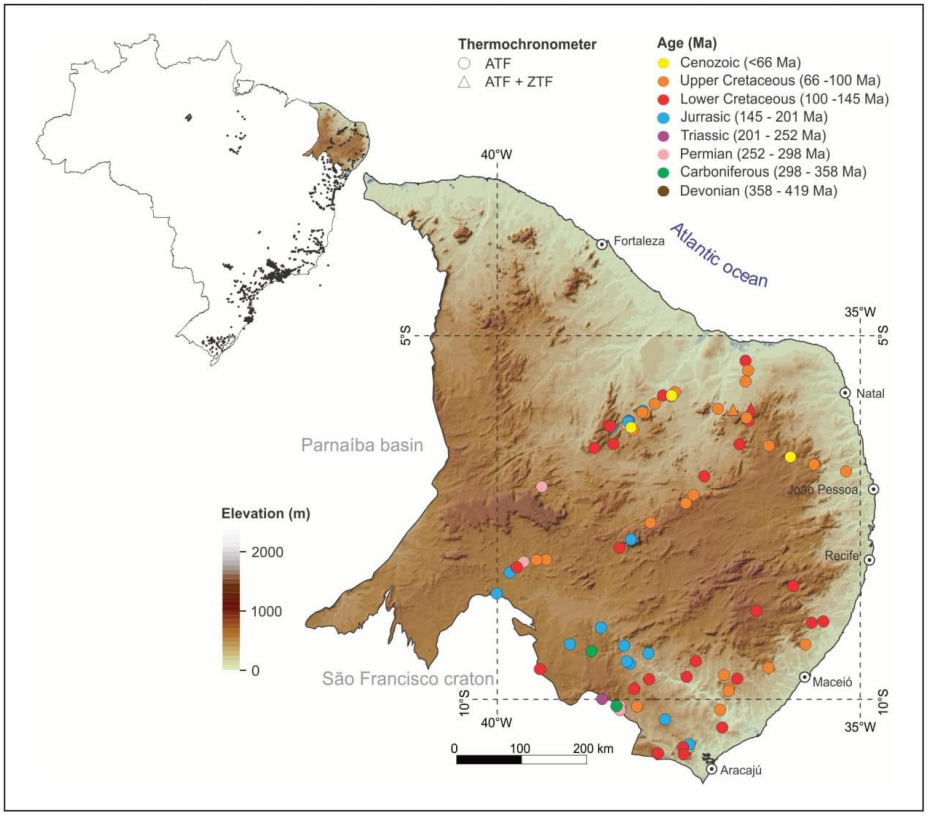

FIGURE 7. Thermochronological data set published in the Borborema province.

unconformity and thermal uplift coeval with volcanic pulses of Trindade plume.

Oliveira et al. (2016b) analyzed apatite fission-track from borehole samples from the Santos basin. The central ages obtained for the basement range from 21.0 ± 1.8 to 157.0 ± 35.0 Ma, and the central ages for borehole samples vary from 6.5 ± 1.1 to 208.0 ± 11.0 Ma. From thermal modeling, an early thermotectonic event is recorded during the late Cretaceous related to uplift and denudation of the Serra do Mar and Serra da Mantiqueira, and also indicates that the oil generation started at 55–25 Ma and continued until the Pliocene-Pleistocene. Besides that, during the Neogene, fast cooling is linked to the reactivation along Precambrian shear zones, which also changed the drainage system of Paraíba do Sul.

2.6.3. Barreiras Formation

Dias et al. (2021b) show ZFT ages from the Barreiras Formation; a Neogene deposit in the Brazilian continental margin. The data range from the Silurian to Late Cretaceous. The authors recognize four groups (429 to 358 Ma, 351 to 274 Ma, 270 to 171 Ma, and 167 to 127 Ma) that reflect the Gondwana and Pangea agglutination and break-up.

2.7. Alkaline provinces

Almeida (1983) defined alkaline provinces as chrono-correlated clusters of alkaline bodies with similar petrographic and geotectonic features. This section brings the main contributions of thermochronology studies in alkaline provinces (Ponta Grossa Arch, Alto Paranaíba, and Poços de Caldas) and Trindade island, in the Brazilian territory (Fig. 8). The data set related to the host rocks of the alkaline intrusions is described in the “Tocantins province” and “Mantiqueira province” sections.

2.7.1. Ponta Grossa arc province

Ponta Grossa arc alkaline province is located at the eastern border of Paraná basin, in southeastern Brazil. Jacupiranga is one of its alkaline bodies, composed of mafic and ultramafic rocks associated with carbonatite (Almeida 1983; Riccomini et al. 2005). The crystallization age of the Jacupiranga alkaline body ranges from ca. 130 to 133 Ma (Renne et al. 1993; Sonoki and Garda 1988; Roden et al. 1985; Amaral 1978; Amaral et al. 1967). Amaral et al. (1997) obtained similar ages with AFT, confirming an early Cretaceous heating period from 130 to 70 Ma, followed by continuous cooling since 70 Ma. The heating

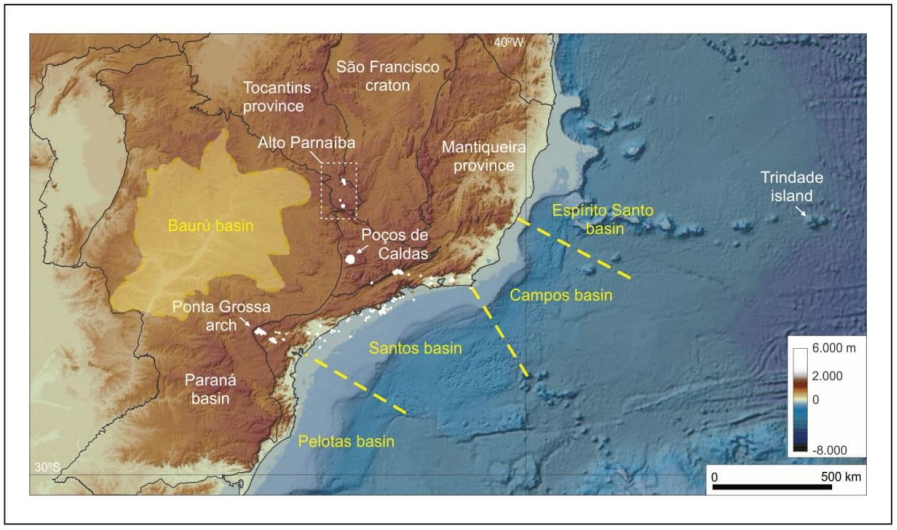

FIGURE 8. Phanerozoic syneclises, marginal basins, and Alkaline provinces (indicated in white).

event suggests the influence of Upper Cretaceous alkaline intrusions or due to the increase of heat flow during crustal thinning during the Santos basin rift event.

Soares et al. (2016) obtained AFT ages from Ipanema (69.1 ± 6.5 Ma), Barra do Itapirapuã (98.2 ± 12.7 Ma) and Jacupiranga (94.9 ± 8.0 Ma) bodies, with modeling indicating a Late Cretaceous fast cooling event. The difference between the crystallization age (ca. 130 Ma) and the AFT age is attributed to the compressive Andean collision, which caused rising and erosion on the boundary of the Paraná basin (Lima 2000), increasing the temperature and resetting the fission-track ages in Jacupiranga, and inducing a slower cooling in Barra do Itapirapuã and Ipanema bodies. Tunas, a felsic alkaline body from the Early Cretaceous (110 Ma K/Ar age), yields an AFT age of 16.95 ± 1.05 Ma. (Gomes et al. 1987; Sonoki and Garda 1988; Ulbrich and Gomes 1981; Franco-Magalhães et al. 2010).

2.7.2. Alto Paranaíba province

The Alto Paranaíba province (Almeida 1983) or the southeastern portion of the Minas–Goiás Alkaline province (Sgarbi and Gaspar 2002) is located in central Brazil, in the northeast border of the Paraná Basin. The apatite fission-track thermochronometry data were analyzed by Eby and Mariano (1992) and compared with the K/Ar data set from Amaral et al. (1967), Hasui and Cordani (1968), and Sonoki and Garda (1988). The alkaline bodies detailed here are Araxá, Catalão II, Tapira, Serra Negra, Salitre I, and II, which yielded ages from the Upper Cretaceous while Catalão II yielded ages from the Lower Cretaceous. For the Araxá body, the AFT mean age for carbonatite/glimmerite rock is 84.4 Ma, phosphate rock is 81.9 Ma and pyrochlore-mineralized carbonatite is 84.4 Ma. K/Ar ages from the glimmerite yielded older values as 89.4 ± 10.1 and 97.7 ± 6.1 Ma and carbonatite (77.4 ± 1.0 Ma), which can indicate that the glimmerite were emplaced earlier than the carbonatite, or that thermal closure for the AFT system did not occur until about 5-13 Ma after the complex's emplacement. At Catalão I, AFT ages range from 110.6 to 116.1Ma, with a mean age of 114 Ma, while for Catalão II, the AFT age is 87.1Ma. The K/Ar dating of an alkali-syenite from Catalão I yielded an age of 85.0 ± 6.9 Ma and Eby and Mariano (1992) suggested that the alkali syenite may be related to Catalão II. For Tapira body, AFT ages are 81.7 ± 7.9 Ma (bebedourite) and 78.6 ± 9.0 Ma (carbonatite) and the K-Ar biotite age of 71.2 ± 5.1 Ma (bebedourite), 87.2 ± 1.2 Ma (phonolite) and 85.6 ± 5.1 Ma (jacupiranguito). Conceição et al. (2020) dated $^{40}Ar/^{39}Ar$ in phlogopite, which indicate at least two magmatic events during the emplacement, the first at > 96.2 ± 0.8 Ma and the second at 79.15 ± 0.6 Ma. Amaral et al. (1997) also analyzed the thermal histories on apatite from Catalão II and Tapira Complex which presents single cooling history since the annealing temperature, characterized by a slow cooling from 95º to 85ºC between 90 and 60 Ma and faster cooling from 85º to 27ºC for the last 60 Ma. Soares et al. (2016) dated apatite fission tracks from Catalão (82.6 ± 5.3 Ma) and Tapira (88.9 ± 7.4 Ma) in agreement with values from other radiometric methods which can be associated with post-magmatic cooling and the confined track length distributions can be related to fast cooling.

The Serra Negra body was dated by K/Ar of biotite from the peridotite and yielded ages of 83.7 - 83.8 ± 2.5 Ma, while AFT age is 79.1 Ma of an apatite-calcite carbonatite. Salitre I was dated by AFT phosphate-rich carbonatite (87.1 Ma) and sanidine trachyte (89.8 Ma) and at Salitre II the bebedourite has an AFT age of 82.6 Ma. Biotite from bebedourite of Salitre was also dated by K/Ar and yielded 86.3 ± 5.7 and 82.5 ± 5.6 Ma and phonolite yielded ages from 79.0 ± 1.2 to 94.5 ± 1.5 Ma. In general, K/Ar dating and AFT dating are in good agreement and they all were emplaced between 88-79 Ma, except for Catalão I. This supports that the alkaline

complexes were emplaced relatively close to the surface and also had a fast cooling at temperatures that the fission tracks were retained in apatite. Besides that, the results suggest that there are two moments of activity, the first one at ca. 80 Ma with the emplacement of Salitre II, Serra Negra, and Tapira; and the second one at ca. 88 Ma refers to the emplacement of Catalão II and Salitre I. (Eby and Mariano 1992; Gomes et al. 1990).

2.7.3. Trindade island

Trindade Island is located in the South Atlantic Ocean, 1170 km from the Brazilian coast. Pires et al. (2016) present new Ar/Ar ages and also a re-evaluation of K/Ar data. The volcanism has a peak between 3.9-2.5 Ma (Trindade Complex) and completely ceased at ca. 0.25 Ma (Paredão Formation). Apatites from the lava flow and dikes from the basal unit

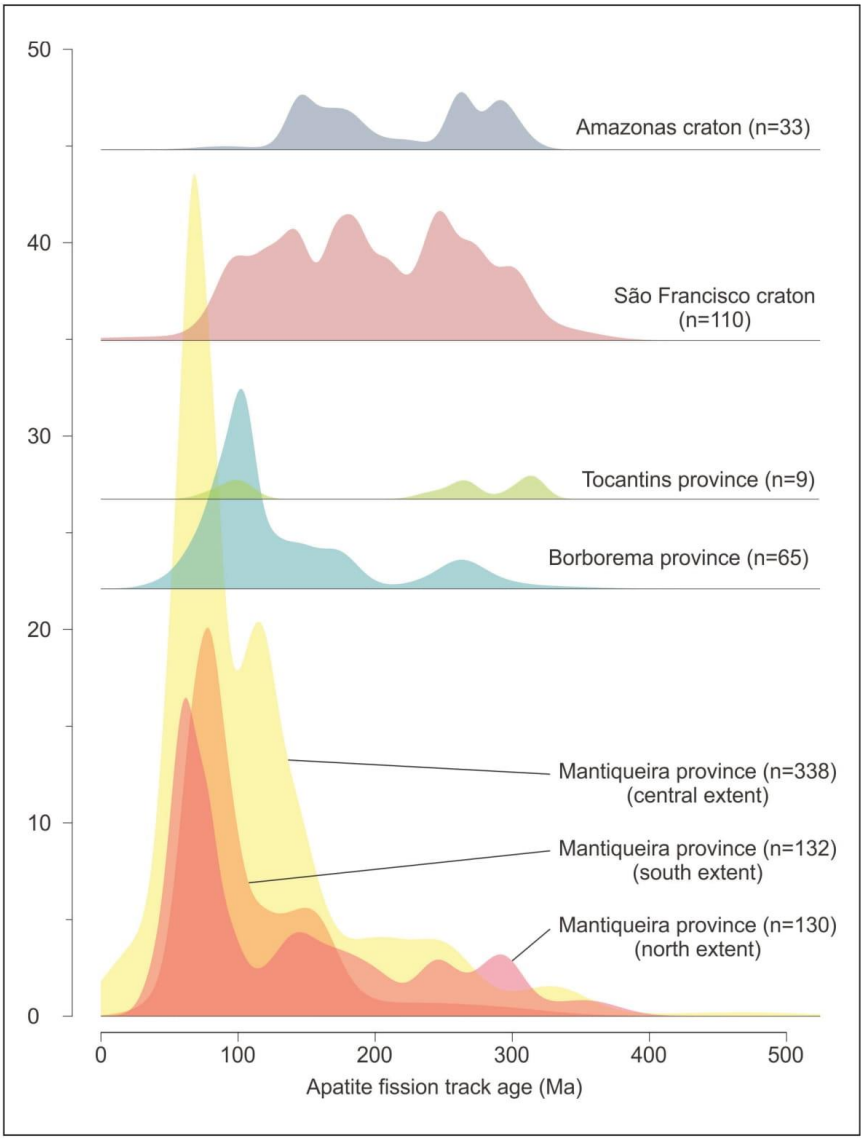

FIGURE 9. Apatite fission-track samples dating histograms for Brazilian tectonic domains. Due to a large amount of data, Mantiqueira province was divided into three sectors: North (13°S to 20°S), Central (20°S to 26 °S), and South (26°S to 33 °S).

(Trindade Complex) yielded ages of 3.53 - 3.0 Ma and the modeling showed cooling between 3.9 and 3.0 Ma, followed by relatively slow erosion rates (Hackspacher et al. 2017).

2.7.4. Poços de Caldas province

In southeastern Brazil, the Serra do Mar magmatism migrated progressively approximately 500 km from Poços de Caldas to Cabo Frio, between 80 and 55 Ma (Thompson et al. 1998; Sonoki and Garda 1988; Amaral et al. 1967). Poços de Caldas alkaline massif is located on the boundary between São Paulo and Minas Gerais. Cogné et al. (2011) combined AHe and AFT ages from samples of the Poços de Caldas alkaline body. The AHe ages suggest slow cooling between 90-60 Ma related to exhumation during Late Cretaceous followed by a fast cooling during Neogene (although this result is in the limit of the method resolution). On the other hand, Silva et al. (2011) showed apatite grains yielding AFT ages from 69.0 ± 4.4 to 42.7 ± 3.4 Ma, with magmatic crystallization age ranging from 89.1 ± 7.1 Ma to 83.6 ± 6.7 Ma. The thermochronological history reveals that shortly after the intrusion, the faster cooling and main exhumation occurred, which lasted for about 11 Myr. Doranti-Tiritan et al. (2014) agree with Silva et al. (2011) and interpreted the data as fast cooling at 80 Ma with the thermal stability of 40°C until approximately 50 Ma when heating occurs from 40° to 75°C until 5 Ma, followed by a fast cooling event to 20°C. Souza et al. (2014) get Eocene to Paleocene AFT ages in the region, and compared with published data (Godoy 2003; Franco et al. 2005; Doranti 2006; Silva 2010; Doranti-Tiritan 2013), highlighting the importance of past tectonic and magmatic events for the regional relief development.

3. Final Remarks

On one hand, the data highlight the importance of the elastic thickness, structural network, and drainage system in the morphotectonic control. On the other hand, the lack of data leaves a series of unsolved questions: i) which forces act in the Brazilian morphotectonic evolution? Compressive, extensional, and plume-related tectonic events could lead to blocks adjustment? What is the role of climate in this interaction? And what could be the implications of a robust data set for gas, oil, and metal deposit studies?

For a more in-depth and robust discussion, it is necessary to acquire a regional fission-track and (U-Th)/He database in zircon and apatite. Brazil still has large areas with no thermochronology data. Advances in the method, like the uranium content reading by mass spectrometers, would exponentially change this scenario. Besides basic data acquisition, an integrated, multi-method, transdisciplinary study is recommended, including sedimentology, geophysics, geomorphology, structural, and tectonics. Complete research like this could lead to an understanding of Brazilian tectono-thermal evolution.

References

Alkmim F.F. 2004. O que faz de um cráton um cráton? O cráton São Francisco e as revelações almeidianas ao delimitá-lo. In: Mantesso-Neto V., Bartorelli A., Carneiro C.D.R., Brito Neves B.B. (ed.). Geologia do continente Sul-Americano: evolução da obra de Fernando Flávio Marques de Almeida. São Paulo, Beca, 17–35.

Almeida F.F.M. 1964. Geologia do centro-oeste mato-grossense. Rio de Janeiro, IBGE, 137. (Boletim 215)

Almeida F.F.M. 1983. Relações tectônicas das rochas alcalinas mesozóicas da região meridional da Plataforma Sul-Americana. Revista Brasileira de Geociências, 13(3), 139–158. Available on line at: http://www.ppegeo.igc.usp.br/index.php/rbg/article/view/12148 / (accessed on 11 December 2021)

Almeida F.F.M., Hasui Y., Brito Neves B.B., Fuck R.A. 1981. Brazilian structural provinces: an introduction. Earth-Science Review, 17, 1–29. https://doi.org/10.1016/0012-8252(81)90003-9

Amaral, G. 1978. Potassium-Argon age studies on the Jacupiranga Alkaline District, State of São Paulo, Brazil. In: International Symposium on Carbonatites, 1st., 297-302.

Amaral G., Born H., Hadler J.C.N., Iunes P.J., Kawashita K., Machado D.L., Oliveira E.P., Paulo S.R., Tello C.A.S. 1997. Fission track analysis of apatites from São Francisco craton and Mesozoic alcaline-carbonatite complexes from central and southeastern Brazil. Journal of South American Earth Sciences, 10, 285–294. https://doi.org/10.1016/S0895-9811(97)00020-5

Amaral G., Bushee J., Cordani U.G., Kawashita K., Reynolds J.H. 1967. Potassium-argon ages of alkaline rocks from southern Brazil. Geochimica et Cosmochimica Acta, 31, 117–142. doi.org/10.1016/S0016-7037(67)80041-3

Amaral-Santos E., Jelinek A., Almeida-Abreu P., Genezine F. 2019. Phanerozoic cooling history of Archean/Paleoproterozoic basement in the southern Espinhaço Range, southeastern Brazil, through apatite fission-track analysis. Journal of South American Earth Sciences, 96. https://doi.org/10.1016/j.jsames.2019.102352

Assumpção M., Azevedo P.A., Rocha M.P., Bianchi M.B. 2017. Lithospheric features of the São Francisco Craton. In: Heilbron M., Cordani U.G., Alkmim F.F. (ed.). São Francisco Craton, Eastern Brazil. Springer, pp 15-25. https://doi.org/10.1007/978-3-319-01715-0

Ault A.K., Gautheron C., King G.E. 2019. Innovations in (U-Th)/He, fission-track, and trapped-charge thermochronometry with applications to earthquakes, weathering, surface-mantle connections, and the growth and decay of mountains. Tectonics, 38, 3705–3739. https://doi.org/10.1029/2018TC005312

Batezelli A., Ladeira F.S.B. 2016. Stratigraphic framework and evolution of the Cretaceous continental sequences of the Bauru, Sanfranciscana, and Parecis basins, Brazil. Journal of South American Earth Sciences, 65, 1–24. https://doi.org/10.1016/j.jsames.2015.11.005

Bicca A., Chemale Jr. F., Jelinek A., Oliveira C., Guadagnin F., Armstrong R. 2013. Tectonic evolution and provenance of the Santa Bárbara Group, Camaquã Mines region, Rio Grande do Sul, Brazil. Journal of South American Earth Sciences, 48, 173-192. https://doi.org/10.1016/j.jsames.2013.09.006

Borba A., Lima E., Vignol-Lelargel M., Mizusakil A., Pimentel A., Sparrenberg I., Barros C. 2003. Significance of Late Paleozoic Fission-track Ages in Volcanic Rocks from the Lavras Do Sul Region, Southernmost Brazil. Gondwana Research, 6, 79- 88. https://doi.org/10.1016/S1342-937X(05)70645-6

Braun, J., Beek, P., Batt, G. 2006. Introduction. In: Braun, J., Beek, P., Batt, G. Quantitative Thermochronology: numerical methods for the interpretation of thermochronological data. p. 1-18. Cambridge: Cambridge University Press. doi:10.1017/CBO9780511616433.002

Braun J., Beek P., Batt G. 2006. Quantitative thermochronology: numerical methods for the interpretation of thermochronological data. Cambridge, Cambridge University Press. https://doi.org/10.1017/CBO9780511616433

Brito Neves B.B. 2002. Main stages of the development of the sedimentary basins of South America and their relationship with the tectonics of supercontinents. Gondwana Research, 5, 175–196. https://doi.org/10.1016/S1342-937X(05)70901-1

Carlson W.D., Donelick R.A., Ketcham R.A. 1999. Variability of apatite fission-track annealing kinetics: I. Experimental results. American Mineralogist, 1213–1223. https://doi.org/10.2138/am-1999-0901

Chew D., Spikings R. 2015. Geochronology and thermochronology using apatite: time and temperature, lower crust to surface. Elements, 11(3), 189-194. https://doi.org/10.2113/gselements.11.3.189

Cogné N., Gallagher K., Cobbold P.R., Riccomini C., Gautheron C. 2012. Post-breakup tectonics in southeast Brazil from thermochronological data and combined inverse-forward thermal history modeling. Journal of Geophysical Research, 117. https://doi.org/10.1029/2012JB009340

Cogné N., Gallagher K., Cobbold P.R. 2011. Post-rift reactivation of the onshore margin of southeast Brazil: Evidence from apatite (U-Th)/

He and fission-track data. Earth and Planetary Science Letters, 309, 118–130. https://doi.org/10.1016/j.epsl.2011.06.025

Conceição F.T., Vasconcelos P.M., Godoy L.H., Navarro G.R.B. 2020. 40Ar/39Ar geochronological evidence for multiple magmatic events during the emplacement of Tapira alkaline-carbonatite complex, Minas Gerais, Brazil. Journal of South American Earth Sciences, 97, 102416. https://doi.org/10.1016/j.jsames.2019.102416

Curvo E.A.C., Carter A., Dias A.N.C., Soares C.J., Nakasuga W.M., Resende R.S., Gomes M.R., Alencar I., Hadler J.C. 2013. Zircon fission track and U–Pb dating methods applied to São Paulo and Taubaté Basins located in the southeast Brazil. Radiation measurements, 50, 172-180. https://doi.org/10.1016/j.radmeas.2012.07.015

Dantas E.L., Hackspacher P.C., Van Schmus W.R., Brito Neves B.B. 1998. Archean accretion in the São José do Campestre massif, Borborema province, Northeast Brazil. Revista Brasileira de Geociências, 28(2), 221-228. Available on line at: https://ppegeo.igc.usp.br/index.php/rbg/article/view/11213 / (accessed on 11 December 2021)

Dias, A.N.C., Chemale Jr F., Candeiro C.R.A., Lana C., Guadagnin F., Sales A.S.W. 2021a. Unraveling multiple tectonic events and source areas in the intracratonic Bauru Basin through combined zircon geo and thermochronological studies. Journal of South American Earth Sciences, 106, 103061. https://doi.org/10.1016/j.jsames.2020.103061

Dias A.N.C., Guadagnin F., Rangel C.V.G.T., Chemale F., Oliveira T.R.P., Moura C.A., Pereira V.Q., Alves J.S.E. 2021b. Provenance of Neogene deposits of Barreiras Formation in the southeastern Brazilian continental margin. International Journal of Earth Sciences, 110(1), 233-249. https://doi.org/10.1007/s00531-020-01949-y

Dias A.N.C., Chemale F., Hackspacher P.C., Soares C.J., O-Aristizabal C.I., Telloet C.A.S. 2018. Fission track and U–Pb double dating of detrital zircon applied to the intracratonic Mesozoic Bauru Basin, Brazil. Geological Journal, 53, 1767–1780. https://doi.org/10.1002/gj.3005

Dias A.N.C., Moura C.A.V., Milhomem Neto J.M., Chemale F., Girelli T.J., Masuyama K.M. 2017. Geochronology and thermochronology of the gneisses of the Brasiliano/Pan-African Araguaia Belt: records of exhumation of West Gondwana and Pangea break up. Journal of South American Earth Sciences, 80, 174–191. https://doi.org/10.1016/j.jsames.2017.09.027

Dias A.N.C, Tello C.A.S., Chemale F., Godoy M.C.T.F., Guadagnin F., Iunes P.J., Soares C.J., Osório A.M.A., Bruckmann M.P. 2011. Fission track and U-Pb in situ dating applied to detrital zircon from the Vale do Rio do Peixe Formation, Bauru Group, Brazil Journal of South American Earth Sciences, 31, 298–305. https://doi.org/10.1016/j.jsames.2011.02.003

Dodson M.H. 1973. Closure temperature in cooling geochronological and petrological systems. Contributions to Mineralogy and Petrology, 40, 259–274. https://doi.org/10.1007/BF00373790

Doranti C. 2006. Estrutura da Paisagem no Leste de São Paulo e Sudoeste de Minas Gerais: relações entre superfícies de erosão e termocronologia por traços de fissão. MSc Dissertation, Universidade Estadual Paulista, Rio Claro, 106. http://hdl.handle.net/11449/92910

Doranti C., Hackspacher P.C., Hadler Neto J.C., Ribeiro M.C.S., Lima H.C. 2008. Evolução do relevo da região do Planalto de Poços de Caldas: correlações entre níveis planálticos e termocronologia por traços de fissão em apatitas. Revista Geografias, 87–92. https://doi.org/10.35699/2237-549X .13255

Doranti-Tiritan C. 2013. Evolução geomórfica e modelagem termocinemática 3D da região do Maciço Alcalino de Poços de Caldas (SP/MG). PhD Thesis, Universidade Estadual Paulista, 160. http://hdl.handle.net/11449/110582

Doranti-Tiritan C., Hackspacher P.C., Ribeiro M.C.S., Glasmacher U.A., Souza D.H. 2014. Relief evolution of Poços de Caldas (SP/MG) Region based in thermochronology data and 3D thermokinematic modeling. Revista Brasileira Geomorfologia, 15, 291–310. https://doi.org/10.20502/rbg.v15i2.491

Eby G.N., Mariano A.N. 1992. Geology and geochronology of carbonatites and associated alkaline rocks peripheral to the Paraná Basin, Brazil-Paraguay. Journal of South American Earth Sciences, 6, 207–216. https://doi.org/10.1016/0895-9811(92)90009-N

Farley K.A. 2000. Helium diffusion from apatite: General behavior as illustrated by Durango fluorapatite. Journal of Geophysical Research Solid Earth, 105(B2), 2903–2914. https://doi.org/10.1029/1999jb900348

Fleischer R.L., Price P.B., Walker R.M. 1975. Nuclear tracks in solids: Principles and applications. Berkeley CA, University of California Press.

Flowers R.M., Ketcham R.A., Shuster D.L., Farley K.A. 2009. Apatite (U-Th)/He thermochronometry using a radiation damage accumulation and annealing model. Geochimica et Cosmochimica Acta, 73, 2347–2365. https://doi.org/10.1016/j.gca.2009.01.015

Fonseca A.C. 1994. Esboço geocronológico da região de Cabo Frio, Estado do Rio de Janeiro. PhD Thesi, Intituto de geociências, Universidade de São Paulo, São Paulo. 207 p. DOI: 10.11606/T.44.1994.tde-17042015-161414

Fonseca A.C.L., Novo T., Nachtergaele S., Fonte-Boa T.M.R., Van Ranst G., De Grave J., 2021. Differential Phanerozoic evolution of cratonic and non cratonic lithosphere from a thermochronological perspective: São Francisco Craton and marginal orogens (Brazil). Gondwana Research, 93, 106-126. https://doi.org/10.1016/j.gr.2021.01.006

Fonseca A.L., Piffer G., Nachtergaele S., Van Ranst G., De Grave J., Novo T. 2020. Devonian to Permian post-orogenic denudation of the Brasília Belt of West Gondwana: insights from apatite fission track thermochronology. Journal of Geodynamics, 137-101733. https://doi.org/10.1016/j.jog.2020.101733

Franco-Magalhães A., Cuglieri M., Hackspacher P., Saad A. 2014. Long-term landscape evolution and post-rift reactivation in the southeastern Brazilian passive continental margin: Taubaté basin. International Journal of Earth Sciences (Geol Rundsch), 103, 441–453. https://doi.org/10.1007/s00531-013-0967-4

Franco-Magalhães A.O.B., Hackspacher P.C., Glasmacher U.A., Saad A.R. 2010. Rift to post-rift evolution of a "passive" continental margin: The Ponta Grossa Arch, SE Brazil. International Journal of Earth Sciences (Geol Rundsch), 99, 1599–1613. https://doi.org/10.1007/s00531-010-0556-8

Franco A.O.B., Hackspacher P.C., Godoy D.F., Ribeiro L.F.B., Guedes S. 2005. História térmica do Maciço Alcalino de Poços de Caldas (SP/MG) e adjacências através da análise de datação por traços de fissão em apatitas. Revista Brasileira Geociências, 35, 351–358. https://doi.org/10.25249/0375-7536.2005353351358

Gallagher K. 2012. Transdimensional inverse thermal history modeling for quantitative thermochronology. Journal Geophysical Research, 117, 1–16. https://doi.org/10.1029/2011JB008825

Gallagher K., Hawkesworth C.J., Mantovani M.S.M. 1994. The denudation history of the onshore continental margin of SE Brazil inferred from apatite fission track data. Journal of Geophysical Research Solid Earth, 99, 18117–18145. https://doi.org/10.1029/94JB00661

Gallagher K., Hawkesworth C.J., Mantovani M.S.M. 1995. Denudation, fission track analysis and the long-term evolution of passive margin topography: application to the southeast Brazilian margin. Journal of South American Earth Sciences, 8, 65-77. https://doi.org/10.1016/0895-9811(94)00042-Z

Gautheron C., Tassan-Got L., Barbarand J., Pagel M. 2009. Effect of alpha-damage annealing on apatite (U-Th)/He thermochronology. Geochimica et Cosmochimica Acta, 266, 157–170. https://doi.org/10.1016/j.chemgeo.2009.06.001

Genaro D. 2008. Contribuição ao Conhecimento de Processos Atuantes no Rifteamento Continental, por Traços de Fissão em Zircões e Apatitas, Aplicados no Rift Continental do Sudeste do Brasil, bacias de Taubaté, Resende, Volta Redonda e Circunvizinhanças. MSc Dissertation, Instituto de Geociências e Ciências Exatas, Universidade Estadual Paulista, 131 p. Available on line at: http://hdl.handle.net/11449/92905 / (accessed on 11 December 2021)

Gezatt J.N., Macdonald D.I.M., Stephenson R., Jelinek A.R., Carter A. 2021. South Atlantic passive margin evolution: A thermochronology case study from the Rio de Janeiro-Três Rios section, SE Brazil. Journal of South American Earth Sciences, 106, 103051. https://doi.org/10.1016/j.jsames.2020.103051

Gleadow A.J.W., Duddy I.R. 1981. A natural long-term track annealing experiment for apatite. Nucl Tracks, 5, 169–174. https://doi.org/10.1016/0191-278X(81)90039-1

Gleadow A.J.W., Duddy I.R., Green P.F., Lovering J.F. 1986. Confined fission track lengths in apatite: a diagnostic tool for thermal history analysis. Contributions to Mineralogy and Petrology, 94, 405–415. https://doi.org/10.1007/BF00376334

Godoy D.F. 2003. História térmica e denudação do maciço alcalino de poços de caldas e circunvizinhanças: área norte. Graduation work, Universidade Estadual Paulista.

Godoy D.F., Hackspacher P., Guedes S., Hadler Neto J. 2006. Reconhecimento da tectônica Mesozóica-Cenozóica na borda leste da bacia do Paraná através da aplicação de traços de fissão em apatitas no Domo de Pitanga (Sudoeste de Rio Claro, SP). Geociências, 25, 151-164. Available on line at: https://www.revistageociencias.com.br/geociencias-arquivos/25_1/15.pdf / (accessed on 11 December 2021)

Gomes C.B., Barbieri M., Beccaluva L., Brotzu P., Conte A., Garbarino C., Macciotta G., Melluso L., Morbidelli L., Ruberti E., Scheibe L.F., Tamura R.M., Traversa G. 1987.

Gomes C.B., Ruperti E., Morbidelli L. 1990. Carbonatite complexes from Brazil: a review. Journal of South American Earth Sciences, 3, 51–63. https://doi.org/10.1016/0895-9811(90)90017-U

Petrological and geochemical studies of alkaline rocks from continental Brazil. 2. The tunas massif, State of Parana. Geochimica Brasiliensis, 1, 201–234.

Gomes C.H., Almeida D. 2019. New insights into the Gondwana breakup at the Southern South America by apatite fission-track analyses. Advances in Geosciences, 47(1–15). https://doi.org/10.5194/adgeo-47-1-2019

Green P.F., Duddy I.R., Gleadow A.J.W., Tingate P.R, MLaslett G. 1986. Thermal annealing of fission tracks in apatite. Chemical Geology: Isotope Geoscience section, 59, 237–253. https://doi.org/http://dx.doi.org/10.1016/0168-9622(86)90074-6

Guenthner W.R., Reiners P.W., Ketcham R.A., Nasdala L., Giester G. 2013. Helium diffusion in natural zircon: radiation damage, anisotropy, and the interpretation of zircon (U-Th)/He thermochronology. American Journal Science, 313, 145–198. https://doi.org/10.2475/03.2013.01

Hackspacher P.C., Biancini J.R.C., Lourenço P.R., Ribeiro MCB. 2017. Rochas vulcânicas da Ilha da Trindade: resfriamento rápido e baixa erosão .In: Secretaria da Comissão Interministerial para os Recursos do Mar. Protrindade: programa de pesquisas científicas na Ilha da Trindade. 10 anos de pesquisas. Brasília, SECIRM. p. 65-69. Available on line at: marinha.mil.br/secirm/sites/www.marinha.mil.br.secirm/files/publicacoes/protrindade/protrindade-10anos.pdf / (accessed on 11 December 2021)

Hackspacher P.C., Godoy D.F., Ribeiro L.F.B., Hadler Neto J.C., Franco A.O.B. 2007. Modelagem térmica e geomorfologia da borda sul do Cráton do São Francisco: termocronologia por traços de fissão em apatita Peter. Revista Brasileira de Geociências, 37, 76–86. Available on line at: http://www.ppegeo.igc.usp.br/index.php/rbg/article/view/9225 / (accessed on 11 December 2021)

Hackspacher P.C., Ribeiro L.F.B., Ribeiro M.C.S., Fetter A.H., Hadler Neto J.C., Tello C.E.S., Dantas E.L. 2004. Consolidation and break-up of the South American Platform in southeastern Brazil: tectonothermal and denudation histories. Gondwana Research, 7, 91–101. https://doi.org/10.1016/S1342-937X(05)70308-7

Harman R., Gallagher K., Brown R., Raza A., Bizzi L. 1998. Accelerated denudation and tectonic/geomorphic reactivation of the cratons of northeastern Brazil during the Late Cretaceous. Journal of Geophysical Research Solid Earth, 103, 27091–27105. https://doi.org/10.1029/98JB02524

Hasebe N., Barbarand J., Jarvis K., Carter A., JHurford A. 2004. Apatite fission-track chronometry using laser ablation ICP-MS. Chemical Geology, 207, 135–145. https://doi.org/10.1016/j.chemgeo.2004.01.007

Hasui Y. 2012. Cráton Amazônico: províncias Rio Branco e Tapajós. In: Carneiro, C.R., Almeida, Fernando F.M., Bartorelli A., Hasui, Y. (org.). Geologia do Brasil. São Paulo, Beca. p 138-175.

Hasui Y., Cordani U.G. 1968. Idade Potássio-Argônio de rochas eruptivas Mesozóicas do oeste mineiro e sul de Goiás. In: Congresso Brasileiro de Geologia, 22, 139-143.

Heilbron M., Cordani U.G., Alkmim F.F. (ed.). 2017. São Francisco Craton, Eastern Brazil: Tectonic Genealogy of a Miniature Continent. Springer, Cham. https://doi.org/10.1007/978-3-319-01715-0

Hiruma S., Riccomini C., Modenesi-Gauttieri M., Hackspacher P., Hadler Neto J., Franco-Magalhães A. 2010. Denudation history of the Bocaina Plateau, Serra do Mar, southeastern Brazil: relationships to Gondwana breakup and passive margin development. Gondwana Research, 18(4), 674-687 https://doi.org/10.1016/j.gr.2010.03.001

Hueck M., Dunkl I., Heller B., Basei M., Siegesmund S. 2018. (U-Th)/He Thermochronology and zircon radiation damage in the South American passive margin: Thermal overprint of the Paraná LIP? Tectonics, 37, 4068–4085, https://doi.org/10.1029/2018TC005041

Hueck M., Dunkl I., Oriolo S., Wemmer K., Basei M., Siegesmund S. 2019. Comparing contiguous high- and low-elevation continental margins: New (U Th)/He constraints from South Brazil and an integration of the thermochronological record of the southeastern passive margin of South America. Tectonophysics, 770, 228222. https://doi.org/10.1016/j.tecto.2019.228222

Hueck M., Oriolo S., Dunkl I., Wemmer K., Oyhantçabal P., Schanofski M., Basei M., Siegesmund S. 2017. Phanerozoic low-temperature evolution of the Uruguayan Shield along the South American passive margin. Journal of the Geological Society, 174. https://doi.org/10.1144/jgs2016-101

Japsen P., Chalmers J.A., Green P.F., Bonow J.M. 2012. Elevated, passive continental margins: Not rift shoulders, but expressions of episodic, post-rift burial and exhumation. Global and Planetary Change, 90–91, 73–86. https://doi.org/10.1016/j.gloplacha.2011.05.004

Jelinek A.R., Bastos Neto A., Lelarge M., Soliani Jr. E. 1999. Apatite fission track dating of fluorite ore veins from Santa Catarina state, Brazil: a complex hydrothermal evolution. Journal of South American Earth Sciences, 12, 367-377. https://doi.org/10.1016/S0895-9811(99)00028-0

Jelinek A.R., Chemale F., van der Beek P.A., Guadagnin F., Cupertino J.A., Viana A. 2014. Denudation history and landscape evolution of the northern East-Brazilian continental margin from apatite fission-track thermochronology. Journal of South American Earth Sciences, 54, 158–181. https://doi.org/10.1016/j.jsames.2014.06.001

Jelinek A.R., Corrêa-Gomes L.C. Bicca, M.M. 2020. Evolução termotectônica fanerozoica da margem continental na área do Rifte Recôncavo-Tucano-Jatobá. Pesquisas em Geociências, 47(1). https://doi.org/10.22456/1807-9806.101330

Jordan T.H. 1978. Composition and development of the continental tectosphere. Nature, 274, 544–548. https://doi.org/10.1038/274544a0

Karl M., Glasmachera U., Kollenz S., Franco-Magalhaes O., Stockli D., Hackspacher P. 2013. Evolution of the South Atlantic passive continental margin in southern Brazil derived from zircon and apatite (U–Th–Sm)/He and fission-track data. Tectonophysics, 604, 224-244. https://doi.org/10.1016/j.tecto.2013.06.017

Ketcham R.A. 2005. Forward and inverse modeling of low-temperature thermochronometry data. Reviews in Mineralogy and Geochemistry, 58(1), 275–314. https://doi.org/10.2138/rmg.2005.58.11

Ketcham R.A., Carter A., Donelick R.A. 2007, Barbarand J., Hurford A. J. Improved modeling of fission-track annealing in apatite. American Mineralogist, 92(5-6), 799–810. https://doi.org/10.2138/am.2007.2281

Ketcham R.A., Donelick R.A., Carlson W.D. 1999. Variability of apatite fission-track annealing kinetics: III. Extrapolation to geological time scales. American Mineralogist, 84, 1235–1255. https://doi.org/10.2138/am-1999-0902

King L.C. 1956. A geomorfologia do Brasil Oriental. Revista Brasileira de Geografia, 18(2), 3–121. Available on line at: https://biblioteca.ibge.gov.br/visualizacao/periodicos/115/rbg_1956_v18_n2.pdf / (accessed on 11 December 2021)

Krob F., Glasmacher U., Karl M., Perner M., Hackspacher P., Stockli D. 2019. Multi chronometer thermochronological modelling of the Late Neoproterozoic to recent t-T-evolution of the SE coastal region of Brazil. Journal of South American Earth Sciences, 92. https://doi.org/10.1016/j.jsames.2019.02.012

Lima C.C. 2000. Ongoing compression across intraplate South America: observations and some implications for petroleum exploitation and exploration. Revista Brasileira Geociências, 30,203–207. https://doi.org/10.25249/0375-7536.2000301203207

Machado J., Jelinek A., Bicca M., Stephenson R., Genezini F. 2019. West Gondwana orogenies and Pangaea breakup: thermotectonic effects on the southernmost Mantiqueira Province, Brazil. Journal of the Geological Society, 176. https://doi.org/10.1144/jgs2019-018

Machado J.P., Jelinek A.R., Stephenson R., O'Sullivan P. 2021. Thermochronology of South America passive margin between Uruguay and southern Brazil: A lengthy and complex cooling history based on (U–Th)/He and fission tracks. Journal of South American Earth Sciences, 106, 103019. https://doi.org/10.1016/j.jsames.2020.103019

Martins-Ferreira M.A.C., Dias A.N.C., Chemale F., Campos J.E.G. 2020. Intracontinental uplift of the Brazilian Central Plateau linked to continental breakup, orogenies, and basin filling, supported by apatite and zircon fission-track data. Arabian Journal of Geosciences, 13(17), 1-14. https://doi.org/10.1007/s12517-020-05885-8

Martins-Neto M.A., Pedrosa-Soares A.C., Lima S.A.A. 2001. Tectono-sedimentary evolution of sedimentary basins from Late Paleoproterozoic to Late Neoproterozoic in the São Francisco craton and Araçuaí fold belt, eastern Brazil. Sedimentary Geology, 141–142, 343–370. https://doi.org/10.1016/S0037-0738(01)00082-3

Milani E.J., Thomas F.A. 2000. Sedimentary basins of South América. In: In: Cordani U.G., Milani E.J., Thomaz Filho A., Campos D.A (ed.). Tectonic evolution of South America. Rio de Janeiro, 31st International Geological Congress. p. 389–449. Available on line at: https://rigeo.cprm.gov.br/handle/doc/19419 / (accessed on 11 December 2021)

Mohriak W., Nemčok M., Enciso G. 2008. South Atlantic divergent margin evolution: rift-border uplift and salt tectonics in the basins of SE Brazil. In: Pankhurst R.J., Trouw R.A.J., Brito Neve BB, Wit M.J. (ed.). West Gondwana: Pre-Cenozoic correlations across the South Atlantic Region. London, Geological Society. p. 365–398. Special Publication 24. https://doi.org/10.1017/s0954102009990587

Morais Neto J.M., Hegarty K.A., Karner G.D., Alkmim F.F. 2009. Timing and mechanisms for the generation and modification of the anomalous topography of the Borborema province, northeastern brazil. Marine and Petroleum Geology, 26(7), 1070-1086. https://doi.org/10.1016/j.marpetgeo.2008.07.002

Neves S.P., Mariano G., Guimarães I.P., Silva Filho A.F., Melo S.C. 2000. Intralithospheric differentiation and crustal growth: evidence from the Borborema province, northeastern Brazil, Geology, 28, 519–522. https://doi.org/10.1130/0091-7613(2000)28<519:IDACGE>2.0.CO;2

Oliveira C.H.E., Jelinek A., Chemale Jr. F., Bernet M. 2016a. Evidence of post Gondwana breakup in Southern Brazilian Shield: Insights from apatite and zircon fission track thermochronology. Tectonophysics, 666, 173–187. http://dx.doi.org/10.1016/j.tecto.2015.11.005

Oliveira C.H.E., Jelinek A., Chemale Jr. F., Cupertino J. 2016b. Thermotectonic history of the southeastern Brazilian margin: Evidence from apatite fission track data of the offshore Santos Basin and continental basement. Tectonophysics, 685, 21–34. http://dx.doi.org/10.1016/j.tecto.2016.07.012

Oliveira C.H.E., Jelinek A.R., Timoteo D., Bernet M. 2018. Thermotectonic history of the Maastrichtian reservoir in Campos Basin. Marine and Petroleum Geology, 93, 331– 343. https://doi.org/10.1016/j.marpetgeo.2018.03.021

Oliveira S.G., Hackspacher P.C., Hadler Neto J.C., Iunes P.J., DE Paulo, S.R., Ribeiro L.F.B., SÁENZ C.A.T. 2000. Constraints on the evolution and thermal history of the continental platform of southeast brazil, São Paulo state, using apatite fission track analysis (afta). Revista Brasileira de Geociências, 30(1), 107– 109. Available on line at: http://www.ppegeo.igc.usp.br/index.php/rbg/article/view/10929/ (accessed on 11 December 2021)

Pedrosa-Soares A.C., Wiedemann-Leonardos C.M. 2000. Evolution of the Araçuaí belt and its connection to the Ribeira Belt, Eastern Brazil. In: Cordani U.G., Milani E.J., Thomaz Filho A., Campos D.A (ed.). Tectonic evolution of South America. Rio de Janeiro, 31st International Geological Congress. p. 265-285. Available on line at: https://rigeo.cprm.gov.br/handle/doc/19419 / (accessed on 11 December 2021)

Pimentel M.M., Jost H., Fuck R.A. 2004. O embasamento da Faixa Brasília e o Arco Magmático de Goiás. In: Mantesso-Neto V., Bartorelli A., Carneiro C.D.R., Brito-Neves B.B. (ed.). Geologia do continente sul-americano: Evolução da obra de Fernando Flávio Marques de Almeida, Beca. p. 324–355. Available on line at: http://sbg.sitepessoal.com/livrosadobados/geologiaSul.pdf / (accessed on 11 December 2021)

Pimentel M.M., Fuck R.A., Jost H., Ferreira Filho C.F., Araújo S.M. 2000. The basement of the Brasília Fold Belt and the Goiás Magmatic Arc. In: Cordani U.G., Milani E.J., Thomaz Filho A., Campos D.A (ed.). Tectonic evolution of South America. Rio de Janeiro, 31st International Geological Congress. p. 195-229. Available on line at: https://rigeo.cprm.gov.br/handle/doc/19419 / (accessed on 11 December 2021)

Pina A.C.M. 2010. Termocronologia por traços de fissão em apatita da borda sul da Bacia do Amazonas, na região de Itaituba (PA). MSc Dissertation, Instituto de Geociências, Universidade Federal do Pará, Belém, 2010. Available on line at: https://rigeo.cprm.gov.br/handle/doc/1155 / (accessed on 11 December 2021)

Pires G.L.C., Bongiolo E.M., Geraldes M.C., Renac C., Santos A.C., Jourdan F., Neumann R. 2016. New 40 Ar/ 39 Ar ages and revised 40 K/ 40 Ar* data from nephelinitic–phonolitic volcanic successions of the Trindade Island (South Atlantic Ocean). Journal of Volcanology and Geothermal Research, 327, 531–538. https://doi.org/10.1016/j.jvolgeores.2016.09.020

Porada H. 1989. Pan-African rifting and orogenesis in southern to Equatorial Africa and Eastern Brazil. Precambrian Research, 44, 103–136. https://doi.org/10.1016/0301-9268(89)90078-8

Price P.B., Walker R.M. 1963. Fossil tracks of charged particles in mica and the age of minerals. Journal of Geophysical Research (U.S.), 68, 4847-4862. https://doi.org/10.1029/JZ068i016p04847

Reiners P.W., Carlson R.W., Renne P.R., Cooper K.M., Granger D.E., McLean N.M., Schoene B. 2017. Geochronology and Thermochronology. John Wiley & Sons. https://doi.org/10.1002/9781118455876

Reiners P.W., Ehlers T.A. 2005. Low-temperature thermochronology: techniques, interpretations, and applications. Virginia, Mineralogical Society of America, v. 58, 620 p. http://www.minsocam.org/msa/rim/rim58.html

Reiners P.W., Farley K.A., Hickes H.J. 2002. He diffusion and (U-Th)/He thermochronometry of zircon: initial results from Fish Canyon Tuff and Gold Butte. Tectonophysics, 349, 297–308. https://doi.org/10.1016/S0040-1951(02)00058-6

Reiners P.W., Spell T.L., Nicolescu S., Zanetti K.A. 2004. Zircon (U-Th)/He thermochronometry: he diffusion and comparisons with 40Ar/39Ar dating. Geochimica et Cosmochimica Acta 68:1857–1887. https://doi.org/10.1016/j.gca.2003.10.021

Reis H.L.S., Alkmim F.F., Fonseca R.C.S., Nascimento T. C., Suss J. F., Prevatti L. D. 2017. The São Francisco Basin Humberto. In: In: Heilbron M., Cordani U., Alkmim F. (ed.). São Francisco Craton, Eastern Brazil. Springer, Cham. p. 117–143. https://doi.org/10.1007/978-3-319-01715-0_7

Renne PR, Mertz DF, Ernesto M., Marques L.S., Teixeira w., Ens H.H., Richards M.A. 1993. Geochronologic constraints on the magmatic and tectonic evolution of the Paraná Province. EOS (Washington), 74(432), 553.

Ribeiro M.C.S., Hackspacher P.C., Ribeiro L.F.B., Neto J. 2011. Evolução tectônica e denudacional da Serra do Mar (SE/Brasil) no limite entre o Cretáceo Superior e Paleoceno, utilizando análises de traços de fissão e U-Th/He em apatitas. Revista Brasileira de Geomorfologia, 12, 3-14. http://dx.doi.org/10.20502/rbg.v12i0.254

Ribeiro L.F.B., Hackspacher P.C., Ribeiro M.C.S., Hadler Neto J.C., Tello S.C.A., Iunes P.J., Franco A.O.B., Godoy D.F. 2005a. Thermotectonic and fault dynamic analysis of Precambrian basement and tectonic constraints with the Parana basin. Radiation Measurements, 39, 669–673. https://doi.org/10.1016/j.radmeas.2004.09.007

Ribeiro L.F.B., Saenz C.A.T., Iunes P.J., Hackspacher P.C., Hadler Neto, J.C., Paulo S.R 2005b. Phanerozoic brittle tectonics in the South American continental platform, southeast Brazil: new insights from fission-track studies on apatite in reactivated fault zones. Revista Brasileira Geociências, 35, 151–164. Available on line at: http://www.ppegeo.igc.usp.br/index.php/rbg/article/view/9443 / (accessed on 11 December 2021)

Riccomini C., Velázquez V.F., Gomes C.B. 2005. Tectonic controls of the Mesozoic and Cenozoic alkaline magmatism in the central-southeastern Brazilian Platform. In: Comin-Chiaramonti P., Gomes C.B. (ed.). Mesozoic to Cenozoic Alkaline Magmatism in the Brazilian Platform. São Paulo, Editora da Universidade de São Paulo. p. 31–57. Available on line at: http://www.livrosabertos.edusp.usp.br/edusp/catalog/book/6 / (accessed on 11 December 2021)

Roden M.F., Murthy V.R., Gaspar J.C. 1985. Sr and Nd Isotopic Composition of the Jacupiranga Carbonatite. The Journal of Geology, 93, 212–220. https://www.jstor.org/stable/30066298

Santos J.O.S, Hartmann L.A., Gaudette H.E., Groves D.I., Mcnaughton N.J., Fletcher I.R. 2000. A new understanding of the provinces of the Amazon craton based onthe integration of field mapping and U-Pb and Sm-Nd geochronology. Gondwana Research, 3, 453-488. https://doi.org/10.1016/S1342-937X(05)70755-3

Sgarbi P.B.A., Gaspar J.C. 2002. Geochemistry of Santo Antônio da Barra Kamafugites, Goiás, Brazil. Journal of South American Earth Sciences, 14, 889–901. https://doi.org/10.1016/S0895-9811(01)00079-7

Silva J.D.S., Glasmacher U.A., Hackspacher P.C., Stoeckli D., Karl M., Sehrt M. 2011. The Poços de Caldas alkaline massif, a key to understand thermal, exhumation, rock and surface uplift history at the " passive " continental margin of Brazil. In: Geophysical Research Abstracts, 13.

Silva J.S. 2010. Reconstrução termocronologica do maciço alcalino de Poços de Caldas e áreas adjacentes por traços de fissão e (U-Th-Sm)\he em apatitas e zircão. PhD Thesis, Universidade Estadual Paulista, 127. http://hdl.handle.net/11449/103034

Soares C.J., Guedes S., Jonckheere R., Hadler J.C., Passarella S.M., Dias A.N.C. 2016. Apatite fission-track analysis of Cretaceous alkaline rocks of Ponta Grossa and Alto Paranaíba Arches, Brazil. Geological Journal, 51, 805–810. https://doi.org/10.1002/gj.2694

Sonoki I.K., Garda G.M. 1988. Idades K-Ar de rochas alcalinas do Brasil meridional e Paraguai oriental: compilação e adaptação às novas constantes de decaimento. Boletim IG-USP. Série Científica 19:63. https://doi.org/10.11606/issn.2316-8986.v19i0p63-85

Souza D.H., Hackspacher P.C., Doranti-Tiritan C., Godoy D.F. 2014. Comparação da dinâmica evolutiva, a longo e curto prazo, entre o planalto de Poços de Caldas e o planalto de São Pedro de Caldas. Revista Brasileira de Geomorfologia, 15. https://doi.org/10.20502/rbg.v15i2.481

Souza D.H., Hackspacher P.C., Silva B.V., Ribeiro M.C., Hiruma S.T. 2020. Temporal and spatial denudation trends in the continental margin of

southeastern Brazil. Journal of South American Earth Science, 105. https://doi.org/10.1016/j.jsames.2020.102931

Shuster D.L., Flowers R.M., Farley K.A. 2006. The influence of natural radiation damage on helium diffusion kinetics in apatite. Earth and Planetary Science Letters, 249, 148–161. https://doi.org/10.1016/j.epsl.2006.07.028

Strutt R.J. 1909. The accumulation of helium in geological time II. Proc. Roy. Soc., London, Series A, 96–99.

Tagami, T. 2005. Zircon fission-track thermochronology and applications to fault studies. Reviews in Mineralogy and Geochemistry, 58(1), 95–122. https://doi.org/10.2138/rmg.2005.58.4

Tagami T., Galbraith R.F., Yamada R., Laslett G.M. 1998. Revised annealing kinetics of fission tracks in zircon and geological implications. In: Van den Haute P., De Corte F. (ed.). Advances in Fission-Track Geochronology. Solid Earth Sciences Library, 99–114, Springer, Dordrecht. https://doi.org/10.1007/978-94-015-9133-1_8

Tassinari C.C.G., Macambira M.J.B. 1999. Geochronological provinces of the Amazonian craton. Episodes, 22(3), 174-182. https://doi.org/10.18814/epiiugs/1999/v22i3/004

Tello Saenz CA, Hackspacher PC, Hadler Neto JC, Iunes P.J., Guedes S., Ribeiro L.F.B, Paulo S.R. 2003. Recognition of Cretaceous, Paleocene, and Neogene tectonic reactivation through apatite fission-track analysis in Precambrian areas of southeast Brazil: Association with the opening of the South Atlantic Ocean. Journal of South American Earth Sciences, 15, 765–774. https://doi.org/10.1016/S0895-9811(02)00131-1

Tello Saenz C.A., Hadler Neto J.C., Iunes P.J., Guedes S., Hackspacher P.C., Ribeiro L.F.B., Paulo S.R., Osorio A.M.A. 2005. Thermochronology of the South American platform in the state of São Paulo, Brazil, through apatite fission tracks. Radiation Measurements, 39, 635–640. https://doi.org/10.1016/j.radmeas.2004.08.005

Thompson R.N., Gibson S.A., Mitghell J.G., Dickin A P., Leonardos O.H., Brod J.A., Greenwood J.C. Migrating Cretaceous–Eocene Magmatismin the Serra do Mar Alkaline Province,SE Brazil: Melts from the Deflected Trindade Mantle Plume?. Journal of Petrology, 39(8), 1493–1526. https://doi.org/10.1093/petroj/39.8.1493

Trouw R.A.J., Heilbron M., Ribeiro A., Paciullo F.V.P., Valeriano C.M., Almeida J.C.H., Tupinambá M., Andreis R.R. 2000. The Central Segment of the Ribeira Belt. In: Cordani U.G., Milani E.J., Thomaz Filho A., Campos D.A (ed.). Tectonic evolution of South America. Rio de Janeiro, 31st International Geological Congress. p. 287- 310. Available on line at: https://rigeo.cprm.gov.br/handle/doc/19419 / (accessed on 11 December 2021)

Turner J.P., Green P.F., Holford S.P., Lawrence S.R. 2008. Thermal history of the Rio Muni (West Africa)-NE Brazil margins during continental breakup. Earth Planet Sci Lett 270(3-4), 354–367. https://doi.org/10.1016/j.epsl.2008.04.002

Ulbrich H.H.G.J., Gomes C.B. 1981. Alkaline rocks from continental Brazil. Earth-Science Reviews, 17, 135–154. https://doi.org/10.1016/0012-8252(81)90009-X

Van Ranst G., Pedrosa-Soares A.C., Novo T., Vermeesch P., Grave J. 2019. New insights from low-temperature thermochronology into the tectonic and geomorphologic evolution of the south-eastern Brazilian highlands and passive margin. Geoscience Frontiers, 11, 303-324. https://doi.org/10.1016/j.gsf.2019.05.011

Wolf R.A., Farley K.A., Silver L.T. 1996. Helium diffusion and low-temperature thermochronometry of apatite. Geochimica et Cosmochimica Acta, 60, 4231–4240. https://doi.org/10.1016/S0016-7037(96)00192-5

Zeitler P.K., Herczeg A.L., McDougall I., Honda M. 1987. U-Th-He dating of apatite: a potential thermochronometer. Geochimica et Cosmochimica Acta, 51, 2865-2868. https://doi.org/10.1016/0016-7037(87)90164-5